

**NEW CHEMISTRY WITH GOLD-NITROGEN COMPLEXES: SYNTHESIS
AND CHARACTERIZATION OF TETRA-, TRI-, AND DINUCLEAR GOLD(I)
AMIDINATE COMPLEXES. OXIDATIVE-ADDITION TO THE DINUCLEAR
GOLD(I) AMIDINATE**

A Dissertation

by

HANAN ELSAYED ABDOU

Submitted to the Office of Graduate Studies of
Texas A&M University
in partial fulfillment of the requirements for the degree of

DOCTOR OF PHILOSOPHY

May 2006

Major Subject: Chemistry

**NEW CHEMISTRY WITH GOLD-NITROGEN COMPLEXES: SYNTHESIS
AND CHARACTERIZATION OF TETRA-, TRI-, AND DINUCLEAR GOLD(I)
AMIDINATE COMPLEXES. OXIDATIVE-ADDITION TO THE DINUCLEAR
GOLD(I) AMIDINATE**

A Dissertation

by

HANAN ELSAYED ABDOU

Submitted to the Office of Graduate Studies of
Texas A&M University
in partial fulfillment of the requirements for the degree of

DOCTOR OF PHILOSOPHY

Approved by:

Chair of Committee,
Committee Members,

Head of Department,

J. P. Fackler, Jr.
P. A. Lindahl
M. Y. Darensbourg
L. Abbott
E.A. Schweikert

May 2006

Major Subject: Chemistry

ABSTRACT

New Chemistry with Gold-Nitrogen Complexes: Synthesis and Characterization of Tetra-, Tri-, and Dinuclear Gold(I) Amidinate Complexes. Oxidative-Addition to the Dinuclear Gold(I) Amidinate. (May 2006)

Hanan Elsayed Abdou, B.S., Zagazig University; M.S., University of Maine

Chair of Advisory Committee: Dr. John P. Fackler, Jr.

Nitrogen ligands have been little studied with gold(I) and almost no chemistry has been described using anionic bridging nitrogen ligands. This dissertation concerns the impact of the bridging ligands amidinate, ArNHC(H)NAr , on the chemistry of gold(I) and, in particular, the effect of substituents on the molecular arrangement. The electronic vs. steric effect of the substituents on the molecular arrangement of gold(I) amidinate complexes is studied in detail. Tetra-, tri-, and dinuclear gold(I) amidinate complexes are synthesized and characterized using X-ray diffraction. Spectroscopic and electrochemical studies of the amidinate complexes are described. Catalytic studies suggest that gold amidinates and related gold nitrogen complexes are the best catalyst precursors for CO oxidation on TiO_2 surface reported to date (87% conversion).

The dinuclear gold(I) amidinate complex with a Au...Au distance of 2.711(3) Å is rare. To our knowledge, there is only one other example of a symmetrical dinuclear gold(I) nitrogen complex. Oxidative-addition reactions to the dinuclear gold(I) complex, $[\text{Au}_2(2,6\text{-Me}_2\text{-form})_2]$ are studied in detail and result in the formation of gold(II)

complexes. The gold(II) amidinate complexes are the first formed with nitrogen ligands. The complexes are stable at room temperature.

Mixed ligand tetranuclear gold(I) clusters and tetranuclear mixed Au-Ag metal clusters of pyrazolate and amidinate ligands are synthesized and characterized using X-ray diffraction.

DEDICATION

This dissertation is dedicated to my parents who brought me to this world; to my husband Dr. Ahmed Mohamed for the love and support; to my two lovely daughters Rowana and Yara for the real pleasure of life.

ACKNOWLEDGEMENTS

I would sincerely thank Dr. John P. Fackler, Jr. for his guidance and support during the past four years, a special period of my life. I am very grateful for his respect to my family and my religious obligations. His door was always open for me for questions and directions.

I am very grateful for the help of Dr. Ahmed Mohamed for doing the X-ray crystallography of this work. His guidance support and encouragement are greatly appreciated.

I also thank Dr. Ibrahim Kani for helping me to get started in the lab and be famlier with the different instruments in the chemistry department.

I would like to thank all the members of the LMSB, past and present. I also thank all other graduate students who made my stay in the chemistry department an enjoyable experience.

TABLE OF CONTENTS

	Page
ABSTRACT.....	iii
DEDICATION.....	v
ACKNOWLEDGEMENTS.....	vi
TABLE OF CONTENTS.....	vii
LIST OF TABLES.....	ix
LIST OF FIGURES.....	xiii
 CHAPTER	
I INTRODUCTION.....	1
II SYNTHESIS AND CHARACTERIZATION OF TETRA-, TRI-, AND DINUCLEAR GOLD(I) AMIDINATE COMPLEXES.....	13
Experimental	14
Crystallographic Studies.....	16
Results and Discussion.....	40
III OXIDATIVE-ADDITION REACTIONS TO THE DINUCLEAR GOLD(I) AMIDINATE COMPLEX, [Au ₂ (<i>o</i> -Me ₂ -form) ₂].....	61
Experimental.....	62
Crystallographic Studies.....	66
Results and Discussion.....	80
IV ELECTROCHEMICAL AND PHOTOPHYSICAL STUDIES OF GOLD(I) AMIDINATE COMPLEXES.....	102
Experimental.....	103
Results and Discussion.....	104
V FORMATION OF MIXED LIGAND MIXED METAL TETRANUCLEAR GOLD(I)-NITROGEN CLUSTERS FROM LIGAND EXCHANGE REACTION WITH THE DINUCLEAR	

CHAPTER	Page
GOLD(I) AMIDINATE COMPLEX $[\text{Au}_2(2,6\text{-Me}_2\text{-form})_2]$	118
Experimental.....	120
Crystallographic Studies.....	123
Results and Discussion.....	131
VI CONCLUSIONS AND SUGGESTIONS FOR FUTURE WORK....	147
REFERENCES.....	152
APPENDIX A.....	157
APPENDIX B.....	161
VITA.....	164

LIST OF TABLES

TABLE	Page
1 Optimized Geometries at MP2 Level and Selected Experimental Structural Parameters for the $[M_2(NHCHNH)_2]$	3
2 Crystal Data and Structure Refinement for N,N'-dinaphthylformamidine, 2 , N,N'-dinaphthylacetamidine, 3 , and N,N'-di(2,6-isopropyl)phenylformamidine, 7	17
3 Crystal Data and Structure Refinement for $[Au_4(ArNC(H)NAr)_4]$, Ar = C ₆ H ₄ -4-OMe, 12 , and Ar = C ₁₀ H ₇ , 13	18
4 Crystal Data and Structure Refinement for $[Au_4(ArNC(H)NAr)_4]$, Ar = C ₆ F ₅ , 14 , and $[Au_4(ArNC(Ph)NAr)_4]$, Ar = C ₆ H ₅ , 16	19
5 Crystal Data and Structure Refinement for $[Au_4(ArNC(CH_3)NAr)_4]$, Ar = C ₆ H ₅ , 17	20
6 Crystal Data and Structure Refinement for $[Au_3(2,6-Me_2-form)_2(THT)Cl]$, 18 , and $[Au_2(2,6-Me_2-form)_2]$, 20	21
7 Selected Bond Distances (Å) and Angles (°) for N,N'-dinaphthylamidine, 2	22
8 Selected Bond Distances (Å) and Angles (°) for N,N'-dinaphthylacetamidine, 3	22
9 Selected Bond Distances (Å) and Angles (°) for N,N'-di(2,6isopropyl)phenylformamidine, 7	23
10 Selected Bond Distances (Å) and Angles (°) for $[Au_4(ArNC(H)NAr)_4]$, Ar = C ₆ H ₄ -4-OMe, 12	24
11 Selected Bond Distances (Å) and Angles (°) for $[Au_4(ArNC(H)NAr)_4]$, Ar = C ₁₀ H ₇ , 13	25
12 Selected Bond Distances (Å) and Angles (°) for $[Au_4(ArNC(H)NAr)_4]$, Ar = C ₆ F ₅ , 14	26
13 Selected Bond Distances (Å) and Angles (°) for $[Au_4(ArNC(Ph)NAr)_4]$ Ar = C ₆ H ₅ , 16	27

TABLE	Page
14 Selected Bond Distances (Å) and Angles (°) for [Au ₄ (ArNC(CH ₃)NAr) ₄] Ar = C ₆ H ₅ , 17	28
15 Selected Bond Distances (Å) and Angles (°) for [Au ₃ (2,6-Me ₂ -form) ₂ (THT)Cl], 18	30
16 Selected Bond Distance(Å) and Angles (°) for [Au ₂ (2,6-Me ₂ -form) ₂], 20	31
17 Different Bond Distances and Angles for N,N'-dinaphthylformamidine, 2 , N,N'-dinaphthylacetamidine, 3 , and N,N'-di(2,6-isopropyl)phenylformamidine, 7	46
18 Average Au...Au Distances (Å) and Au...Au...Au Angles (°) of Tetranuclear Gold(I) Amidinate Clusters, [Au ₄ (ArNC(H)NAr) ₄], and Related Tetranuclear Gold(I) Clusters.....	49
19 Crystal Data and Structure Refinement for [Au ₂ (<i>o</i> -Me ₂ -form) ₂ Cl ₂], 21 , and [Au ₂ (<i>o</i> -Me ₂ -form) ₂ X ₂][Au ₂ (<i>o</i> -Me ₂ -form) ₂]·CH ₂ ClCH ₂ Cl, X = Cl, 22 ·CH ₂ ClCH ₂ Cl.....	67
20 Crystal Data and Structure Refinement for [Au ₂ (<i>o</i> -Me ₂ -form) ₂ Br ₂], 23 and [Au ₂ (<i>o</i> -Me ₂ -form) ₂ X ₂][Au ₂ (<i>o</i> -Me ₂ -form) ₂] X = Br, 24	68
21 Crystal Data and Structure Refinement for [Au ₂ (<i>o</i> -Me ₂ -form) ₂ I ₂], 25 , and [Au ₂ (<i>o</i> -Me ₂ -form) ₂ CH ₃ I], 26	69
22 Crystal Data and Structure Refinement for [Au ₂ (2,6-Me ₂ -form) ₂].2Hg(CN) ₂ .2THF, 27 , and [Au ₂ (<i>o</i> -Me ₂ -form) ₂ (PhCOO) ₂], 28	70
23 Selected Bond Distances (Å) and Angles (°) for [Au ₂ (<i>o</i> -Me ₂ -form) ₂ Cl ₂], 21	71
24 Selected Bond Distances (Å) and Angles (°) for [Au ₂ (<i>o</i> -Me ₂ -form) ₂ X ₂][Au ₂ (<i>o</i> -Me ₂ -form) ₂], X = Cl, 22	72
25 Selected Bond Distances (Å) and Angles (°) for [Au ₂ (<i>o</i> -Me ₂ -form) ₂ Br ₂], 23	73
26 Selected Bond Distances (Å) and Angles (°) for [Au ₂ (<i>o</i> -Me ₂ -form) ₂ X ₂][Au ₂ (<i>o</i> -Me ₂ -form) ₂], X = Br, 24	74

TABLE	Page
27 Selected Bond Distances (Å) and Angles (°) for [Au ₂ (<i>o</i> -Me ₂ -form) ₂ I ₂], 25	75
28 Selected Bond Distances (Å) and Angles (°) for [Au ₂ (<i>o</i> -Me ₂ -form) ₂ CH ₃ I], 26	76
29 Selected Bond Distances (Å) and Angles (°) for [Au ₂ (2,6-Me ₂ -form) ₂] · 2Hg(CN) ₂ · 2THF, 27	77
30 Selected Bond Distances (Å) and Angles (°) for [Au ₂ (<i>o</i> -Me ₂ -form) ₂ (PhCOO) ₂], 28	79
31 Au(II)-Au(II), Au(I)...Au(I) and Au-Cl (Å) distances(Å) in [Au ₂ (<i>o</i> -Me ₂ -form) ₂ X ₂][Au ₂ (<i>o</i> -Me ₂ -form) ₂], X = Cl, 22 and [Au ₂ (<i>o</i> -Me ₂ -form) ₂ X ₂], XII	94
32 Dinuclear Au(II) ylide and amidinate complexes characterized by X-ray studies.....	101
33 Crystal Data and Structure Refinement for [Au ₂ (2,6-Me ₂ -form) ₂][Au ₄ (4-Me-form) ₄] · 2THF, 29 · 2THF, and [Au ₂ (3,5-Ph ₂ pz) ₂ Ag ₂ (2,6-Me ₂ -form) ₂] · 2THF, 33 · 2THF.....	124
34 Crystal Data and Structure Refinement for [Au ₄ (3,5-Ph ₂ pz) ₂ (2,6-Me ₂ -form) ₂] · 2THF, 31 · 2THF, and [Au ₄ (3,5-Ph ₂ pz) ₃ (2,6-Me ₂ -form)] · THF, 32 · THF.....	125
35 Selected Bond Distances (Å) and Angles (°) for [Au ₂ (2,6-Me ₂ -form) ₂][Au ₄ (4-Me-form) ₄] · 2THF, 29 · 2THF.....	126
36 Selected Bond Distances (Å) and Angles (°) for [Au ₄ (3,5-Ph ₂ pz) ₂ (2,6-Me ₂ -form) ₂] · 2THF, 31 · 2THF.....	127
37 Selected Bond Distances (Å) and Angles (°) for [Au ₄ (3,5-Ph ₂ pz) ₃ (2,6-Me ₂ -form)] · THF, 32 · THF.....	128
38 Selected Bond Distance(Å) and Angles (°) for [Au ₂ (3,5-Ph ₂ pz) ₂ Ag ₂ (2,6-Me ₂ -form) ₂] · 2THF, 33 · 2THF.....	129
39 Tetranuclear Gold(I) Amidinate Cluster.....	147
40 Dinuclear Au(II) Amidinate Complexes Characterized by X-ray Studies.....	149

TABLE	Page
41 Crystal Data and Structure Refinement for [Au ₄ (tbo) ₄], tbo = 1,3,6-triazabicyclo[3.3.0]oct-4-ene, 34	159
42 Selected Bond Distances (Å) and Angles (°) for [Au ₄ (tbo) ₄], tbo = 1,3,6-triazabicyclo[3.3.0]oct-4-ene, 34	160

LIST OF FIGURES

FIGURE	Page
1 Schematic representation of the mechanism of CO oxidation.....	6
2 Non-relativistic and quasi-relativistic level of the gold frontier orbitals.....	9
3 The relativistic contraction of the 6s shell in the elements Cs to Fm.....	9
4 Schematic representation of the reaction between amidinate ligands and Au(THT)Cl.....	43
5 Thermal ellipsoid plot of 2 is drawn at the 50% probability level Hydrogen atoms are removed for clarity	46
6 Thermal ellipsoid plot of 3 is drawn at the 50% probability level. Hydrogen atoms are removed for clarity.....	47
7 Thermal ellipsoid plot of 7 is drawn at the 50% probability level. Hydrogen atoms are removed for clarity.....	47
8 Thermal ellipsoid plot of 12 is drawn at the 50% probability level. Hydrogen atoms are removed for clarity.....	51
9 Thermal ellipsoid plot of 13 is drawn at the 50% probability level. Hydrogen atoms are removed for clarity.....	53
10 Thermal ellipsoid plot of 14 is drawing at the 50% probability level. Hydrogen atoms are removed for clarity.....	54
11 Thermal ellipsoid plot of 16 is drawn at the 50% probability level. Hydrogen atoms are removed for clarity.....	56
12 Thermal ellipsoid plot of 17 is drawn at the 50% probability level. Hydrogen atoms are removed for clarity.....	57
13 Thermal ellipsoid plot of 18 is drawing at the 50% probability level. Hydrogen atoms are removed for clarity.....	59
14 Thermal ellipsoid plot of 20 is drawn at the 50% probability level. Hydrogen atoms are removed for clarity.....	60

FIGURE	Page
15 Schematic representation of the reactions between Hg(CN) ₂ and the dinuclear gold(I) dithiophosphinate, dinuclear gold(I) ylide and the dinuclear Au(I) amidinate complexes.....	84
16 Schematic representation of the replacement reactions of [Au ₂ (<i>o</i> -Me ₂ -form) ₂ (PhCOO) ₂], 28 , in CH ₃ CN.....	86
17 Thermal ellipsoid plot of 21 is drawn at the 50% probability level. Hydrogen atoms are removed for clarity.....	88
18 Thermal ellipsoid plot of 23 is drawn at the 50% probability level. Hydrogen atoms are removed for clarity.....	89
19 Thermal ellipsoid plot of 25 is drawn at the 50% probability level. Hydrogen atoms are removed for clarity.....	90
20 Thermal ellipsoid plot of 22 is drawn at the 50% probability level. Hydrogen atoms are removed for clarity.....	92
21 Thermal ellipsoid plot of 24 is drawn at the 50% probability level. Hydrogen atoms are removed for clarity.....	93
22 Thermal ellipsoid plot of 26 is drawn at the 50% probability level. Hydrogen atoms are removed for clarity.....	95
23 Thermal ellipsoid plot of 27 is drawn at the 50% probability level. Hydrogen atoms are removed for clarity.....	97
24 (a) Thermal ellipsoid plot of 27 is drawn at the 50% probability level. Hydrogen atoms are removed for clarity. (b) Coordination environment of gold with the four nitrogen atoms in 27 . (c) Packing diagram of 27 showing the THF solvent in the voids.....	98
25 Thermal ellipsoid plot of 28 is drawn at the 50% probability level. Hydrogen atoms are removed for clarity.....	100
26 UV-Vis spectra of the ligand (Hform), IV , R = 4-OMe and 12 , (1.8 x 10 ⁻⁵ M), in CH ₂ Cl ₂	105
27 Excitation and emission spectrum of 12 , at 77 K.....	107
28 Emission spectrum of 13 , at 77 K.....	109

FIGURE	Page
29 Emission spectrum of 15 , at 77 K.....	110
30 Emission spectrum of 20 , at 77 K.....	112
31 Cyclic voltammogram of 12 in CH ₂ Cl ₂ with 0.1M NBu ₄ PF ₆ electrolyte. The potentials are referenced to the Ag/AgCl electrode.....	114
32 Cyclic voltammogram of 16 in CH ₂ Cl ₂ with 0.1M NBu ₄ PF ₆ electrolyte. The potentials are referenced to the Ag/AgCl electrode.....	115
33 Cyclic voltammogram of 20 in CH ₂ Cl ₂ with 0.1M NBu ₄ PF ₆ electrolyte. The potentials are referenced to the Ag/AgCl electrode.....	117
34 Schematic representation of the exchange reactions between XII , I and II	132
35 ¹ H NMR spectra of 30 in CDCl ₃ at 25 °C.....	133
36 Density Functional Theory calculations of the tetranuclear and dinuclear amidinate complexes at both the Gaussian 98 and ADF levels.....	136
37 Thermal ellipsoid plot of 29 is drawn at the 50% probability level. Hydrogen atoms are removed for clarity.....	138
38 Thermal ellipsoid plot of 31 is drawn at the 50% probability level. Hydrogen atoms are removed for clarity.....	139
39 Thermal ellipsoid plot of 32 is drawn at the 50% probability level. Hydrogen atoms are removed for clarity.....	141
40 Thermal ellipsoid plot of 33 is drawn at the 50% probability level. Hydrogen atoms are removed for clarity.....	142
41 UV -Vis spectra of XII , 29 , and 30 in CH ₂ Cl ₂	143
42 Emission spectra of XII , 29 , and 30 in the solid state at 77K.....	144
43 Emission spectra of 31 and 32 in the solid state at 77K.....	146
44 Thermal ellipsoid plot of 34 is drawn at the 50% probability level. Hydrogen atoms are removed for clarity.....	158

FIGURE	Page
45 Thermal ellipsoid plot of 35 is drawn at the 50% probability level. Hydrogen atoms are removed for clarity.....	163

CHAPTER I

INTRODUCTION

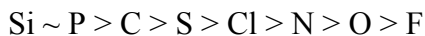
Nitrogen ligands have been little used with gold(I) and almost no chemistry has been described using anionic bridging nitrogen ligands. Dinuclear gold(I) complexes containing either one or two bridging ligands such as ylides and thiolates and their oxidative-addition products have attracted great attention for many years. Numerous number of complexes with two bridging ylide ligands and two gold atoms in a metallacyclic array, $[\text{Au}_2\{(\text{CH}_2)_2\text{PR}_2\}_2]$, are known in addition to a wide variety of complexes with S-Au-PR₃ coordination.¹

Gold(I) complexes with N-donor ligands are much less common than those with P-donor ligands. However, the affinity of gold for nitrogen can be increased if a phosphine ligand is present because of the efficient π -acceptor nature of the phosphine.¹ Therefore, the majority of the gold(I) complexes with anionic N-donor ligands (L^-) are complexes of the type R_3PAuL . For example, $\text{Ph}_3\text{PAu}(\text{bis}(\text{trimethylsilyl})\text{amide})$ and $\text{Ph}_3\text{PAu}(4\text{-nitro-anilide})$. Other complexes with L^- representing differently substituted pyrazoles, imidazoles and benzylimidazoles are also known.¹ The nitrogen chemistry of pyrazoles will be discussed in the next few pages. The gold(I) amidinate complexes to be reported here are symmetrical with the Au atom bonded to only a N atom.

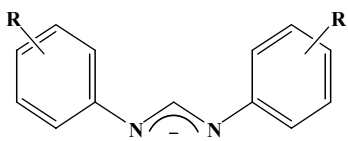
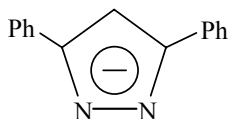
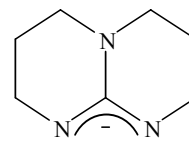
Gold(I) with its $[\text{Xe}]4\text{f}^{14}5\text{d}^{10}$ electronic configuration is often described as a soft metal ion and therefore might be expected to have a preference for soft donor ligands

This dissertation follows the format and style of *Inorganic Chemistry*.

such as sulfur and carbon, over hard donor ligands such as those which bond through nitrogen or oxygen.² For example, when bifunctional ligands with two different donor atoms are used, the gold atom will bind to the bifunctional ligands through the atom with the higher donor strength according to the sequence¹



The bifunctional ligands 2-pyridylphosphines, thioamides and the 1,1-dicyanoethylene-2,2-dithiolate for example are coordinated to gold through the P and S atoms but not N, since P and S atoms are better donor atoms than N according to the sequence above.¹ Therefore, it is generally assumed that the gold(I) will not effectively coordinate to a donor nitrogen atom.¹ However, the interesting chemistry of the anionic bridging ligands, amidines, ArNHC(H)NAr , **I**, to be described here, does not bare this out.

**I****II****III**

Cotton has been able to exploit the amidine ligands for the synthesis of a variety of complexes spanning the transition elements.³ Previous trials by his group to use the anionic bridging ligand amidines with gold were not successful and indicated that in the case of $[\text{M}_2(\text{ArNC(H)NAr})_2]$ compounds, $\text{Ar} = \text{C}_6\text{H}_4\text{-4-Me}$ and $\text{M} = \text{Ag}, \text{Cu}, \text{Au}$, the stability series must be $\text{Cu} \sim \text{Ag} \gg \text{Au}$.⁴ The gold amidinate complexes reported here

are synthesized in open air at room temperature and are stable at room temperature for several months.

Theoretical studies by Pyykko for $[M_2(NHCHNH)_2]$ systems, $M = Cu, Ag,$ and Au , predicted the M-M distances at the MP2 level.⁵ Experimentally, systems containing amidine ligands are known with Cu and Ag and unknown with Au . The results for the models containing silver and copper are close to the experimental structures of $[M_2(ArNC(H)NAr)_2]$, $Ar = C_6H_4-4-Me$ and $M = Ag, Cu$. The $Ag-Ag$ distance is 2.705 and 2.712 Å and the $Cu-Cu$ distance is 2.497 and 2.528 Å at the experimental and theoretical level, Table 1. The hypothetical dinuclear gold amidinate compound would have an $Au-Au$ distance at the MP2 level of 2.728 Å.⁵ The dinuclear gold(I) amidinate complex to be reported here with $Au-Au$ distance 2.71 Å prove the predicted $Au-Au$ distance to be true.

Table 1. Optimized Geometries at MP2 Level and Selected Experimental Structural Parameters for the $[M_2(NHCHNH)_2]$.⁵

System	M-M(Å)	N-M(Å)
$[Au_2(NHCHNH)_2]$	2.728	2.005
$[Ag_2(NHCHNH)_2]$	2.712	2.043
$[Cu_2(NHCHNH)_2]$	2.528	1.834
experimental structural parameters for the $[M_2(NHCHNH)_2]$, $M = Ag$ and Cu		
$Cu_2(ArNC(H)NAr)_2$, $Ar = C_6H_4-4-Me$	2.497	1.886
$Ag_2(ArNC(H)NAr)_2$, $Ar = C_6H_4-4-Me$	2.705	2.116

Only very few examples of gold(II) nitrogen compounds are known. There is only one gold(II) nitro complex, $\text{Au}_2(\text{ylide})_2(\text{NO}_2)_2$ reported by Schmidbaur in the book, *Gold Progress in Chemistry, Biochemistry, and Technology*, which was synthesized by Fackler and co-workers.¹ The great majority of compounds with gold nitrogen bonds occur with gold in its oxidation states +I and +III with the electronic configuration $[\text{Xe}]4f^{14}5d^{10}6s^06p^0$ and $[\text{Xe}]4f^{14}5d^86s^06p^0$ respectively.¹ There is a strong tendency for disproportionation from Au^{2+} to give Au^+ and Au^{3+} because the odd electron in d^9 metal complexes is in the $d_{x^2-y^2}$ orbital (octahedral, tetragonally distorted or square planar) which has a high energy and can be easily ionized.⁶

Surprisingly, several gold(II) amidinate complexes have been produced in this research project. The Au(II) amidinate complexes reported here are the first formed with nitrogen ligands. The complexes are stable at room temperature.

The anionic amidinate ligands, **I**, are known for their remarkable ability to bridge between the metal ions, facilitating the formation of short metal-metal distances and for their flexible coordination modes, leading to various molecular arrangements.⁷ The use of these amidinate ligands in the coordination chemistry of the transition metals has produced complexes with extraordinarily short M-M distances.³ These short distances are due, at least in part, to the ability of the amidinate anion to delocalize the negative charge while strongly donating sigma electron density to the metal atoms, supporting bond formation.⁸ Previous studies have shown that the amidinate ligands form dinuclear Ag(I) and Cu(I) complexes.^{4,9,10} Placing alkyl substituents on the amidinate NCN carbon atom influences the formation of tetranuclear and trinuclear structural motifs with

Ag(I).¹¹ The effect of the substituents on the structural chemistry in general is not well understood. Clearly the substituents play a role in determining the nuclearity and molecular arrangement of the complexes.

Pyrazolate ligands, **II**, have been studied extensively in our laboratory. The nitrogen ligand chemistry with pyrazolate ligands has produced mainly trinuclear complexes of group 11 with the structure, $[M(\mu\text{-}3,5\text{-Ph}_2\text{Pz})]_3$, $M = \text{Cu}, \text{Ag(I)}, \text{Au(I)}$. The hexanuclear gold complex $[\text{Au}(\mu\text{-}3,5\text{-Ph}_2\text{Pz})]_6$ also has been obtained, although in low yield.¹² Tetranuclear gold(I) pyrazolates were isolated only with a 3,5-diisobutyl substituted pyrazolate.¹³

The guanidinate-type anion ligand hpp (1, 3, 4, 6, 7, 8-hexahydro-H-pyrimido[1,2-a]pyrimidine), **III**, forms complexes with extra short M-M bonding distances and stabilizes metals in high oxidation states.¹⁴ Recent work from our laboratory with hpp anion, **III**, produced a dinuclear Au(II) complex, $[\text{Au}_2(\text{hpp})_2\text{Cl}_2]$, which has the shortest Au-Au bond distance reported to date 2.4 Å. The synthesis involved the reaction of the hpp anion with (THT)AuCl (THT = tetrahydrothiophene) in THF and CH_2Cl_2 .¹⁵ A tetranuclear $[\text{Au}_4(\text{hpp})_4]$, was also isolated when the reaction was carried out using ethanol as the solvent.¹⁶ The remarkable chemistry of the anionic bridging nitrogen ligands **II** and **III** suggests that an interesting chemistry may exist with gold(I) coordinates to the amidinate, ArNHC(H)NAr , **I**. This chemistry has challenged us to consider the effect of substituents on the molecular arrangement of gold(I) complexes.

In the past few years there has been an explosion of interest in gold catalysis. It is well known now that gold has unique properties as a catalyst for many reactions. One of the most fascinating observations of the late twentieth century is the discovery in the 1980's that finely supported divided nanoparticles of gold could act as catalysts for reactions at low temperatures.¹⁷ It has been recognized that supported gold nano-crystals can be highly effective catalysts for oxidation of CO at very low temperatures, below 0 °C. This high activity of gold is not replicated by other metals. The low temperature

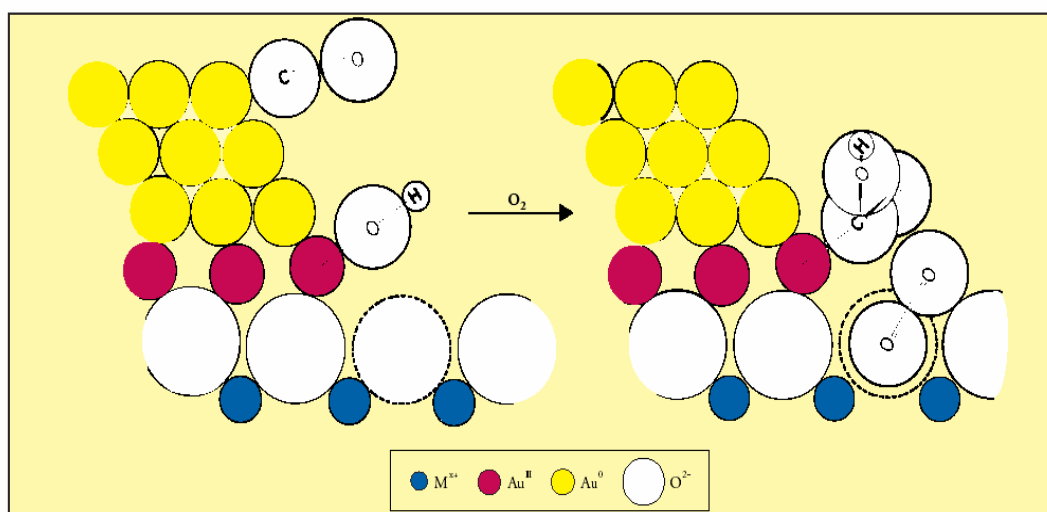


Figure 1. Schematic representation of the mechanism of CO oxidation.¹⁷

activity has produced a great deal of interest in gold research today. Many of the active gold catalysts for CO oxidation are typically found to consist of small crystallites, 2-4 nm in diameter, of gold supported on an oxide. There is debate concerning the nature of the active site for these catalysts. A proposed model by Bond and Thompson is shown in

Figure 1. The Au atoms at the interface between the Au particle and the oxide are the active oxidation centers, Figure 1. However it remains unclear whether Au^{3+} or Au^0 is the active form of gold.¹⁷

Recent catalytic studies, in collaboration with Professor D. W. Goodman's group, suggest that the tetranuclear gold amidinate complexes reported here and related gold nitrogen complexes are the best catalyst precursors for CO oxidation on a TiO_2 surface reported to date (87% conversion).¹⁸ The advantages of gold amidinate clusters as catalyst precursors are due to their low oxide residues after calcinations and the fact that the clusters do not contain elements which may be potential catalyst poisons. These complexes only contain C, H, N and sometimes O and/or halogens.¹⁸

Gold(I) cluster complexes have attracted great attention due to their structural diversity which involved short metal–metal interactions.¹ An understanding of the interactions between closed shell d^{10} gold centers was first discussed by Schmidbaur in the 1980s who introduced the term ‘aurophilic attractions’ or ‘aurophilicity’ based on crystallographic evidence of short distances between the gold(I) atoms.¹⁹ Closed-shell metal cations such as $\text{Au(I)}([\text{Xe}]4f^{14}5d^{10})$ are expected to repel one another.¹⁹ The attractive aurophilic interactions between two-coordinate, closed-shell Au(I) ions occur when the Au...Au separations are less than 3.6 Å. The “bond” strength is similar to hydrogen bonds, ca. 7-11 kcal/mol. Theoretical studies have shown that this weakly bonding interaction is the result of a combination of correlation effects and relativistic factors.²⁰ This is clearly seen in the tetranuclear gold(I) complexes where short Au...Au contacts are often observed as a result of these effects.¹

Many unusual properties of gold chemistry compared to the other elements of group 11 can be explained in part by the relativistic and correlation effects, Figure 2.¹⁹ The main effects on the atomic orbitals are radial contraction and energetic stabilization of the s and p shells, and radial expansion and energetic destabilization of the outer d and f shells. The contraction of the 6s shell in the elements Cs (Z= 55) to Fm (Z=100) is shown in Figure 3.¹⁹ The contraction increases gradually as the 4f shell is filled and reaches a maximum when the 5d shell is completely filled at gold, (5d)¹⁰(6s)¹.¹⁹

An important objective of this dissertation is to study the effects of substituents on the nuclearity in gold amidinates. Three different amidinate structures are examined, symmetrical diaryl substituted, ArNH(CH)NAr, symmetrical dialkyl substituted, RNH(CH)NR and unsymmetrical aryl-alkyl substituted RNHC(H)NAr. The main focus is the study of the symmetrical diaryl substituted complexes. The results are described in Chapter II which examines the electronic vs. the steric effect of the substituents on the molecular arrangement of gold amidinate complexes. A series of symmetrical diaryl substituted amidinate ligands, ArNH(CH)NAr, has been synthesized. The substituents on the ligand *N*-aryl groups are varied from electron withdrawing to electron donating, **IV**, **VII**, and their reaction with gold is described. Different substituents on the amidinate NCN carbon are also prepared and studied, **V**, **VI**. Chapter II, proves that the 2,6-substituents on the ligand *N*-aryl groups, **VIII**, **IX**, play a key role in determining the cluster nuclearity. This chapter also describes the synthesis and crystallographic characterization of a series of tetranuclear, trinuclear, and dinuclear gold(I) amidinate complexes.

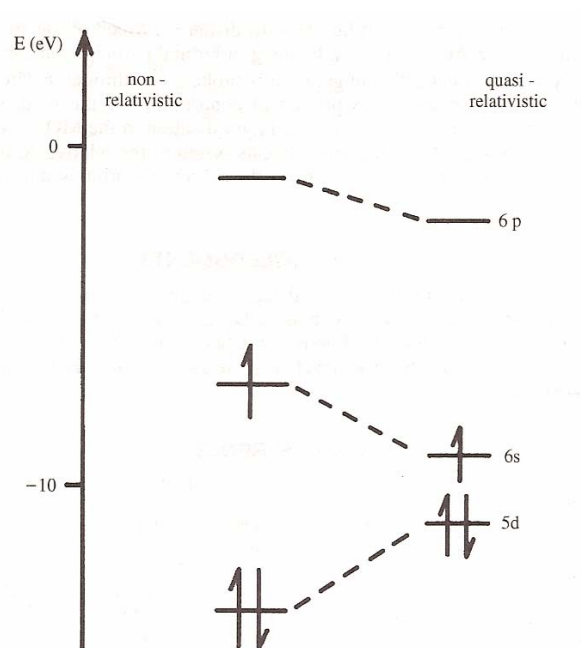


Figure 2. Non-relativistic and quasi-relativistic level of the gold frontier orbitals.¹⁹

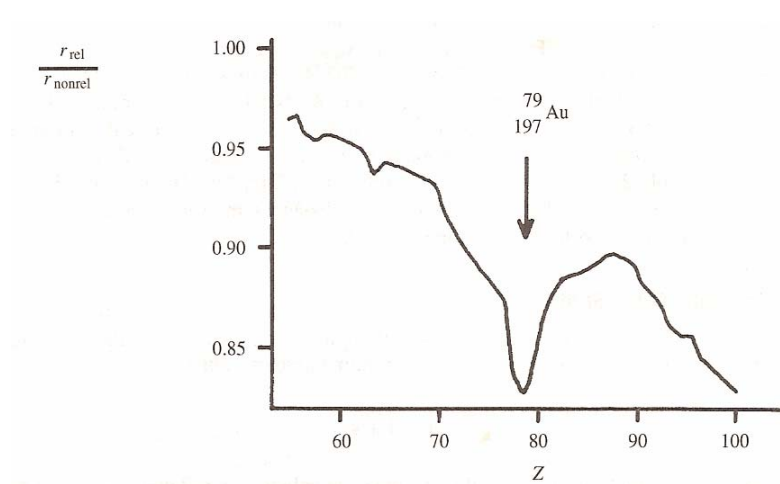
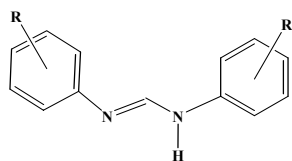
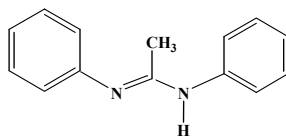


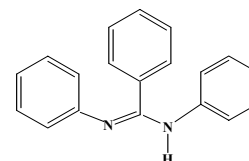
Figure 3. The relativistic contraction of the 6s shell in the elements Cs to Fm.¹⁹



IV

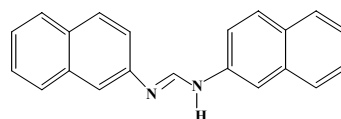


V

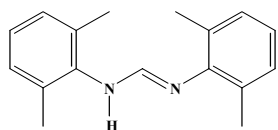


VI

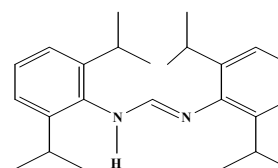
**R = 4-Me, 4-OMe, 3-CF₃,
3,5-Cl, 2,3,4,5,6-pentafluoro**



VII



VIII



IX

The effect of the solvent and temperature on the synthesis of the gold(I) amidinates is also investigated by carrying out the synthesis using different solvents such as ethanol, pyridine, and tetrahydrofuran and at different temperatures.

The tetranuclear gold(I) amidinate clusters exhibit aurophilic Au...Au bonding commonly found in many gold complexes, as explained earlier.^{21,22} The dinuclear gold(I) amidinate complex with a Au...Au distance 2.711(3) Å is rare.²³ To our knowledge, there is only one other example of a symmetrical dinuclear gold(I) nitrogen complex, {Au₂[(Me₃SiN)₂C(Ph)]₂}, which has a Au...Au distance of 2.646 Å.²⁴ Surprisingly Density Functional Theory calculations done in our group showed that the ground state

for the dinuclear gold(I) complex has a HOMO which is δ metal-metal antibonding,²³ not σ metal-metal antibonding as has been observed with the dinuclear gold(I) ylides.²⁵

Oxidative addition reactions to the dinuclear gold(I) complex, $[\text{Au}_2(2,6\text{-Me}_2\text{-form})_2]$, 2,6-Me₂-form = **VIII-H**, are described in Chapter III. The reactions result in the formation of Au(II) complexes. The Au(II) amidinate complexes are the first formed with nitrogen ligands. The complexes are stable at room temperature.²³ Oxidative-addition reactions have been widely studied with bridged dinuclear metal complexes. Earlier work with the ylides and sulfur bonded ligands (*vide infra*) has led to the formation of many Au(II)-Au(II) bonded complexes. Furthermore, no stable organometallic alkyl halide addition products have been characterized with other (non ylide) ligands.²⁶

Spectroscopic and electrochemical studies of the amidinate complexes are discussed in Chapter IV. The tetranuclear gold(I) clusters are the first tetranuclear gold(I) cluster species from group 11 elements that show fluorescence at room temperature.^{21,22} Chapter V describes a new idea for changing the nuclearity of the gold(I) amidinate complexes based on Density Functional Theory calculations. These calculations show that the dinuclear gold(I) complex, $[\text{Au}_2(2,6\text{-Me}_2\text{-form})_2]$, is less stable than the tetranuclear gold(I) amidinate clusters. Introducing less steric amidinate ligands as well as other anionic ligands such as 3,5-diphenylpyrazolate results in the formation of new Au(I) amidinate complexes and mixed ligand complexes with higher gold nuclearity.²⁷

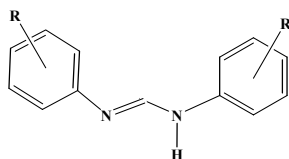
The ligand exchange of the sterically bulky ligands to form mixed ligand species provides a facile procedure for the synthesis of mixed ligand complexes with increased nuclearity. This approach has led to several new mixed ligands, mixed metal complexes. Chapter V describes the utilization of this approach to the synthesis of tetranuclear mixed Au-Ag complexes of pyrazolate and amidinate ligands. These complexes were obtained by reacting the trinuclear Ag(I) pyrazolate, $[\text{Ag}(\mu\text{-}3,5\text{-Ph}_2\text{Pz})]_3$, with the dinuclear gold(I) amidinate complex in different stoichiometric ratios.

The results from each chapter are brought together in Chapter VI which reiterates the results of the main theme of the dissertation, new chemistry with gold nitrogen complexes, and gives suggestions for future work with the gold amidinate complexes.

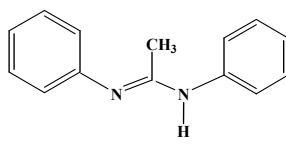
CHAPTER II
SYNTHESIS AND CHARACTERIZATION OF TETRA-, TRI-, AND
DINUCLEAR GOLD(I) AMIDINATE COMPLEXES*

As stated in the introduction, the structural arrangement of group 11 amidinate complexes is determined by the substituents on the amidinate aryl groups as well as on the NCN carbon.^{4,9,10,11} The electronic vs. steric effect of the substituents on the molecular arrangement of gold(I) amidinates complexes is studied in detail in this chapter. Changing the substituents on the aryl groups focuses on the following ligand influences: a) substituents with electronic effect such as electron withdrawing and donating groups, **V**. b) substituents with obvious steric constrains, **VI**, **VII**, **VIII**, **IX** and **X**. Other amidinate structures such as symmetrical dialkyl substituted, RNH(CH)NR (R = tert-butyl), **X** and unsymmetrical aryl, alkyl substituted RNHC(H)Ar (R = tertbutyl, Ar = *p*-tolyl), **XI** were also prepared and studied.

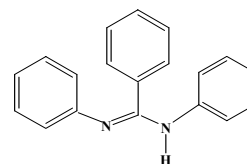
*Reproduced in part from *Inorg. Chem.*, *44*, 166-168, **2005**, Abdou, H. E.; Mohamed, A. A.; Fackler, Jr., J. P., "Synthesis and X-ray Structures of Dinuclear and Trinuclear Gold(I) and Dinuclear Gold(II) Amidinate Complexes", copyright 2005 American Chemical Society; from *J. Cluster Sci.*, *15*, 397-411, **2004**, Abdou, H. E.; Mohamed, A. A.; López-de-Luzuriaga, J. M.; Fackler, Jr., J. P., "Tetranuclear Gold(I) Clusters with Nitrogen Donor Ligands: Luminescence and X-Ray Structure of Gold(I) Naphthyl Amidinate Complex", copyright 2004, and from *J. Cluster Sci.*, *14*, 253-266, **2003**, Mohamed, A. A.; Abdou, H. E.; Irwin, M. D.; López-de-Luzuriaga, J. M.; Fackler, J. P., Jr., "Gold(I) Formamidinate Clusters: The Structure, Luminescence, and Electrochemistry of the Tetranuclear, Base-Free [Au₄(ArNC(H)NAr)₄]" copyright 2003 reprinted with kind permission of Springer Science and Business media.



IV

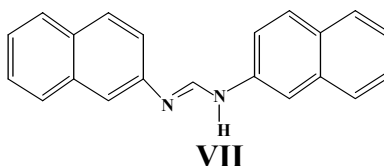


V

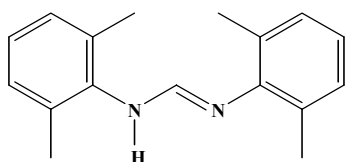


VI

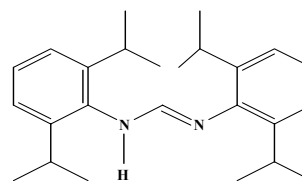
**R = 4-Me, 4-OMe, 3-CF₃,
3,5-Cl, 2,3,4,5,6-pentafluoro**



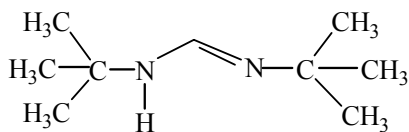
VII



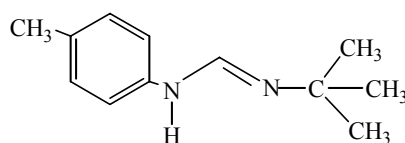
VIII



IX



X



XI

EXPERIMENTAL

General Procedures

All glassware was oven-dried prior to use. Triethyl orthoformate (orthoester), triethylorthoacetate, 1-aminonaphthalene, *p*-toluidine, aniline, 2,6-isopropylaniline, 2,3,4,5,6-pentafluoro aniline, 3-trifluoromethaneaniline, KOH, NaOH, acetic acid were

purchased from Aldrich. N,N'-diphenylbenzamidine was purchased from Lancaster. 2,6-dimethylaniline was purchased from Acros. Tetrahydrothiophene was purchased from TCI, Tokyo. The solvents, THF, hexanes, toluene and ether were purchased from Aldrich and used as received. Au(THT)Cl was prepared by reacting H₂AuCl₄ with the tetrahydrothiophene, (THT). The ligands N,N'-4-methyldiphenylamidine, N,N'-3,5-dichlorodiphenylamidine and their tetranuclear gold complexes, [Au₄(ArNC(H)NAr)₄], Ar = C₆H₄-4-Me and Ar = C₆H₄-3,5-Cl were synthesized previously in our group.²¹

Physical Measurements

Elemental analyses were performed by Guelph Chemical laboratories Ltd. & Chemisar Laboratories Inc, Guelph, Ontario, Canada. UV-Vis spectra were recorded on a Shimadzu UV-2501 PC spectrometer. ¹H and ¹⁹F NMR spectra were recorded on a Unity Plus 300 NMR spectrometer, using solvent peaks to reference chemical shifts (δ).

CRYSTALLOGRAPHIC STUDIES

X-ray data were collected using a Siemens (Bruker) SMART CCD (charge coupled device) based diffractometer equipped with a LT-2 low temperature apparatus operating at 110 K. A suitable crystal was chosen and mounted on a glass fiber using cryogenic grease. Data were measured using omega scans of 0.3° per frame for 60 s. The first 50 frames were recollected at the end of data collection as a monitor for decay. No decay was detected. Cell parameters were retrieved using SMART software and refined using SAINT on all observed reflections.²⁷ Data reductions were performed using SAINT software.²⁸ The structures were solved by direct methods using SHELXS-97 and refined by least squares on F², with SHELXL-97 incorporated in SHELXTL-PC V 5.03.^{29,30} The structures were determined in the space groups reported in Tables 2, 3, 4, 5 and 6 by analysis of systematic absences. Hydrogen atom positions were calculated by geometrical methods and refined as a riding model. Cell parameters and refinement results for the amidine ligands **2**, **3**, **7** and gold(I) amidinate complexes are summarized in Tables 2, 3, 4, 5 and 6. Tables 7, 8, 9 show the important interatomic distances and angles for the amidine ligands **2**, **3** and **7**. Tables 10-16 show the important interatomic distances and angles for gold(I) amidinate complexes.

Table 2. Crystal Data and Structure Refinement for N,N'-dinaphthylformamidinium, **2**, N,N'-dinaphthylacetamidinium, **3**, and N,N'-di(2,6-isopropyl)phenylformamidinium, **7**.

Compound	2	3	7
Formula	C ₂₁ H ₁₆ N ₂	C ₂₂ H ₁₈ N ₂	C ₁₅ H ₃₅ N ₂
FW	296.36	310.38	243
Space Group	P $\bar{1}$	<i>P2₁/c</i>	P $\bar{1}$
<i>a</i> (Å)	7.8205(16)	25.520(13)	12.84(2)
<i>b</i> (Å)	8.0828(16)	15.596(8)	13.56(3)
<i>c</i> (Å)	13.853(3)	8.265(4)	16.48(4)
α	73.929(4)	90.00	78.10(6)
β	78.189(4)	90.00	67.30(3)
γ	65.493(4)	90.00	62.01(4)
<i>V</i> (Å ³)	761.6(3)	3289(3)	2337(9)
<i>Z</i>	2	8	4
<i>d</i> _{calc} (g/cm ⁻³)	1.292	1.254	2.155
μ (mm ⁻¹)	0.076	0.074	12.556
λ (Å)	0.71073	0.71073	0.71073
T (K)	110(2)	110(2)	110(2)
R1, wR2	0.088, 0.091	0.152, 0.208	0.0704, 0.1663

$$^a R1 = \frac{\sum ||F_o| - |F_c||}{\sum |F_o|}$$

$$^b wR2 = \left[\frac{\sum [w(F_o^2 - F_c^2)^2]}{\sum [w(F_o^2)]} \right]^{1/2}; w = 1/[\sigma^2(F_o^2) + (aP)^2 + (bP)], \text{ where } P = [\max(F_o^2 \text{ or } 0) + 2(F_c^2)]/3$$

Table 3. Crystal Data and Structure Refinement for [Au₄(ArNC(H)NAr)₄], Ar = C₆H₄-4-OMe, **12**, and Ar = C₁₀H₇, **13**.

Compound	12	13
Formula	C ₆₀ H ₆₀ Au ₄ N ₈ O ₈	C ₈₄ H ₆₀ Au ₄ N ₈
FW	1809.03	1969.28
Space Group	<i>P2₁/c</i>	<i>P2₁/n</i>
<i>a</i> (Å)	14.906(3)	15.081(5)
<i>b</i> (Å)	20.501(4)	20.823(8)
<i>c</i> (Å)	22.226(5)	20.736(7)
α	90.00	90.00
β	95.602(4)	90.669(7)
γ	90.00	90.00
<i>V</i> (Å ³)	6759(3)	6511(4)
<i>Z</i>	4	4
<i>d</i> _{calc} (g/cm ⁻³)	1.778	2.009
μ (mm ⁻¹)	8.708	9.041
λ (Å)	0.71073	0.71073
T (K)	110(2)	110(2)
R1, wR2	0.071, 0.215	0.047, 0.092

$$^a R1 = \frac{\sum ||F_o| - |F_c||}{\sum |F_o|}$$

$$^b wR2 = \left[\frac{\sum [w(F_o^2 - F_c^2)^2]}{\sum [w(F_o^2)^2]} \right]^{1/2}; w = 1/[\sigma^2(F_o^2) + (aP)^2 + (bP)], \text{ where } P = [\max(F_o^2 \text{ or } 0) + 2(F_c^2)]/3$$

Table 4. Crystal Data and Structure Refinement for [Au₄(ArNC(H)NAr)₄], Ar = C₆F₅, **14**, and [Au₄(ArNC(Ph)NAr)₄] Ar = C₆H₅, **16**.

Compound	14	16
Formula	C ₅₂ H ₄ Au ₄ F ₄₀ N ₈	C ₇₂ H ₆₀ Au ₄ N ₈
FW	2288.51	1825.15
Space Group	<i>C2/c</i>	<i>P2₁/c</i>
<i>a</i> (Å)	30.64(3)	12.723(10)
<i>b</i> (Å)	11.701(10)	16.483(12)
<i>c</i> (Å)	21.78(2)	33.57(3)
α	90.00	90.00
β	133.891(15)	100.161(14)
γ	90.00	90.00
<i>V</i> (Å ³)	5676(9)	6929(9)
<i>Z</i>	4	4
<i>d</i> _{calc} (g/cm ⁻³)	2.679	1.750
μ (mm ⁻¹)	10.489	8.488
λ (Å)	0.71073	0.71073
T (K)	110(2)	110(2)
R1, wR2	0.128, 0.213	0.062, 0.166

$$^a R1 = \sum \left| |F_o| - |F_c| \right| / \sum |F_o|$$

$$^b wR2 = [\sum [w(F_o^2 - F_c^2)^2] / \sum [w(F_o^2)^2]]^{1/2}; w = 1/[\sigma^2(F_o^2) + (aP)^2 + (bP)], \text{ where } P = [\max(F_o^2 \text{ or } 0) + 2(F_c^2)]/3$$

Table 5. Crystal Data and Structure Refinement for [Au₄(ArNC(CH₃)NAr)₄], Ar = C₆H₅, **17**.

Compound	17
Formula	C ₅₆ H ₅₂ Au ₄ N ₈
FW	1624.92
Space Group	Cc
<i>a</i> (Å)	13.588(3)
<i>b</i> (Å)	20.060(4)
<i>c</i> (Å)	19.093(4)
α	90.00
β	103.918(4)
γ	90.00
<i>V</i> (Å ³)	5051.5(16)
<i>Z</i>	4
<i>d</i> _{calc} (g/cm ⁻³)	2.137
μ (mm ⁻¹)	11.627
λ (Å)	0.71073
<i>T</i> (K)	110(2)
R1, wR2	0.062, 0.110

$$^a R1 = \frac{\sum ||F_o| - |F_c||}{\sum |F_o|}$$

$$^b wR2 = \frac{[\sum [w(F_o^2 - F_c^2)^2]]^{1/2}}{\sum [w(F_o^2)^2]}; w = 1/[\sigma^2(F_o^2) + (aP)^2 + (bP)], \text{ where } P = [\max(F_o^2 \text{ or } 0) + 2(F_c^2)]/3$$

Table 6. Crystal Data and Structure Refinement for [Au₃(2,6-Me₂-form)₂(THT)Cl], **18**, and [Au₂(2,6-Me₂-form)₂], **20**.

Compound	18	20
Formula	C ₃₈ H ₄₆ Au ₃ ClN ₄ S	C ₃₄ H ₃₈ Au ₂ N ₄
FW	1217.22	896.62
Space Group	<i>P</i> 2 ₁ / <i>n</i>	<i>P</i> $\bar{1}$
<i>a</i> (Å)	10.8294(6)	7.354
<i>b</i> (Å)	21.4450(13)	9.661(7)
<i>c</i> (Å)	16.7756(10)	11.421 (10)
α	99.00	81.74(5)
β	99.5270(10)	99.5270(10)
γ	99.00	86.07(9)
<i>V</i> (Å ³)	3842.2(4)	760.1(4)
<i>Z</i>	4	1
<i>d</i> _{calc} (g/cm ⁻³)	2.137	2.679
μ (mm ⁻¹)	8.678	10.768
λ (Å)	0.71073	0.71073
<i>T</i> (K)	110(2)	110(2)
R1, wR2	0.086, 0.167	0.047, 0.124

$$^a R1 = \frac{\sum ||F_o| - |F_c||}{\sum |F_o|}$$

$$^b wR2 = \frac{[\sum [w(F_o^2 - F_c^2)^2]]^{1/2}}{\sum [w(F_o^2)]^{1/2}}; w = 1/[\sigma^2(F_o^2) + (aP)^2 + (bP)], \text{ where } P = [\max(F_o^2 \text{ or } 0) + 2(F_c^2)]/3$$

Table 7. Selected Bond Distances (Å) and Angles (°) for N,N'-dinaphthylamidine, **2**.

N1-C1	1.285(3)	N2-C1	1.341(3)
N1-C2	1.421(3)	N2-C12	1.407(3)
N1-C1-N2	123.3(2)	C1-N1-C2	116.0(2)
C1-N2-C12	123.4(2)		

Table 8. Selected Bond Distances (Å) and Angles (°) for N,N'-dinaphthylacetamidine, **3**.

N-C11	1.361(5)	N2-C1	1.429(5)
N2-C11	1.287(6)	C1-C12	1.514(7)
C11-N2-C1	121.6(4)	N2-C11-C12	125.9(4)
N2-C11-N1	119.9(4)	N1-C11-C12	114.2(4)

Table 9. Selected Bond Distances (Å) and Angles (°) for N,N'-di(2,6-isopropyl)phenylformamidine, **7**.

N2-C1	1.336(5)	C11-C13	1.527(6)
N2-C14	1.427(5)	C7-C6	1.406(5)
N1-C1	1.317(5)	C7-C2	1.424(6)
C11-C7	1.519(6)	C8-C10	1.525(6)
C11-C12	1.527(7)	C8-C9	1.545(7)
C1-N2-C14	120.5(3)	C7-C11-C12	111.5(4)
C1-N1-C2	119.1(3)	C7-C11-C13	112.6(3)
C2-C3-C8	121.7(3)	C12-C11-C13	110.1(4)
C4-C3-C8	119.4(4)	N1-C1-N2	121.4(4)
C6-C7-C2	118.3(4)		

Table 10. Selected Bond Distances (Å) and Angles (°) for [Au₄(ArNC(H)NAr)₄], Ar = C₆H₄-4-OMe, **12**.

Au(1)⋯ Au(2)	2.9016(8)	Au(1)–N(8)	2.047(11)
Au(2)⋯ Au(3)	3.0057(9)	Au(2)–N(7)	2.029(11)
Au(3)⋯ Au(4)	2.9265(9)	Au(2)–N(6)	2.057(11)
Au(1)⋯ Au(4)	2.9447(10)	C(1)–N(1)	1.322(17)
Au(1)–N(1)	2.022(11)	C(1)–N(2)	1.306(17)
Au(1)⋯ Au(4)⋯ Au(3)	109.62(2)	N(3)–C(16)–N(4)	127.2(12)
Au(2)⋯ Au(3)⋯ Au(4)	70.273(18)	N(2)–C(2)–N(1)	126.5(13)
Au(3)⋯ Au(2)⋯ Au(1)	108.62(2)	N(7)–Au(4)–N(6)	173.6(5)
Au(4)⋯ Au(1)⋯ Au(2)	71.473(18)	N(5)–Au(3)–N(4)	175.2(4)
N(2)⋯ Au(4)⋯ Au(3)	100.8(3)	N(7)–Au(2)–N(6)	173.3(4)
N(4)⋯ Au(3)⋯ Au(2)	104.0(3)	N(1)–Au(1)–N(8)	175.8(4)
N(5)⋯ Au(3)⋯ Au(2)	79.8(3)	N(4)⋯ Au(3)⋯ Au(4)	82.0(3)

Table 11. Selected Bond Distances (Å) and Angles (°) for [Au₄(ArNC(H)NAr)₄], Ar = C₁₀H₇, **13**.

Au(2)–N(2)	2.024(7)	Au(2)...Au(1)	3.0139(11)
N(1)–C(1)	1.306(12)	Au(2)...Au(3)	2.9920(9)
Au(4)...Au(3)	2.9721(11)	Au(4)...Au(1)	2.9944(10)
Au(1)–N(1)	2.022(7)	Au(3)–N(4)	2.033(7)
N(3)–Au(2)–N(2)	171.0(3)	N(3)...Au(2)...Au(1)	97.3(2)
N(2)...Au(2)... Au(1)	85.16(18)	N(3)...Au(2)...Au(3)	81.3(2)
Au(1)...Au(2)...Au(3)	68.59(2)	N(2)...Au(2)...Au(3)	107.58(19)
N(1)–Au(1)–N(8)	165.9(3)	N(6)–Au(4)–N(7)	172.1(3)
N(1)–C(1)–N(2)	126.2(8)	N(6)...Au(4)...Au(1)	105.7(2)
C(1)–N(1)–Au(1)	132.4(6)	Au(1)...Au(4)...Au(3)	69.11(2)
N(3)–C(22)–N(4)	126.1(8)	N(5)...Au(3)...Au(2)	105.5(2)
Au(2)...Au(1)...Au(4)	110.07(2)	Au(2)...Au(3)...Au(4)	111.29(2)

Table 12. Selected Bond Distances (Å) and Angles (°) for [Au₄(ArNC(H)NAr)₄], Ar = C₆F₅, **14**.

Au1–N4	1.96(4)	Au2–N3	2.04(4)
Au1...Au2A	2.954(4)	Au2...Au1A	2.954(4)
Au1...Au2	2.971(4)	N3–C14	1.35(6)
Au2–N2	2.02(4)	C14–N4A	1.40(6)
N4–Au1–N1	168.1(17)	N3...Au2...Au1A	82.3(11)
N4...Au1...Au2A	82.4(13)	N2...Au2...Au1	78.8(10)
N1...Au1...Au2A	107.6(13)	N3...Au2...Au1	107.6(11)
N4...Au1...Au2	102.6(12)	Au1...Au2...Au1A	87.06(10)
N1...Au1...Au2	83.5(13)	N3–C14–N4A	124(4)
Au2...Au1...Au2A	92.54(10)	C14–N4A–Au1A	127(3)
N2–Au2–N3	171.9(15)		
N2...Au2...Au1A	103.3(10)		

Table 13. Selected Bond Distances (Å) and Angles (°) for [Au₄(ArNC(Ph)NAr)₄] Ar = C₆H₅, **16**.

Au2–N2	2.018(11)	Au1–N1	2.035(13)
Au2–N3	2.042(11)	Au3–N4	2.022(12)
Au2...Au3	2.9270(18)	Au3–N5	2.045(12)
Au2...Au1	2.982(2)	N1–C1	1.339(19)
Au4–N7	2.018(12)	N1–C8	1.396(19)
Au4–N6	2.030(12)	N2–C1	1.365(18)
Au4...Au1	2.9252(18)	C2–C3	1.35(2)
Au4...Au3	2.955(2)	C2–C7	1.42(2)
Au1–N8	2.003(12)	C2–C1	1.49(2)
N2...Au2...Au3	110.8(3)	N1...Au1...Au4	104.0(3)
N3...Au2...Au3	80.1(3)	N8...Au1...Au2	109.2(3)
N2...Au2...Au1	80.4(3)	N6...Au4...Au3	79.2(3)
N3...Au2...Au1	106.6(4)	N1...Au1...Au2	81.3(4)
Au3...Au2...Au1	82.37(2)	Au4...Au1...Au2	97.10(3)
N7–Au4–N6	165.1(5)	N4–Au3–N5	170.0(5)
N7...Au4...Au1	79.8(4)	N4...Au3...Au2	83.1(4)
N6...Au4...Au1	113.3(4)	N5...Au3...Au2	102.0(4)
N7...Au4...Au3	110.6(3)	N4...Au3...Au4	107.8(4)
Au1...Au4...Au3	82.86(2)	N5...Au3...Au4	80.2(4)
N8–Au1–N1	167.7(5)	Au2...Au3...Au4	97.66(3)

Table 14. Selected Bond Distances (Å) and Angles (°) for [Au₄(ArNC(CH₃)NAr)₄] Ar = C₆H₅, **17**.

N1–C1	1.30(2)	Au3–N4	2.069(16)
N1–C3	1.48(2)	Au3...Au4	2.9078(12)
N1–Au1	1.994(16)	Au4–N7	1.993(15)
Au1–N8	1.980(16)	Au4–N6	2.001(15)
Au1...Au4	2.8970(12)	N7–C43	1.34(2)
Au1...Au2	2.9996(12)	N2–C1	1.28(2)
Au2–N3	2.028(17)	C1–C2	1.64(3)
Au2–N2	2.081(19)	C43–C44	1.52(2)
Au2...Au3	2.9796(13)	C15–C16	1.49(3)
Au3–N5	2.053(16)		
C1–N1–C3	115.7(17)	N7...Au4...Au1	80.1(4)
C1–N1–Au1	130.9(15)	N6...Au4...Au1	102.7(4)
C3–N1–Au1	113.3(12)	N7...Au4...Au3	106.0(4)
N8–Au1–N1	169.8(7)	N6...Au4...Au3	80.5(4)
N8...Au1...Au4	79.3(5)	Au1...Au4...Au3	91.14(3)
N1...Au1...Au4	107.4(5)	C43–N7–C45	120.2(15)
N8...Au1...Au2	111.3(5)	C43–N7–Au4	123.6(13)
N1...Au1...Au2	77.0(5)	C45–N7–Au4	115.4(12)
Au4...Au1...Au2	88.29(3)	C43–N8–Au1	126.9(13)
N3–Au2–N2	169.8(7)	C15–N3–Au2	124.4(13)

Table 14

Continued

N3...Au2... Au3	81.8(4)	C15-N4-Au3	129.7(15)
N2...Au2...Au3	106.6(5)	C1-N2-Au2	122.9(16)
N3...Au2...Au1	105.7(5)	N2-C1-N1	124(2)
N2...Au2...Au1	80.7(5)	N2-C1-C2	115.1(19)
Au3...Au2...Au1	87.78(3)	N1-C1-C2	119.5(19)
N5-Au3-N4	170.2(6)	N8-C43-N7	119.8(17)
N5...Au3...Au4	80.9(4)	N8-C43-C44	120.8(17)
N4...Au3...Au4	104.0(4)	N7-C43-C44	119.3(17)
N5...Au3...Au2	110.0(4)	N4-C15-N3	121.0(19)
N4...Au3...Au2	78.9(5)	N4-C15-C16	120.4(19)
Au4...Au3...Au2	88.47(3)	N3-C15-C16	118.5(18)
N7-Au4-N6	173.0(6)		

Table 15. Selected Bond Distances (Å) and Angles (°) for [Au₃(2,6-Me₂-form)₂(THT)Cl], **18**.

Au(3)-N(4)	2.019(15)	Au(3)-Cl(1)	2.258(6)
N(1)-C(1)	1.30(2)	Au(3)...Au(2)	3.0181(10)
Au(2)-N(3)	2.042(17)	N(2)-C(1)	1.29(2)
S(1)-C(35)	1.85(2)	Au(2)-N(2)	2.055(16)
Au(1)-N(1)	2.044(16)	Au(1)...Au(2)	3.0132(12)
Au(1)-S(1)	2.245(6)		
N(4)-Au(3)-Cl(1)	174.1(5)	N(1)-Au(1)-S(1)	176.9(4)
Au(1)...Au(2)...Au(3)	72.15(3)	N(4)-Au(3)...Au(2)	80.5(4)
N(2)-Au(2)...Au(1)	78.6(4)	N(2)-Au(2)...Au(3)	110.3(4)
N(3)-Au(2)...Au(1)	112.2(5)	N(3)-Au(2)-N(2)	167.5(7)
N(4)-C(18)-N(3)	128.0(18)	N(2)-C(1)-N(1)	125.0(18)

Table 16. Selected Bond Distances (Å) and Angles (°) for [Au₂(2,6-Me₂-form)₂], **20**.

Au(1)-N(2)	2.026(13)	Au(1)-N(1)	2.018(13)
Au(1)...Au(1)	2.712(2)	Au(2)-N(4)	2.028(13)
Au(2)-N(3)	2.042(12)	N(1)-C(1)	1.36(2)
Au(2)...Au(2)	2.712(2)	N(2)-C(1)	1.31(2)
N(2)-Au(1)-N(1)	171.1(6)	N(2)-Au(1)...Au(1)	85.3(4)
N(4)-Au(2)-N(3)	168.3(5)	N(1)-Au(1)...Au(1)	85.7(4)
N(4)-Au(2)...Au(2)	84.1(4)	N(3)-Au(2)...Au(2)	84.2(4)
N(3)-C(18)-N(4)	127.6(16)	N(2)-C(1)-N(1)	127.8(15)

Synthesis of Formamidine Ligands

N,N'-di(4-methoxy)phenylformamidine, 1. Triethylorthoformate (orthoester) (2.96 mL, 0.2 mol) and the o-anisidine (4-methoxyaniline), (4.92 mL, 0.04 mol) were mixed and the reaction mixture was heated to 140–160 °C in a reflux vessel for 1–2 hr. The reaction mixture was distilled at the same temperature to remove ethanol and left at room temperature to solidify. The solid was extracted with warm toluene and left overnight at room temp or in the refrigerator to give white blocks in yields of 85%. ¹H NMR (CDCl₃, ppm): 3.77 (s, 24H, CH₃), 8.04 (s, 1H, CH amidine).

N,N'-dinaphthylformamidine, 2. 1-Aminonaphthalene (11.45 g, 0.08 mol) and triethylorthoformate (orthoester) (5.92 mL, 0.04 mol) were mixed and the mixture was heated to 140–160 °C in a reflux vessel for 1–2 h. The reaction mixture was distilled at the same temperature to remove ethanol and left at room temperature to solidify. The solid was extracted with warm toluene and left overnight at room temperature or in the refrigerator to give white blocks in yields of 70%. The ligand was characterized by X-ray crystallography. ¹H NMR (CDCl₃, ppm): 8.3(s, 1H, CH amidine), 7.2-8.2 (m, 14H, CH naphthyl).

N,N'-dinaphthylacetamidine, 3. 1-Aminonaphthalene (6.76 g, 0.04 mol) was mixed with triethylorthoacetate (3.24 mL, 0.02 mol). The reaction mixture was heated to 140–160 °C until it became viscous, about 1-2 h. The mixture was distilled at the same temperature to remove ethanol, then it was layered with toluene and left at room temperature to solidify. The dark solid was dissolved in THF, layered with hexanes and left overnight at room temperature to give a white crystalline product in yield of 40%.

The ligand was characterized by X-ray crystallography. ^1H NMR (CDCl_3 , ppm): 1.9 (s, 3H, CH_3), 7.2-8.2(m, 14H, CH naphthyl).

N,N'-di(4-methyl)phenylacetamidine, 4. Triethylorthoacetate (3.24 mL, 0.02 mol) was mixed with P-Toluidine (4.28 g, 0.04 mol) in round bottom flask and 1 mL of acetic acid was added. The reaction mixture was heated to 140–160 °C in a reflux vessel for 1 h where upon oil product formed. The product was dissolved in toluene and layered with petroleum ether then left overnight in the refrigerator to form white crystal in yields of 65%. ^1H NMR (CDCl_3 , ppm): 1.9 (s, 3H, CH_3), 2.3 (s, 6H, CH_3).

N,N'-phenylacetamidine, 5. Aniline (6.2 mL, 0.06 mol) and triethylorthoformate (orthoester) (5.4 mL, 0.03 mol) were mixed and the mixture was heated to 140–160 °C in a reflux vessel for 1–2 h. The reaction mixture was distilled at the same temperature to remove ethanol and left at room temperature to solidify. The solid was extracted with warm toluene and left overnight at room temperature to give white crystal in 75% yield. ^1H NMR (CDCl_3 , ppm): 2.0 (s, 3H, CH_3), 7.0-7.3 (m, 10H, CH phenyl).

N,N'-di(2,6-methyl)phenylfarmamidine, 6. 2,6-Dimethylaniline (19.4 mL, 0.04 mol) was mixed with triethylorthoformate (orthoester) (11.8 mL, 0.02 mol) in round bottom flask. The reaction mixture was heated to a temperature between 140-160 °C for 1 to 2 hr and then distilled at the same temperature to remove ethanol. The viscous reaction mixture was cooled to ambient temperature then layered with hexanes to form white fiber solid product in 77% yield. ^1H NMR (CDCl_3 , ppm): 2.31 (s, 12H, CH_3), 7.39 (s, 1H, CH amidine).

N,N'-di(2,6-isopropyl)phenylformamidine, 7. 2,6-Diisopropyl (11.8 mL, 0.06 mol) was mixed with triethylorthoformate (orthoester) (4.9 mL, 0.03 mol) in a round bottom flask. The reaction mixture was heated to a temperature between 140-160 °C for 1 to 2 h and then distilled at the same temperature to remove ethanol. The viscous reaction mixture was cooled to ambient temperature then layered with hexanes and left at room temperature to form white crystal in 45% yield. ¹H NMR (CDCl₃, ppm): 1.46 (s, 12H, CH₃), 2.9 (2H, CH), 7.48 (s, 1H, CH amidine).

N,N'-di(3-CF₃)phenylformamidine, 8. 3-trifluoromethaneaniline (6.44 g, 0.04 mol) were mixed with (2.96 mL, 0.019 mol) of triethylorthoformate (orthoester) in a round bottom flask. The reaction mixture was heated to a temperature between 140-160 °C for 1 to 2 hr and then distilled at the same temperature to remove ethanol. The viscous reaction mixture was cooled to ambient temperature, whereupon it solidified. The solid was extracted with warm toluene and left overnight at room temp to give white crystalline solid in 70% yield. F¹⁹ NMR (CDCl₃, ppm): 129.41 (s, 2CF₃). ¹H NMR (CDCl₃, ppm): 7.26- 7.49 (m, 8H, CH phenyl), 8.23 (s, 1H, CH formamidine).

N,N'-di(2,3,4,5,6-pentafluoro)phenylformamidine, 9. Triethylorthoformate (orthoether) (1.4 mL, 0.01 mol) and pentafluoroaniline (3.66 g, 0.02 mol) were mixed in a round bottom flask and acetic acid (1 mL) was added. The reaction mixture was heated to a temperature 140–160 °C for 30–40 min until the mixture became viscous. It was left at room temp to solidify. The dark solid was extracted with warm toluene and layered with petroleum ether and left overnight at room temperature or in the refrigerator to give a white needle crystalline product in 81% yield. ¹H NMR (CDCl₃, ppm): 8.3 (s, 1H, CH

formamidine). ^{19}F NMR (CDCl_3 , ppm): 31.7 (t, F3); 36.8 (t, F2 and F4); 41.7 (d, F1 and F5).

N,N'-di-*t*-butyl-formamidine, 10. A round bottom flask containing triethylorthoformate (orthoether) (14.8 mL, 0.1 mol) and catalytic amount of acetic acid (1 mL) were fitted to a reflux condenser and heated to 165 °C, and *t*-butyl amine (14.6 mL, 0.2 mol) was added dropwise during 15 min. The mixture was then refluxed at 165 °C for 30 min to 1 hour and then distilled at the same temperature for 2 hour to remove ethanol. The reaction mixture was cooled to ambient temperature then layered with hexanes and left at room temperature or in the refrigerator overnight to form white crystals in 45% yield. The ligand is characterized by x-ray and ^1H NMR (CDCl_3 , ppm): 1.39 (m, 18 H, CH_3), 7.3 (s, 1H amidine).

N-*p*-tolyl- N'-*t*-butyl-formamidine, 11. triethylorthoformate (orthoether) (3.7 mL, 0.025 mol) was mixed with *p*-tolyl (2.67 mL, 0.025 mol) and catalytic amount of acetic acid (1 mL) in a round bottom flask fitted to a reflux condenser. The reaction mixture was heated to 165 °C for and *t*-butylamine (1.83 mL, 0.025 mol) was added drop wise during 20 min. The mixture was then refluxed at 165 °C for 30 min to 1 hour and then distilled at the same temperature for 2 hour to remove ethanol. The reaction mixture was cooled to ambient temperature then layered with hexanes and left at room temperature or in the refrigerator over night to form off-white product in 55% yield. ^1H NMR (CDCl_3 , ppm): 1.24 (m, 9 H, CH_3), 2.19 (m, 3H, CH_3), 7.63 (br, 1 H amidine).

Synthesis of Tetranuclear Gold(I) Amidinate Complexes

[Au₄(ArNC(H)NAr)₄], Ar = C₆H₄-4-OMe, 12. N,N'-di(4-OMe)phenylformamidine (256 mg, 1 mmol) was stirred with (40 mg, 1 mmol) of NaOH in THF for 1 hr. Gradually the colorless solution turned yellow. Au(THT)Cl (320 mg, 1 mmol) was added and stirring continued for additional 12 hr. The volume was decreased under vacuum and ether was added to form an off-white precipitate. The product was filtered and washed with cold ether to give the tetranuclear gold(I) cluster product. The product is air stable in the solid state and in a THF solution, yield 50%. ¹H NMR (CDCl₃, ppm): 3.71 (s, 24H, CH₃), 8.20 (s, 4H, CH amidinate). UV-Vis(CH₂Cl₂): λ_{max} (nm), ε (L/M⁻¹cm⁻¹): 315, 28000; 360, 13000; 260, 50000.

[Au₄(ArNC(H)NAr)₄], Ar = C₁₀H₇, 13. N,N'-dinaphthylformamidine (301 mg, 1 mmol) was stirred with (56 mg, 1 mmol) of KOH powder in THF for 1 h. The colorless solution turned yellow. Au(THT)Cl (320 mg, 1 mmol) was added and stirring was continued for additional 4 h. The volume was decreased under reduced pressure and hexanes was added to form an of-white precipitate. The product was filtered and recrystallized from THF/hexanes to give the tetranuclear gold(I) cluster product. The product is air stable in the solid state. Anal. Calcd. for C₈₄H₆₀Au₄N₈: C, 50.79; H, 3.85. Found: C, 50.72; H, 4.11. Yield: 31%. ¹HNMR (CDCl₃, ppm): 8.3 (4H, CH amidinate). UV-Vis(CH₂Cl₂): λ_{max} (nm), ε (L/M⁻¹cm⁻¹): 333, 64900.

[Au₄(ArNC(H)NAr)₄], Ar = C₆F₅, 14. N,N'-di(2,3,4,5,6-pentafluoro)phenylformamidine (376 mg, 1 mmol) was stirred with (40 mg, 1 mmol) of NaOH in THF for 24 hr. Gradually the colorless solution turned yellow. Au(THT)Cl

(320 mg, 1 mmol) was added and stirring continued for additional 4-5 hr. The solution was filtered and volume was decreased under reduced pressure and hexanes was added to form an off-white precipitate. The product was filtered and recrystallized from THF/hexanes to give the tetranuclear gold(I) cluster product in yield of 77%. Anal. Calcd. for $C_{52}H_4F_{40}N_8Au_4$: C, 27.27; N, 4.89. Found: C, 27.75; N, 4.64. ^{19}F NMR ($CDCl_3$, ppm): 30 (t, F3); 34 (t, F2 and F4); 43 (d, F1 and F5). 1H NMR ($CDCl_3$, ppm): 8.3 (4H, CH amidinate). UV-Vis(CH_2Cl_2): λ_{max} (nm), ϵ ($L/M^{-1}cm^{-1}$): 260, 102800; 285, 76900; 300 46700 .

$[Au_4(ArNC(H)NAr)_4]$, Ar = $C_6H_4-3-CF_3$, 15. N,N'-di(3- CF_3)phenylformamidine (320 mg, 1 mmol) was stirred with (40 mg, 1 mmol) of NaOH in 25 mL of THF for 24 hr. The colorless solution turned yellow. Au(THT)Cl (320 mg, 1 mmol) was added and stirring continued for additional 4-5 hr. The solution was filtered and volume was decreased under reduced pressure to 5 mL and hexanes was added to form an off-white precipitate. The product was filtered and recrystallized from THF/hexanes to give white crystals in yield of 42%. Anal. Calcd. for $C_{60}H_{36}F_{24}N_8Au_4$: C, 34.08; H, 1.71; N, 5.30. Found: C, 34.29; H, 2.06; N, 5.28. ^{19}F NMR ($CDCl_3$, ppm): 129 (singlet, 24 F, CF_3). 1H NMR ($CDCl_3$, ppm): 8.3 (s, 4H, CH amidine). UV-Vis(CH_2Cl_2): λ_{max} (nm), ϵ ($L/M^{-1}cm^{-1}$): 266, 68000; 306, 45000 ; 330, 31000.

$[Au_4(ArNC(Ph)NAr)_4]$ Ar = C_6H_5 , 16. N,N'-diphenylbenzamidine (272 mg, 1 mmol) was stirred with (56 mg, 1 mmol) of KOH in 25 mL of THF for 24 hr. Gradually the colorless solution turned yellow. Au(THT)Cl (320 mg, 1 mmol) was added and stirring continued for additional 4-5 hr. The solution was filtered and volume

was decreased under reduced pressure to 5 mL and hexanes was added to form an off-white precipitate. The product was filtered and recrystallized from THF/hexanes to give white crystals in yield of 47%. Anal. Calcd. for $C_{72}H_{60}Au_4N_8$: C, 48.73; H, 3.20. Found: C, 50.21; H, 3.54. 1H NMR ($CDCl_3$, ppm): 6.7-6.9(br, 60 H, CH phenyl). UV-Vis(CH_2Cl_2): λ_{max} (nm), ϵ ($L/M^{-1}cm^{-1}$): 226, 53000; 284, 29000; 344, 11000.

[Au₄(ArNC(CH₃)NAr)₄] Ar = C₆H₅, 17. N,N'-phenylacetamidine(210 mg, 1 mmol) was stirred with (56 mg, 1 mmol) of KOH in 25 mL of THF for 24 hr. Au(THT)Cl (320 mg, 1 mmol) was added and stirring continued for additional 4-5 hr. The solution was filtered and hexanes was added to form an of-white precipitate. The product was filtered and recrystallized from THF/hexanes to give off-white crystals in yield of 70%. 1H NMR ($CDCl_3$, ppm): 1.7 (mult., 3H, 4(CH₃)), 6.9-7.1 (br, 40 H, CH phenyl). Anal. Calcd. for $C_{56}H_{52}Au_4N_8$: C, 41.38; H, 3.20. Found: C, 41.56; H, 3.12. UV-Vis(CH_2Cl_2): λ_{max} (nm), ϵ ($L/M^{-1}cm^{-1}$): 226, 84000; 264, 83000; 305, 50000.

Synthesis of Tri- and Dinuclear Gold(I) Formamidinate Complexes

[Au₃(2,6-Me₂-form)₂(THT)Cl], 18. N,N'-di(2,6-methyl)phenylformamidine (252 mg, 1 mmol) was stirred with (56 mg, 1 mmol) of KOH in THF for 2 hr. The solution was colorless. Au(THT)Cl (480 mg, 1.5 mmol) was added and stirring continued for additional 4-5 hr. The solution was filtered and hexanes was added to form an off-white precipitate. The product was filtered and recrystallized from THF/hexanes to give white crystals in yield of 80%. X-ray studies confirmed the product as trinuclear gold(I) complex, [Au₃(2,6-Me₂-form)₂(THT)Cl], (THT= tetrahydrothiophene ligand), 1H

NMR (CDCl₃, ppm): 1.9 (b, 4H, CH₂, THT), 3.0 (4H, CH₂, THT), 2.47 (s, 24H, CH₃), 7.5 (s, 1H, CH amidine).

[Au₃(2,6-*i*-pr₂-form)₂(THT)Cl], 19. N,N'-di(2,6- isopropyl)phenylformamidine (363 mg, 1 mmol) was stirred with (40 mg, 1 mmol) of NaOH in 20 mL THF for 2 hr. The solution was colorless. Au(THT)Cl (480 mg, 1.5 mmol) was added and stirring continued for additional 4-5 hr. The solution was filtered and hexanes was added to form an off-white precipitate. The product was filtered and recrystallized from THF/hexanes to give white crystals in yield of 80%. X-ray studies confirmed the product as trinuclear gold(I) complex, , [Au₃(2,6-*i*-pr₂-form)₂(THT)Cl], (THT= tetrahydrothiophene ligand). ¹H NMR (CDCl₃, ppm): 1.9 (b, 2H, 2(CH₂), THT), 3.0 (2H, 2(CH₂), THT), 7.49 (s, 1H, 2(CH) amidine).

[Au₂(2,6-Me₂-form)₂], 20. N,N'-di(2,6methyl)phenylformamidine (126 mg, 0.5 mmol) was stirred with (28 mg, 0.5 mmol) of KOH in 20 mL THF for 24 hr. The solution was colorless. Au(THT)Cl (160 mg, 0.5 mmol) was added and stirring continued for additional 4-5 hr. The solution was filtered and hexanes was added to form an off-white precipitate. The product was filtered and recrystallized from THF/hexanes to give white crystals in yield of 75%. X-ray studies confirmed the product as dinuclear gold(I) complex, [Au₂(2,6-Me₂-form)₂]. Anal. Calcd. for C₃₄H₃₈Au₂N₄: C, 45.53; H, 4.24. Found: C, 45.67; H, 4.45. ¹H NMR (CDCl₃, ppm): 2.48 (3H, 8(CH₃)), 7.44 (1H, 2(CH) amidine). UV-Vis(CH₂Cl₂) : λ_{max} (nm), ε (L/M⁻¹cm⁻¹): 259, 60800.

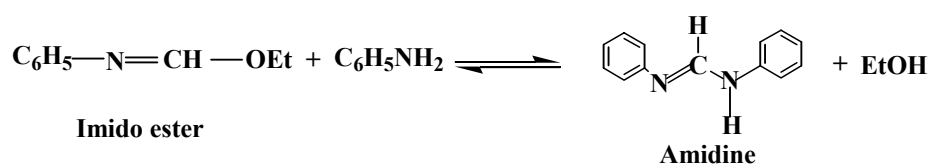
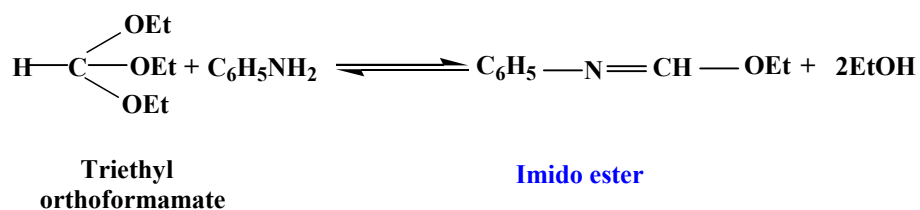
RESULTS AND DISCUSSION

Synthesis of Amidine Ligands

A series of symmetrical diaryl substituted amidinate ligands, $\text{ArNH}(\text{CH})\text{NAr}$, is synthesized. The substituents on the NCN aryl group are vary from electron withdrawing group such as $-\text{C}_6\text{F}_5$, $3\text{-CF}_3\text{-C}_6\text{H}_4$, $3,5\text{-Cl-C}_6\text{H}_3$ to donating groups such as $4\text{-OMe-C}_6\text{H}_4$, $4\text{-Me-C}_6\text{H}_4$, C_{10}H_7 , **V**, **IX**. Ligands with sterically bulky groups in the ortho positions such as $2,6\text{-(CH}_3)_2\text{-C}_6\text{H}_3$, **VIII** and $2,6\text{-}(\text{iPr})_2\text{-C}_6\text{H}_3$, **X** as well as on the NCN carbon, $\text{NC}(\text{Me})\text{N}$, $\text{NC}(\text{Ph})\text{N}$, **VI**, **VII**, are also prepared. All amidine ligands were synthesized by modified literature procedures.¹¹ In the preparations, the reaction time, temperature, and the method of recrystallization varied for some ligands. The aniline derivative (0.2 mol) and triethylorthoformate (orthoester) (0.1 mol) were mixed and the reaction mixture was heated to $140\text{--}160^\circ\text{C}$ in a reflux vessel for 1–2 hr to form the imido ester.³¹ The reaction mixture was distilled at the same temperature to remove ethanol and form the amidine ligands. Adding catalytic amount of acetic acid (1mL) to the synthesis helps to improve the yield.

Symmetrical and unsymmetrical substituted formamidine, $\text{RNH}(\text{CH})\text{NR}$ ($\text{R} = \text{tert-butyl}$), $\text{RNHC}(\text{H})\text{Ar}$ ($\text{R} = \text{tert-butyl}$, $\text{Ar} = p\text{-tolyl}$) were synthesized by modified literature procedures.³² Triethylorthoformate (orthoether) (0.1 mol) and catalytic amount of acetic acid (1 mL) were heated to 165°C , and *t*-butyl amine (0.2 mol) added drop wise during 15 min. The mixture was refluxed at 165°C for 30 min to 1 hour and then distilled at the same temperature for 2 hour to remove ethanol and form the desired product. All amidine ligands were characterized by $^1\text{HNMR}$. *N,N'*-naphthylamidine, **2**,

N,N'-Naphthylaceamidine, **3**, N,N'-di(2,6-isopropyl)phenylformamidine, **7** and N,N'-di-t-butyl-formamidine, **10** were characterized by X-ray crystallography.



Synthesis of Gold Amidinate Complexes

Tetranuclear gold(I) amidinate complexes are synthesized by the reaction of Au(THT)Cl with the potassium or sodium salt of the amidinate in THF, Figure 4. The reaction is stirred for few hours before filtrating off the KCl. A pale yellow product is isolated in a good yield. The yields vary for the synthesis of different gold(I) amidinates. For example, in the synthesis of the naphthyl derivative the yield is 31 versus 77% for the pentafluorophenyl complex. A violet or pink color is observed after adding the Au(THT)Cl. Stirring the reaction mixture for 1-2 hour give a pale yellow product. The reaction product forms rapidly after adding the gold precursor and it is crystallized from THF/hexanes. Drying a drop of the reaction mixture on a filter paper produces a spot

with a strong green luminescence under a hand-held UV lamp. The clusters are stable at room temperature for weeks and show gray coloration after standing for months in the light and open air.

Syntheses involving various substituted amidinates resulted in tetranuclear gold(I) clusters, $[\text{Au}_4(\text{ArNC}(\text{H})\text{NAr})_4]$. No change in the nuclearity was found by using substituents such as electron donating groups, $\text{Ar} = 4\text{-Me-C}_6\text{H}_4$, $4\text{-OMe-C}_6\text{H}_4$, C_{10}H_7 and electron withdrawing groups, $3, 5\text{-Cl-C}_6\text{H}_3$, C_6F_5 , $3\text{-CF}_3\text{-C}_6\text{H}_4$, Figure 4. In trials to investigate the effect of the solvents on the nuclearity of gold(I) amidinates, solvents such as ethanol, pyridine, CH_2Cl_2 , CHCl_3 and tetrahydrofuran were used. Only the reported tetranuclear clusters were isolated. The effect of the temperature was also investigated. *N,N'*-di(4-methoxy)phenylformamidine sodium salt is mixed with $\text{Au}(\text{THT})\text{Cl}$ in THF and the reaction temperature was raised to $45\text{ }^\circ\text{C}$. The synthesis was repeated at $55\text{ }^\circ\text{C}$ and $69\text{ }^\circ\text{C}$. The crystal formed from carrying the syntheses at 45 , 55 , $69\text{ }^\circ\text{C}$ showed no change in the nuclearity this was confirmed by X-rays crystallography as the tetranuclear $[\text{Au}_4(\text{ArNC}(\text{H})\text{NAr})_4]$, $\text{Ar} = \text{C}_6\text{H}_4\text{-4-OMe}$, **12**.

The C-functionalized substituted amidine $\text{ArNC}(\text{Ph})\text{NAr}$, $\text{Ar} = \text{C}_6\text{H}_5$ and $\text{ArNC}(\text{Me})\text{NAr}$, $\text{Ar} = \text{-C}_6\text{H}_5$, $\text{-4-MeC}_6\text{H}_5$, $\text{-C}_{10}\text{H}_7$ were synthesized and reacted with $\text{Au}(\text{THT})\text{Cl}$. Although the $\text{ArNC}(\text{Me})\text{NAr}$, $\text{Ar} = 4\text{-MeC}_6\text{H}_5$, **4**, and $\text{Ar} = \text{C}_{10}\text{H}_7$, **3**, are characterized by X-ray, unfortunately the reaction of their sodium salt with $\text{Au}(\text{THT})\text{Cl}$ resulted in the formation of twin crystals. However, the reactions of $\text{ArNC}(\text{Me})\text{NAr}$, $\text{Ar} = \text{C}_6\text{H}_5$ and $\text{ArNC}(\text{Ph})\text{NAr}$, $\text{Ar} = \text{C}_6\text{H}_5$ resulted in the formation of tetranuclear gold (I) amidinate complexes, Figure 4.

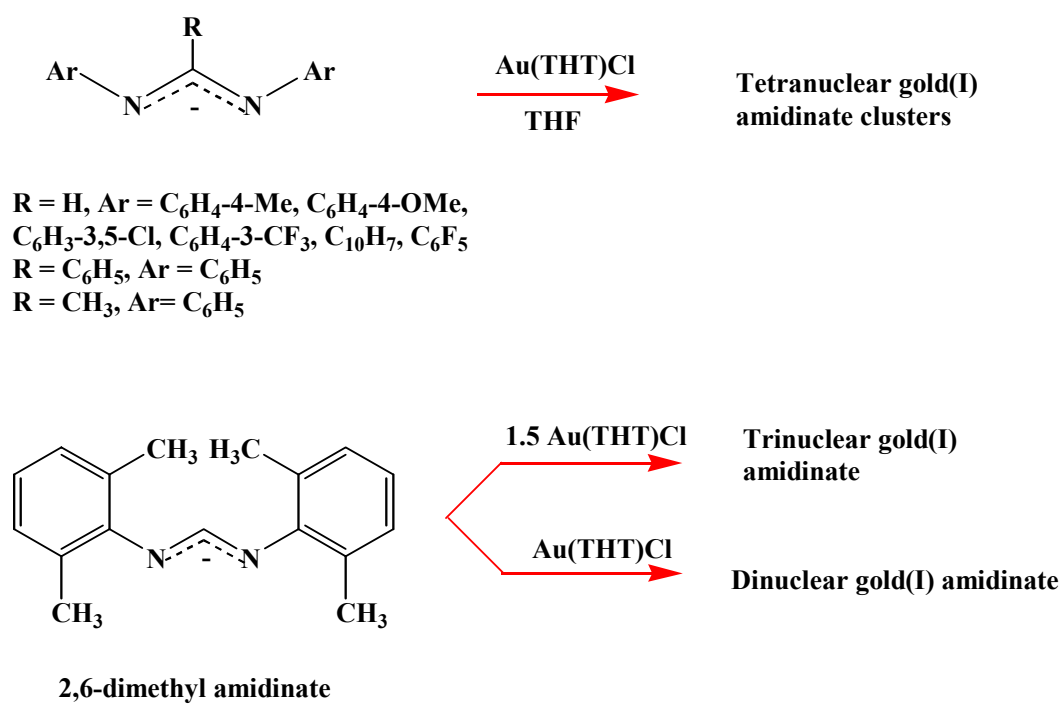
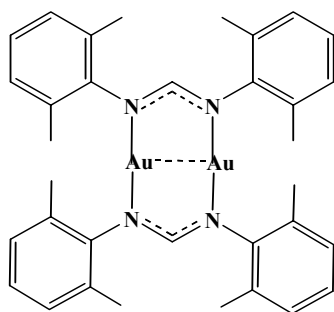
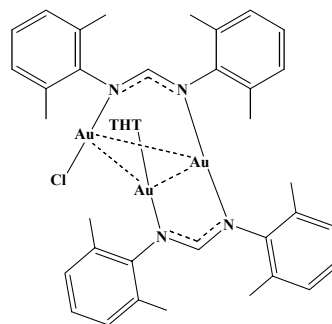


Figure 4. Schematic representation of the reaction between amidinate ligands and Au(THT)Cl.

Using sterically bulky groups in the ortho positions of the phenyl groups in ArNH(CH)NAr such as $\text{Ar} = 2,6\text{-(CH}_3\text{)}_2\text{-C}_6\text{H}_3$, **VIII** and $\text{Ar} = 2,6\text{-}(\text{i}\text{pr})_2\text{-C}_6\text{H}_3$, **IX** suggested that steric factors lead to the formation of di- and trinuclear gold(I) amidinates. Blocking formation of the tetranuclear species with **VIII**, di- and trinuclear gold(I) amidinate were isolated, **XII**, **XIII**. A trinuclear species was isolated using 2,6- $(\text{i}\text{pr})_2\text{-C}_6\text{H}_3$, **IX**. Previous work indicate formation of dinuclear products $\{\text{Au}_2[(\text{Me}_3\text{SiN})_2\text{C(Ph)}]_2\}$ and $[\text{Au}_2(\text{hpp})_2\text{Cl}_2]$ with the ligands indicated.^{15, 24}

**XII****XIII**

The trinuclear species $[\text{Au}_3(2,6\text{-Me}_2\text{-form})_2(\text{THT})\text{Cl}]$, **XIII** and $[\text{Au}_3(2,6\text{-}^i\text{pr}_2\text{-form})_2(\text{THT})\text{Cl}]$, **19** were isolated by the reaction of the potassium salt of the formamidinate ligand **VIII**, **IX** with $(\text{THT})\text{AuCl}$ in a (1:1.5) stoichiometric ratio, Figure 4. Attempts to obtain a tetranuclear gold species with these ligands, using different stoichiometric ratios, were not successful, and instead, the dinuclear **XII** was only

isolated. ^1H NMR of the trinuclear species showed the characteristic resonances of the tetrahydrothiophene ligand. The dinuclear complex $[\text{Au}_2(2,6\text{-Me}_2\text{-form})_2]$, **XII**, is isolated in quantitative yield by the reaction of $(\text{THT})\text{AuCl}$ with the potassium salt of 2,6-Me₂-form in a 1:1 stoichiometric ratio, Figure 4.

The reaction of the sodium salt of symmetrical and unsymmetrical substituted formamidinate ligand N,N'-di-*t*-butyl-formamidinate, **X** and N-*p*-tolyl-N'-*t*-butyl-formamidinate, **XI** with $\text{Au}(\text{THT})\text{Cl}$ was not successful and resulted in the formation of Au(0) and decomposition products.

Crystallographic Studies

Amidine ligands. The amidine ligands N,N'-Naphthylformamidinate, **2**, N,N'-Naphthylacetamidinate, **3**, N,N'-di(2,6-isopropyl)phenylformamidinate, **7** and N,N'-di-*t*-butyl-formamidinate, **10**, are characterized by X-rays. Selected bond distances and angles for **2**, **3** and **7** are summarized in Table 17. The X-ray structures of **2** and **3** showed independent molecular units without hydrogen bonds, Figure, 5, 6. Many amidine ligand structures reported as dimers linked through hydrogen bonding as the case in N,N'-di(4-methoxy)phenylformamidinate.³³ The C–N amidine distances of 1.285(3) and 1.341(3) Å in **2** average to 1.306 (12) Å in complex **13**, indicating delocalization upon coordination with gold. The naphthyl rings are in the plane of the ligand in **2** and perpendicular to it in **3**. The C–N amidine distances in **3** are 1.287(6), 1.361(5) Å and 1.317(5), 1.336(5) in **7**, Figure 7. The N-C-N angle decreased from 124.70° in N,N'-di(4-methoxy)phenylformamidinate, **1**, to 123.3(2), 121.4(4) and 119.9(4)° in **2**, **7** and **3**

respectively. The X-ray structure of **10** even at 77 K is not sufficiently well resolved due to disorder in the phenyl rings.

Table 17. Different Bond Distances and Angles for N,N'-dinaphthylformamide, **2**, N,N'-dinaphthylacetamide, **3**, and N,N'-di(2,6-isopropyl)phenylformamide, **7**.

Compound	C-N amidine Å	C-Namide Å	N-C-N °
N,N'-Naphthylformamide, 2	1.285(3)	1.341(3)	123.3(2)
N,N'-Naphthylacetamide, 3	1.287(6)	1.36(5)	119.9(4)
N,N'-di(2,6-isopropyl)phenylformamide, 7 .	1.317(5)	1.336(5)	121.4(4)

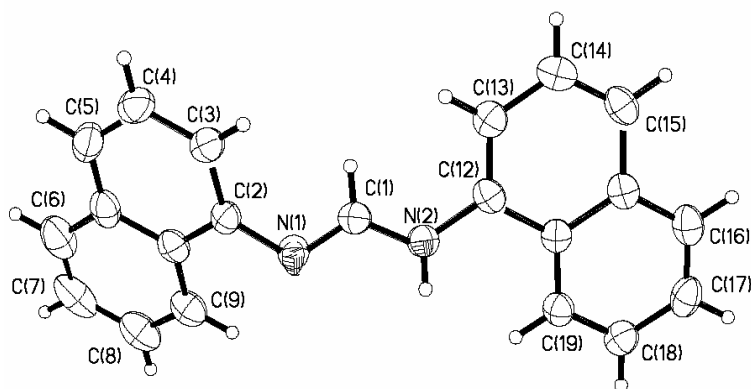


Figure 5. Thermal ellipsoid plot of **2** is drawn at the 50% probability level. Hydrogen atoms are removed for clarity.

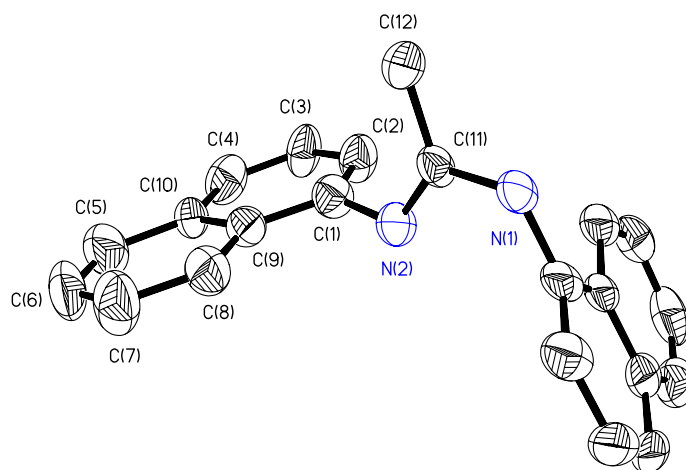


Figure 6. Thermal ellipsoid plot of **3** is drawn at the 50% probability level. Hydrogen atoms are removed for clarity.

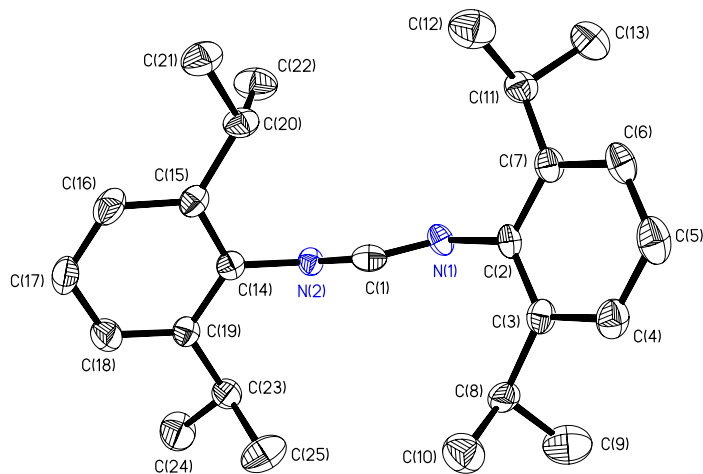


Figure 7. Thermal ellipsoid plot of **7** is drawn at the 50% probability level. Hydrogen atoms are removed for clarity.

Tetranuclear Au(I) Amidinate Complexes

In all the tetranuclear Au(I) formamidinate complexes $[\text{Au}_4(\text{ArNC}(\text{H})\text{NAr})_4]$, the NC bond length in NCN is $\sim 1.3 \text{ \AA}$, indicating delocalization across the amidinate bridge. The four gold atoms are located at the corners of a rhomboid with the amidinate ligands bridged above and below the near plane of the four gold(I) atoms. The average Au...Au distance is $\sim 3.0 \text{ \AA}$, typical of Au(I)...Au(I) aurophilic interaction. Table 18 gives Au...Au distances with Au...Au...Au and ligand N–Au–N angles for several homobridged tetranuclear Au(I) complexes and tetranuclear gold amidinate complexes characterized in our laboratory. Similar structural arrangements have been found in the tetrameric 1,3-diphenyltriazenidogold(I) complex, $[\text{Au}(\text{PhNNNPh})_4]$ (Au...Au = 2.85 \AA),³⁴ $[\text{Au}_4(\text{CH}_3\text{CS}_2)_4]$ (Au...Au = 3.01 \AA)³⁵ and the tetranuclear gold pyrazolate complex $[\text{Au}(\text{l-4-tBu-pz})_4]$ (Au...Au = 3.11 \AA).¹³ The Au(I) atoms bridged by the more flexible amidinate ligands show shorter Au...Au distances than those bridged by the rigid pyrazolate ligands (i.e., 2.9 \AA versus 3.1 \AA).³⁶

Table 18. Average Au...Au Distances (Å) and Au...Au...Au Angles (°) of Tetranuclear Gold(I) Amidinate Clusters, $[\text{Au}_4(\text{ArNC}(\text{H})\text{NAr})_4]$, and Related Tetranuclear Gold Clusters.

Complex	Au...Au	Au(1)...Au(2)...Au(3)	N-Au-N	Ref
$[\text{Au}(\text{PhNNNPh})_4]$	2.85	89.92	176	31
$[\text{Au}_4(\text{CH}_3\text{CS}_2)_4]$	3.01	89.95	167	32
$[\text{Au}(3,5\text{-tbu-pz})_4]$	3.11		175	10
Amidinate clusters $[\text{Au}_4(\text{ArNC}(\text{H})\text{NAr})_4]$, Ar =				
$\text{C}_6\text{H}_4\text{-4-OMe}$	2.94	70.87, 109.12	174	- ^a
$\text{C}_6\text{H}_3\text{-3,5-Cl}$	2.91	88.30, 91.53	177	6
$\text{C}_6\text{H}_4\text{-4-Me}$	3.03	63.59, 116.4	172	6
C_{10}H_7	2.98	68.52, 110.88	170	- ^a
C_6F_5	2.96	92.3, 87.5	169	- ^a
$\text{C}_6\text{H}_4\text{-2-CF}_3$	2.92	84.6, 95.3	176	- ^b
Amidinate clusters $[\text{Au}_4(\text{phNC}(\text{R})\text{Nph})_4]$, R =				
C_6H_5	2.94	82.86, 97.66	173	- ^a
CH_3	2.93	88.47, 91.14	168	- ^a

^a Reported here.

^b Synthesis reported, but the structures, even at 77 K is not sufficiently well resolved because of fluorine atom disorder.

The tetranuclear Au(I) formamidinate complex $[\text{Au}_4(\text{ArNC}(\text{H})\text{NAr})_4]$, $\text{Ar}=\text{C}_6\text{H}_4\text{-OMe}$, **12**, crystallizes as colorless needles in the monoclinic space group $P2_1/c$. The molecular structure of **1** is shown in Figure 8. The four gold atoms are located at the corner of a rhomboid with the formamidinate ligands bridged above and below the near plane of the four Au(I) atoms. The average Au...Au distance is 2.94 Å, typical of Au(I)...Au(I) interactions. The angles at Au...Au...Au are acute (70.26(2)–71.47(2)°) and obtuse (108.64(2)–109.62(2)°). The N–Au–N angles of 175° (av.) show a deviation from linearity consistent with Au...Au interactions. The four gold atoms in **12** lie in a near plane with a small torsion angle of 0.7° at Au(1)Au(2)Au(3)Au(4). The rhomboidal geometry of the four Au units seems to be attributable to steric factors. The AuNCNAu ring is twisted by weak crossing aurophilic interaction between Au(2) and Au(4) (3.417 Å). As a result, a torsion angle emerged at Au(3)N(5)N(6)Au(4) of 11.5°. The angle at NCN increased from 124.70° in the ligand, **1**, which crystallizes as dimers linked through NH...N hydrogen bonds, to 126.05° in the complex.³³ There is a slight twist of the aryl rings out of the formamidinate plane.

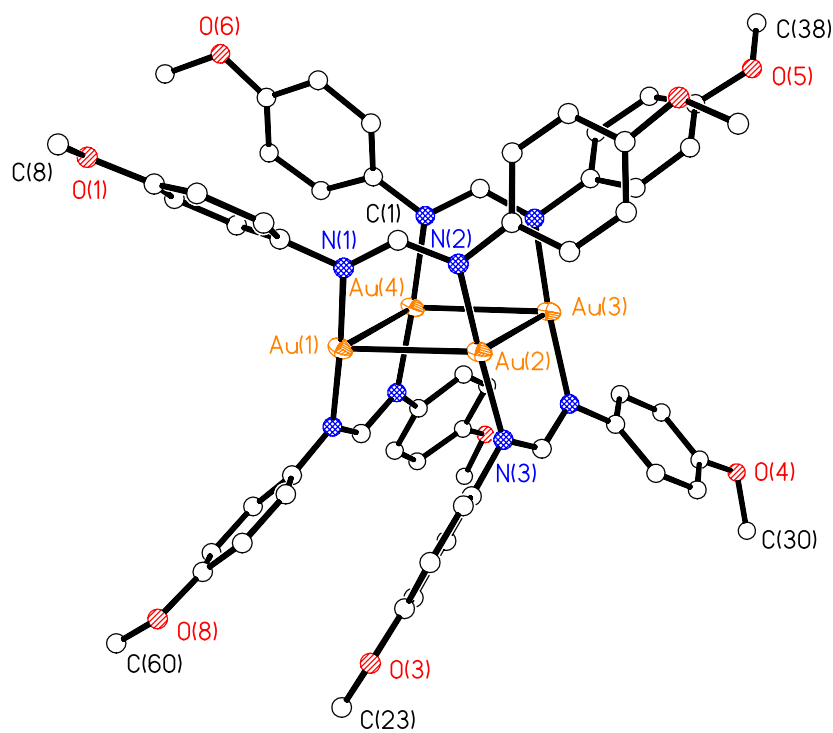


Figure 8. Thermal ellipsoid plot of **12** is drawn at the 50% probability level. Hydrogen atoms are removed for clarity.

The molecular structure of naphthyl derivative, $[\text{Au}_4(\text{ArNC}(\text{H})\text{NAr})_4]$, $\text{Ar} = \text{C}_{10}\text{H}_7$, **13** is shown in Figure 9. The gold atoms are arranged in a parallelogram ($\text{Au}\dots\text{Au}\dots\text{Au} = 68\text{--}110^\circ$). Each of the gold atoms is coordinated to two amidinate ligands in a nearly linear coordination. The average Au–N and Au...Au bond lengths are comparable with those observed in other gold–nitrogen complexes.³⁷ The bite distance in **13** is $\sim 2.33 \text{ \AA}$.

The four gold atoms are arranged in a square ($\text{Au}\dots\text{Au}\dots\text{Au} = 87\text{--}92^\circ$) in the tetranuclear structures $[\text{Au}_4(\text{ArNC}(\text{H})\text{NAr})_4]$, $\text{Ar} = \text{C}_6\text{F}_5$, **14** and a distorted square ($\text{Au}\dots\text{Au}\dots\text{Au} = 84\text{--}95^\circ$) in the trifluoromethylphenyl derivative, $\text{Ar} = \text{C}_6\text{H}_4\text{-3-CF}_3$, **15**. The molecular structure of **14** is shown in Figure 10. The amidinate ligands bridged above and below the near plane of the four Au(I) atoms. The packing diagram of **14** shows weak F...F ($\sim 2.44 \text{ \AA}$), Au...F ($\sim 3.14 \text{ \AA}$, intramolecular), and Au...F ($\sim 3.51 \text{ \AA}$, intermolecular) interactions. The N–Au–N angles of 172° (av.) show a deviation from linearity consistent with Au...Au interactions. The average Au–N and Au...Au bond lengths are comparable with those observed in other gold–nitrogen complexes.³⁷ The bite distance in **14** is $2.34\text{--}2.43 \text{ \AA}$. The X-ray structure of **15** even at 77 K is not sufficiently well resolved because of fluorine atom disorder, while the Au(I) atoms and the amidinates ligand atoms refine well. The Au...Au Distances and Au...Au...Au Angles for **15** are given in Table 18.

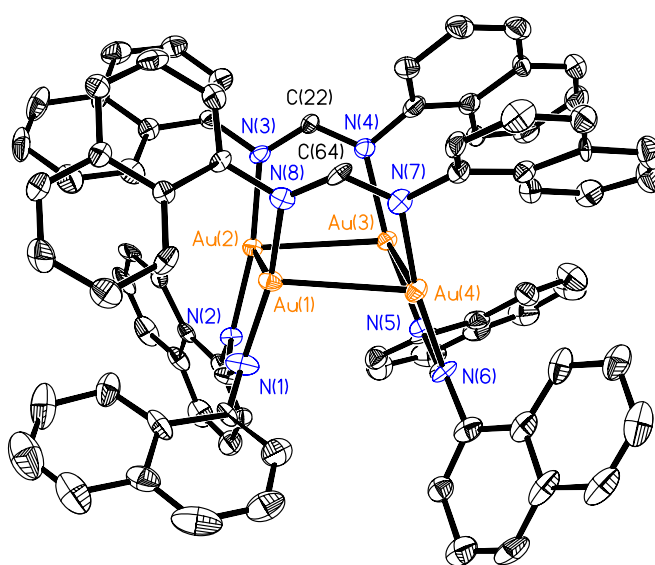


Figure 9. Thermal ellipsoid plot of **13** is drawn at the 50% probability level. Hydrogen atoms are removed for clarity.

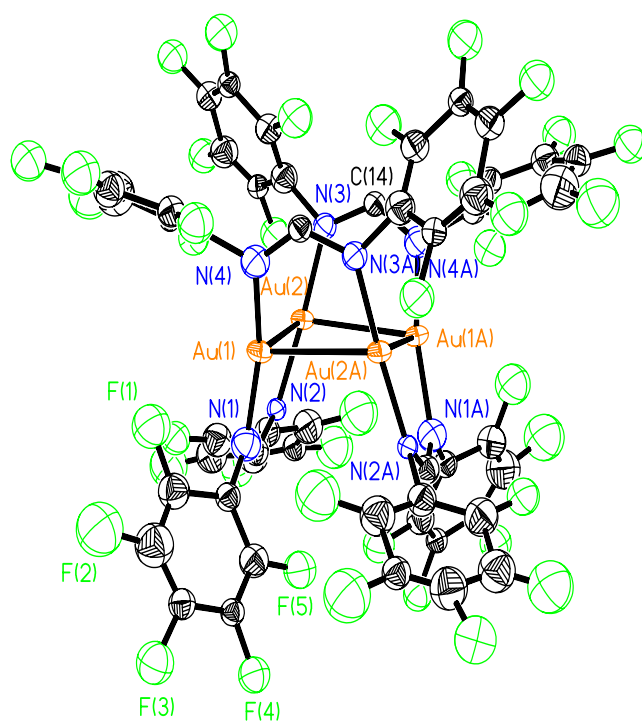


Figure 10. Thermal ellipsoid plot of **14** is drawing at the 50% probability level. Hydrogen atoms are removed for clarity.

Figures 11 and 12 show the thermal ellipsoid plots of **16** and **17**, $[\text{Au}_4(\text{ArNC}(\text{Ph})\text{NAr})_4]$, $[\text{Au}_4(\text{ArNC}(\text{CH}_3)\text{NAr})_4]$, Ar = C₆H₅ respectively. The captions provide selected bond distances and angles. The average Au...Au distance is 2.94 Å, typical of Au(I)...Au(I) interactions. The gold atoms are arranged in a square (Au...Au...Au = 88-91°) in **17** and a distorted square (Au...Au...Au = 82-97°) in **16**. The N-Au-N angles of 170° (av.) show a deviation from linearity consistent with Au...Au interactions. The four gold atoms lie in a near plane with a small torsion angle of 0.78° in **16** and a larger one of 15.8° in **17** at Au(2)Au(1)Au(4)Au(3). The NCN angle is 122(av.).

The trinuclear species $[\text{Au}_3(2,6\text{-Me}_2\text{-form})_2(\text{THT})\text{Cl}]$, **18** and $[\text{Au}_3(2,6\text{-}i\text{-pr}_2\text{-form})_2(\text{THT})\text{Cl}]$, **19** are isolated as monoclinic ($P2_1/n$), prismatic crystals. The structures of **18** and **19** each have two short Au...Au distances of ~3.01 Å, 3.05 and two long Au...Au distance of 3.66, 3.55 Å, respectively. The Au-S and Au-Cl distances in **18** and **19** are 2.245(6) Å and 2.258(6) Å, respectively. The N-Au-N angles of 167.5° show a deviation from linearity consistent with Au...Au interactions. The X-ray structure of **15**

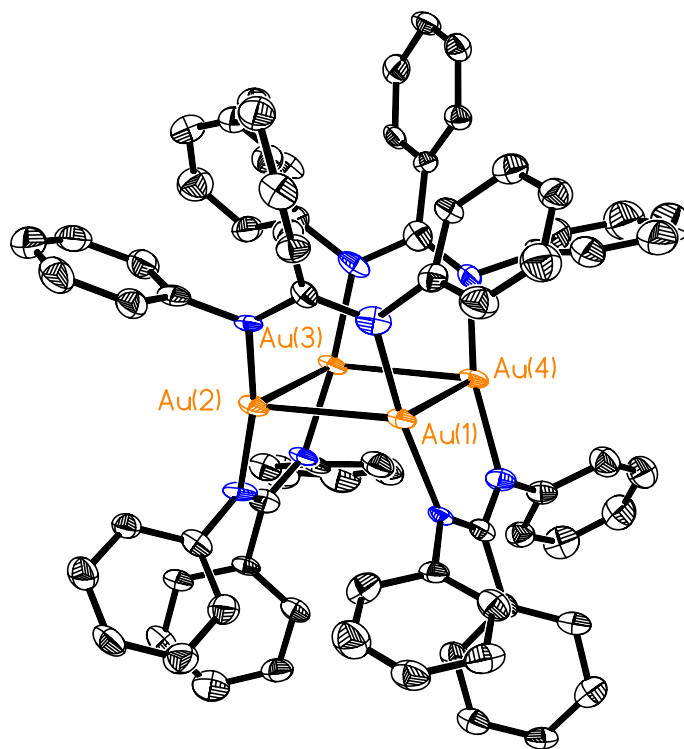


Figure 11. Thermal ellipsoid plot of **16** is drawn at the 50% probability level. Hydrogen atoms are removed for clarity.

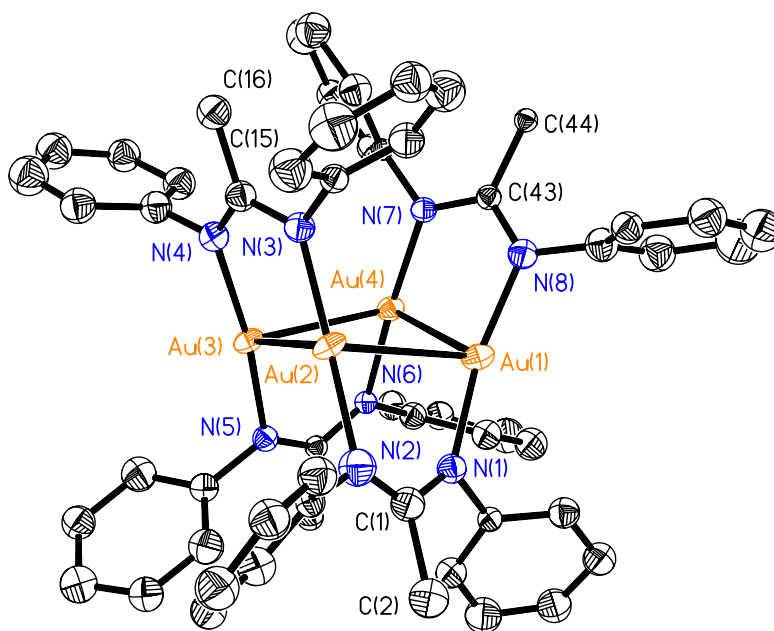


Figure 12. Thermal ellipsoid plot of **17** is drawn at the 50% probability level. Hydrogen atoms are removed for clarity.

even at 77 K is not sufficiently well resolved due to disorder in the phenyl and THT rings. The X-ray structure of N,N'-di(2,6-isopropyl)phenylformamidine, **7** is shown in Figure 7. Selected bond distances and angles are summarized in Table 17. The X-ray structure of **18** is shown in Figure 13.

The dinuclear complex, $[\text{Au}_2(2,6\text{-Me}_2\text{-form})_2]$, **20** is isolated in the space group $P\bar{1}$, Figure 14. The Au...Au distance is 2.711(3) Å, and the N-Au-N angle is 170.2(3)°. To our knowledge, there is only one other example of a symmetrically bridged dinuclear gold(I) nitrogen complex, $\{\text{Au}_2[(\text{Me}_3\text{SiN})_2\text{C}(\text{Ph})]_2\}$, which has a Au...Au distance of 2.646 Å.²⁴ The Au...Au distance in **20** is 2.711 Å. This is shorter than in the xanthate $[\text{Au}_2(\text{}^n\text{Bu-xanthate})_2]$ (2.849 Å),³⁸ the dithiophosphate $[\text{AuS}_2\text{PPh}_2]_2$ (3.085 Å),³⁹ ylides $[\text{Au}(\text{CH}_2)_2\text{PPh}_2]_2$ (2.977 Å),⁴⁰ and dithiophosphonate $[\text{AuS}_2\text{PPh}(\text{OEt})_2]_2$ (3.042 Å);⁴¹ however, closer to the bond distances in the dithiolates $[\text{PPN}]_2[\text{Au}_2(\mu^2\text{-}\eta^2\text{-CS}_3)_2]$ (2.799 Å),⁴² $[n\text{-Bu}_4\text{N}][\text{Au}(\text{S}_2\text{C}=\text{C}(\text{CN})_2)_2]$ (2.796 Å),⁴³ and $[\text{Au}(\text{S}_2\text{C}-\text{N}(\text{C}_5\text{H}_{11})_2)]_2$ (2.769 Å).⁴⁴

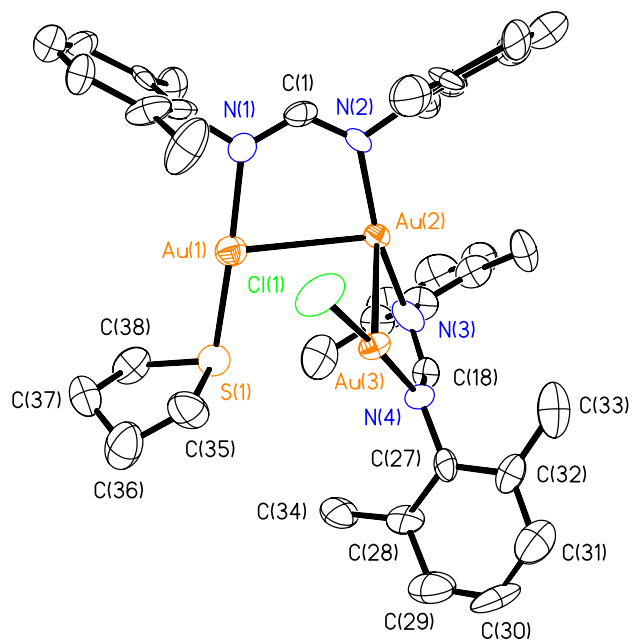


Figure 13. Thermal ellipsoid plot of **18** is drawing at the 50% probability level. Hydrogen atoms are removed for clarity.

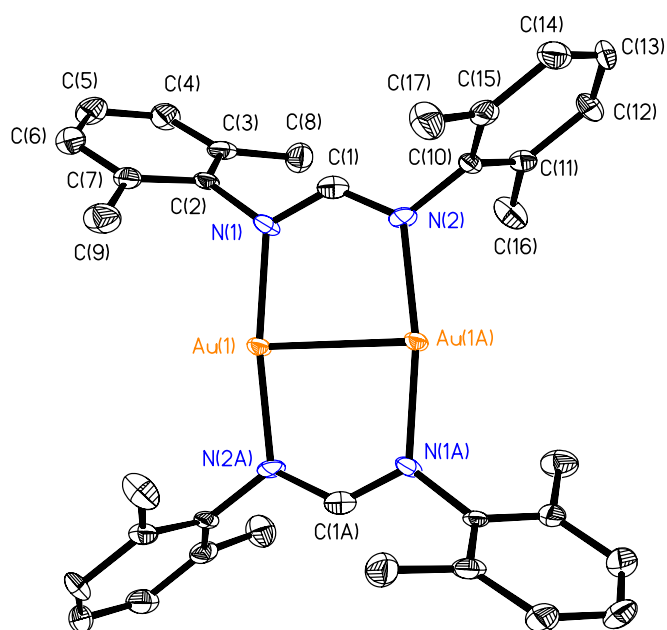


Figure 14. Thermal ellipsoid plot of **20** is drawn at the 50% probability level. Hydrogen atoms are removed for clarity.

CHAPTER III

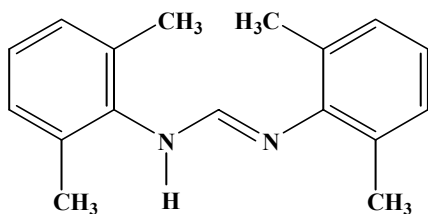
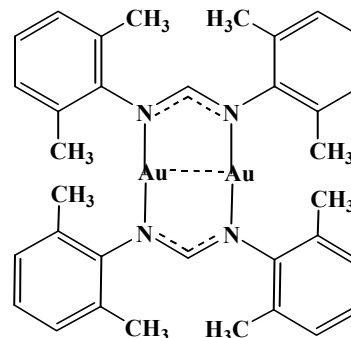
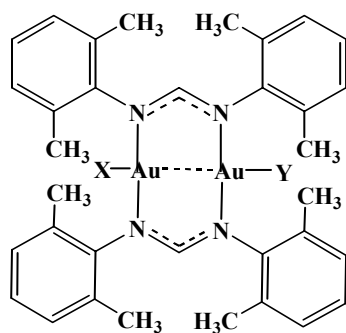
OXIDATIVE-ADDITION REACTIONS TO THE DINUCLEAR GOLD(I)

AMIDINATE COMPLEX, $[\text{Au}_2(o\text{-Me}_2\text{-form})_2]^*$

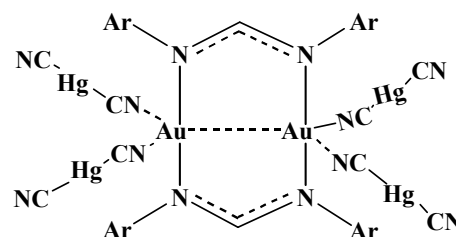
The dinuclear gold(I) amidinate complex, $[\text{Au}_2(o\text{-Me}_2\text{-form})_2]$, **XII**, is isolated by using sterically bulky groups in the ortho positions of the phenyl ring in the formamidine $\text{ArNH}(\text{CH})\text{NAr}$, $\text{Ar} = 2,6\text{-Me}_2\text{-C}_6\text{H}_3$, **VIII**. The oxidative-addition reactions of halogens and other groups to the dinuclear gold(I) amidinate complex, **XII**, are described thoroughly in this chapter. Various reagents such as Cl_2 , Br_2 , I_2 , benzoyl peroxide and CH_3I add to the dinuclear gold(I) amidinate complex to form oxidative addition gold (II) products, **XIV**.^{23,45} The Au(II) amidinate complexes are stable at room temperature. The oxidative addition of benzoyl peroxide leads to the isolation of the first stable dinuclear gold (II) nitrogen complex possessing Au-O bonds, $[\text{Au}_2(o\text{-Me}_2\text{-form})_2(\text{PhCO}_2)_2]$. The reaction with $\text{Hg}(\text{CN})_2$ results in the formation of the 2D

*Reproduced in part from *Inorg. Chem.*, *44*, 166-168, **2005**, Abdou, H. E.; Mohamed, A. A.; Fackler, Jr., J. P., "Synthesis and X-ray Structures of Dinuclear and Trinuclear Gold(I) and Dinuclear Gold(II) Amidinate Complexes" copyright 2005 American Chemical Society, from *Inorg. Chem.*, *45*, 11-12, **2006**, Mohamed, A. A.; Abdou, H. E.; Fackler, Jr., J. P., "Mercury(II) Cyanide Coordination Polymer with Dinuclear Gold(I) Amidinate. Structure of the 2-D $[\text{Au}_2(2,6\text{-Me}_2\text{-formamidinate})_2] \cdot 2\text{Hg}(\text{CN})_2 \cdot 2\text{THF}$ Complex", copyright 2006 American Chemical Society and from *Z. Naturforsch., B:Chem. Sci.*, *59B*, 1480-1482, **2004**, Abdou, H. E.; Mohamed, A. A.; Fackler, J. P., Jr., "Oxidative Addition of Methyl Iodide to Dinuclear Gold(I) Amidinate Complex: Schmidbaur's Breakthrough Reaction Revisited with Amidinates" copyright 2004 Verlag der Zeitschrift für Naturforschung.

mercury(II) cyanide coordination polymer, $[\text{Au}_2(o\text{-Me}_2\text{-form})_2] \cdot 2\text{Hg}(\text{CN})_2 \cdot 2\text{THF}$, **XV**, not the expected oxidative-addition product.⁴⁶

**VIII****XII**

X=Y=Cl, Br, I, PhCOO
X=CH₃ and Y=I

XIV

Ar = 2,6-(CH₃)₂-C₆H₃

XV

EXPERIMENTAL

General Procedures

All glassware was oven-dried prior to use. Triethyl orthoformate (orthoester) and 2,6-dimethylaniline were purchased from Aldrich. Tetrahydrothiophene ligand was purchased from TCI, Tokyo. The solvents THF, CH₂Cl₂, hexanes, toluene and ether

were purchased from Aldrich and used as received. Br₂, I₂, CH₃I, CCl₄, CBr₄, Cl₄, CH₂Br₂, CH₂I₂, ClCH₂CH₂Cl, BrCH₂CH₂Br, ICH₂CH₂I, PhICl₂, tetrabutylammonium bromide and Hg(CN)₂ were purchased from Aldrich. Au(THT)Cl was prepared by reacting HAuCl₄ with tetrahydrothiophene ligand, THT. The dinuclear gold(I) amidinate complex, [Au₂(2,6-Me₂-form)₂], **20**, was prepared as explained in chapter II. IR spectra were recorded using a Perkin Elmer 16 PC FT-IR spectrometer or a Bruker Tensor 27 spectrometer. Elemental analyses were performed by Guelph Chemical laboratories Ltd. & Chemisar Laboratories Inc, Guelph, Ontario, Canada. UV-Vis spectra were recorded on a Shimadzu UV-2501 PC spectrometer. ¹H spectra were recorded on a Unity Plus 300 NMR spectrometer using solvent peaks to reference the chemical shifts (δ).

Synthesis of Gold (II) Amidinate Compounds

[Au₂(*o*-Me₂-form)₂Cl₂], **21** and [Au₂(*o*-Me₂-form)₂X₂][Au₂(*o*-Me₂-form)₂], X = Cl, **22**. Compound **21** is prepared by using several oxidizing agents, Cl₂, CCl₄, CH₂Cl₂, ClCH₂CH₂Cl and aqua regia. [Au₂(*o*-Me₂-form)₂], (0.31 g, 0.03 X 10⁻² mol) was dissolved in 5 mL THF and stirred for 15 min. PhICl₂, (0.095 g, 0.03 X 10⁻² mol) was added, the color of the solution change to dark green immediately. The reaction mixture was stirred for 3 h then filtered and the filtrate left overnight at room temperature for slow evaporation. The next day, green crystals of **21** formed. Yield: 80%. Anal. Calcd. for C₃₄H₃₈Au₂N₄Cl₂: C, 42.20; H, 3.95. Found: C, 41.77; H, 3.88. ¹H NMR (CDCl₃, ppm): 7.97 (s, 2H (CH amidinate)), 2.51 (s, 24H (CH₃)). UV-Vis (CH₂Cl₂): λ_{max} (nm), ε (L/M⁻¹cm⁻¹): 346, 29,400; 456, 5535. The oxidation by halogenated solvents, (0.31 g, 0.03 X 10⁻² mol) of [Au₂(*o*-Me₂-form)₂] was mixed with 5-10 mL

(excess) of the solvent and the mixture stirred for 2-3 days (7 d in the case of CH_2Cl_2), then filtered and the filtrate left overnight at room temperature for slow evaporation. A crystalline product in which there was an equal amount of oxidized and unoxidized complexes in the same unit cell, $[\text{Au}_2(o\text{-Me}_2\text{-form})_2\text{X}_2][\text{Au}_2(o\text{-Me}_2\text{-form})_2]$, $\text{X} = \text{Cl}$, **22** was isolated when the reaction stopped after 3-4 h of stirring before oxidizing all the Au(I) material.

$[\text{Au}_2(o\text{-Me}_2\text{-form})_2\text{Br}_2]$, **23** and $[\text{Au}_2(o\text{-Me}_2\text{-form})_2\text{X}_2][\text{Au}_2(o\text{-Me}_2\text{-form})_2]$, $\text{X} = \text{Br}$, **24**. Several oxidizing agents Br_2 , CBr_4 , $\text{BrCH}_2\text{CH}_2\text{Br}$ and CH_2Br_2 can be used to prepare compound **23**, an example is given. $[\text{Au}_2(o\text{-Me}_2\text{-form})_2]$, (0.22 g, 2.5×10^{-4} mol) was dissolved in 10 mL THF and stirred for 15 min. CBr_4 (0.08 g, 2.5×10^{-4} mol) was added, after 20 min of stirring the color of the reaction mixture change to light brown. The reaction mixture was stirred for 2-3 d then filtered and the filtrate left overnight at room temperature for slow evaporation to form yellow crystals of **23**. Yield: 85%. Anal. Calcd. for $\text{C}_{34}\text{H}_{38}\text{Au}_2\text{N}_4\text{Br}_2$: C, 41.81; H, 3.92. Found: C, 42.22; H, 3.54. ^1H NMR (CDCl_3 , ppm): 8.13 (s, 2H (CH amidinate)), 2.54 (s, 24H, (CH_3)). UV-Vis (CH_2Cl_2): λ_{max} (nm), ϵ ($\text{L}/\text{M}^{-1}\text{cm}^{-1}$): 379, 27,200. A crystalline product in which there was an equal amount of oxidized and unoxidized complexes in the same unit cell, $[\text{Au}_2(o\text{-Me}_2\text{-form})_2\text{X}_2][\text{Au}_2(o\text{-Me}_2\text{-form})_2]$, $\text{X} = \text{Br}$, **24** was isolated when the reaction stopped after 3-4 h of stirring before oxidizing all the Au(I) material.

$[\text{Au}_2(o\text{-Me}_2\text{-form})_2\text{I}_2]$, **25**. Several oxidizing agents I_2 , Cl_4 , CH_2I_2 and $\text{ICH}_2\text{CH}_2\text{I}$ can be used to prepare compound **25**, an example is given. $[\text{Au}_2(o\text{-Me}_2\text{-form})_2]$, (0.22 g, 2.5×10^{-4} mol) was dissolved in 10 mL THF and stirred for 15 min. I_2 (0.07 g, 2.5×10^{-4}

mol) was added, the color of the reaction mixture change to dark green after 5 min. The reaction mixture was stirred for 2 h then filtered and the filtrate left overnight at room temperature for slow evaporation to form green crystals of **25**. The oxidation by halogenated solvents resulted in the isolation of the same product, **25**, after stirring the reaction mixtures for 2 h. Yield: 80%. Anal. Calcd. for $C_{34}H_{38}Au_2N_4I_2$: C, 35.49; H, 3.32. Found: C, 34.73; H, 3.66. 1H NMR ($CDCl_3$, ppm): 8.19 (s, 2H, (CH amidinate)); 2.55 (s, 24H (CH_3)). UV-Vis (CH_2Cl_2): λ_{max} (nm), ϵ ($L/M^{-1}cm^{-1}$): 379, 17,300.

[Au₂(*o*-Me₂-form)₂CH₃I], 26. To 0.23 g (2.5×10^{-4} mmol) of the dinuclear gold amidinate $[Au_2(o-Me_2-form)_2]$ in 20 ml freshly distilled ether in round bottom flask a 0.5 ml (excess) of CH_3I was added. After stirring for 2 h under N_2 stream in ice bath in absence of light the brown product was filtered, 85% yield. 1H NMR ($CDCl_3$, ppm): 1.37 (s, 3H (Au- CH_3)). Anal. Calcd. for $C_{35}H_{41}Au_2I_2N_4$: C, 40.47; H, 3.97. Found: C, 39.91; H, 4.05.

[Au₂(*o*-Me₂-form)₂] \cdot 2Hg(CN)₂ \cdot 2THF, 27. (0.11 g, 1.2×10^{-4} mol) of $[Au_2(o-Me_2-form)_2]$ was dissolved in 10 mL THF and stirred for 15 min. $Hg(CN)_2$ (0.06 g, 2.4×10^{-4} mol) was added to the previous mixture, no color change is observed after mixing. The reaction mixture was stirred for 6 h at room temperature then left for slow evaporation to form white crystals of **27** and a yellow powder. The white crystals change to yellow powder upon grinding. Yield: 65%. IR (NaCl plates, cm^{-1}): 2147 (s, $C\equiv N$).

[Au₂(*o*-Me₂-form)₂(PhCOO)₂], 28. $[Au_2(o-Me_2-form)_2]$, (0.11 g, 1.2×10^{-4} mol) was dissolved in 10 mL toluene and stirred for 15 min. $(PhCO)_2O_2$, (0.03 g, 1.2×10^{-4} mol) was added, the color of the reaction mixture gradually change to dark brown. The

reaction mixture was stirred for 3 h then filtered and the filtrate left overnight at room temperature for slow evaporation. Dark brown crystals of **28** formed after two days. Yield: 85%. Anal. Calcd. for $C_{48}H_{48}Au_2N_4O_4 \cdot 0.5\text{toluene}$: C, 52.20; H 4.42. Found: C, 52.40; H, 4.67. $^1\text{H NMR}$ (CDCl_3 , ppm): 7.97 (s, 2H (CH amidinate)); 2.54 (s, 24H (CH_3)). UV-Vis (CH_2Cl_2): λ_{max} (nm), ϵ ($\text{L/M}^{-1}\text{cm}^{-1}$): 345, 30,600.

CRYSTALLOGRAPHIC STUDIES

Cell parameters and refinement results of Au(II) amidinate compounds **21**, **22**, **23**, **24**, **25**, **26**, **27** and **28** are summarized in Tables 19, 20, 21 and 22. Tables 23-30 show the important interatomic distances and angles. X-ray data were collected using a Siemens (Bruker) SMART CCD (charge coupled device) based diffractometer equipped with a LT-2 low temperature apparatus operating at 110 K. A suitable crystal was chosen and mounted on a glass fiber using cryogenic grease. Data were measured using omega scans of 0.3° per frame for 60 s. The first 50 frames were recollected at the end of data collection as a monitor for decay. No decay was detected. Cell parameters were retrieved using SMART software and refined using SAINT on all observed reflections.²⁸ Data reductions were performed using SAINT software.²⁹ The structures were solved by direct methods using SHELXS-97 and refined by least squares on F², with SHELXL-97 incorporated in SHELXTL-PC V 5.03.^{30, 31} The structures were determined in the space groups reported in Tables 19, 20, 21 and 22 by analysis of systematic absences. Hydrogen atom positions were calculated by geometrical methods and refined as a riding model.

Table 19. Crystal Data and Structure Refinement for $[\text{Au}_2(o\text{-Me}_2\text{-form})_2\text{Cl}_2]$, **21** and $[\text{Au}_2(o\text{-Me}_2\text{-form})_2\text{X}_2][\text{Au}_2(o\text{-Me}_2\text{-form})_2]\cdot\text{CH}_2\text{ClCH}_2\text{Cl}$, X = Cl, **22**·CH₂ClCH₂Cl.

compound	21	22 ·CH ₂ ClCH ₂ Cl
empirical formula	C ₃₇ H ₄₁ Au ₂ N ₄ Cl ₂	C ₇₀ H ₈₀ Au ₄ N ₈ Cl ₄
fw	1006.58	1962.1
crystal system	Monoclinic	monoclinic
space group	<i>P2₁/c</i>	<i>P2₁/n</i>
<i>a</i> (Å)	11.012(2)	16.597(3)
<i>b</i> (Å)	18.464(4)	10.606(2)
<i>c</i> (Å)	19.467(4)	19.809(3)
α	90.00	90.00
B (°)	94.86(4)	94.155(6)
γ	90.00	90.00
V (Å ³)	3943.7(14)	3477.9(11)
Z	4	2
λ (Å)	0.71073	0.71073
d_{calc} (g/cm ⁻³)	1.695	1.969
μ (mm ⁻¹)	7.595	8.690
T (K)	110(2)	110(2)
R1 ^a , wR2 ^b	0.0742, 0.1924	0.1003, 0.2796
Goodness-of -fit ^c	1.089	1.259

$$^a \text{R1} = \frac{\sum \left| |F_o| - |F_c| \right|}{\sum |F_o|}$$

$$^b \text{wR2} = \left[\frac{\sum [w(F_o^2 - F_c^2)^2]}{\sum [w(F_o^2)^2]} \right]^{1/2}; w = 1/[\sigma^2(F_o^2) + (aP)^2 + (bP)], \text{ where } P = [\max(F_o^2 \text{ or } 0) + 2(F_c^2)]/3$$

$$^c \text{Goodness-of -fit} = \left[\frac{\sum [w(F_o^2 - F_c^2)^2]}{(N_{\text{obs}} - N_{\text{param}})} \right]^{1/2}, \text{ based on all data}$$

Table 20. Crystal Data and Structure Refinement for $[\text{Au}_2(o\text{-Me}_2\text{-form})_2\text{Br}_2]$, **23** and $[\text{Au}_2(o\text{-Me}_2\text{-form})_2\text{X}_2][\text{Au}_2(o\text{-Me}_2\text{-form})_2]$ X = Br, **24**.

compound	23	24
empirical formula	$\text{C}_{34}\text{H}_{38}\text{Au}_2\text{N}_4\text{Br}_2$	$\text{C}_{68}\text{H}_{76}\text{Au}_4\text{N}_8\text{Br}_2$
fw	1056.43	1951.03
crystal system	Monoclinic	monoclinic
space group	$P2_1/n$	$P2_1/n$
a (Å)	16.967(3)	16.967(3)
b (Å)	10.783(2)	10.783(2)
c (Å)	20.060(4)	20.060(4)
α	90.00	90.00
β (°)	93.77 (3)	93.77(3)
γ	90.00	90.00
V (Å ³)	3662.1(13)	3662.1(13)
Z	6	2
λ (Å)	0.71073	0.71073
d_{calc} (g/cm ⁻³)	2.498	1.769
μ (mm ⁻¹)	15.247	9.120
T (K)	110(2)	110(2)
R1 ^a , wR2 ^b	0.100, 0.2429	0.1000, 0.2429
Goodness-of-fit ^c	0.966	0.966

$$^a R1 = \frac{\sum ||F_o| - |F_c||}{\sum |F_o|}$$

$$^b wR2 = \left[\frac{\sum [w(F_o^2 - F_c^2)^2]}{\sum [w(F_o^2)^2]} \right]^{1/2}; w = 1/[\sigma^2(F_o^2) + (aP)^2 + (bP)], \text{ where } P = [\max(F_o^2 \text{ or } 0) + 2(F_c^2)]/3$$

$$^c \text{Goodness-of-fit} = \left[\frac{\sum [w(F_o^2 - F_c^2)^2]}{(N_{\text{obs}} - N_{\text{param}})} \right]^{1/2}, \text{ based on all data}$$

Table 21. Crystal Data and Structure Refinement for [Au₂(*o*-Me₂-form)₂I₂], **25**, and [Au₂(*o*-Me₂-form)₂CH₃I], **26**.

compound	25	26
empirical formula	C ₃₈ H ₄₆ Au ₂ I ₂ N ₄ O	C ₃₅ H ₄₁ Au ₂ N ₄ I
fw	1150.43	1038.62
crystal system	Triclinic	Monoclinic
space group	<i>P</i> $\bar{1}$	<i>P</i> 2 ₁ / <i>n</i>
<i>a</i> (Å)	8.0611(12)	16.688(6)
<i>b</i> (Å)	10.956(16)	10.672(4)
<i>c</i> (Å)	11.352 (17)	19.953(7)
α	84.815(2)	90.00
β	78.352(2)	94.565(7)
γ	88.577(2)	90.00
<i>V</i> (Å ³)	977.9(3)	3542(2)
<i>Z</i>	1	4
λ (Å)	0.71073	0.71073
<i>d</i> _{calc} (g/cm ⁻³)	2.076	1.956
μ (mm ⁻¹)	9.105	8.746
T (K)	110(2)	110(2)
R1, wR2	0.0422, 0.1204	0.0581, 0.1329
Goodness-of -fit ^c	1.062	1.133

$$^a R1 = \frac{\sum ||F_o| - |F_c||}{\sum |F_o|}$$

$$^b wR2 = \frac{[\sum [w(F_o^2 - F_c^2)^2]]^{1/2}}{[\sum [w(F_o^2)^2]]^{1/2}}; w = 1/[\sigma^2(F_o^2) + (aP)^2 + (bP)], \text{ where } P = [\max(F_o^2 \text{ or } 0) + 2(F_c^2)]/3$$

$$^c \text{Goodness-of -fit} = [\sum [w(F_o^2 - F_c^2)^2]/(N_{\text{obs}} - N_{\text{param}})]^{1/2}, \text{ based on all data}$$

Table 22. Crystal Data and Structure Refinement for [Au₂(2,6-Me₂-form)₂].2Hg(CN)₂.2THF, **27**, and [Au₂(*o*-Me₂-form)₂(PhCOO)₂], **28**.

compound	27	28
formula	C ₄₆ H ₅₄ Au ₂ Hg ₂ N ₈ O ₂	C ₄₈ H ₄₈ Au ₂ N ₄ O ₄
fw	1546.09	1138
crystal system	Monoclinic	triclinic
space group	<i>P2₁/c</i>	<i>P</i> $\bar{1}$
<i>a</i> (Å)	18.936(4)	11.160 (3)
<i>b</i> (Å)	14.500(3)	12.112(3)
<i>c</i> (Å)	19.897(4)	12.364(3)
α	90.00	115.168(4)
β	118.12(3)	161.112(4)
γ	90.00	106.253(5)
<i>V</i> (Å ³)	4818.3(17)	1355.4 (6)
<i>Z</i>	4	2
λ (Å)	0.71073	0.71073
<i>d</i> _{calc} (g/cm ⁻³)	2.143	2.393
μ (mm ⁻¹)	12.534	10.867
T (K)	110(2)	110(2)
R1, wR2	0.0708, 0.0883	0.0691, 0.1964
Goodness-of-fit ^c	0.986	1.193

$$^a R1 = \frac{\sum ||F_o| - |F_c||}{\sum |F_o|}$$

$$^b wR2 = \left[\frac{\sum [w(F_o^2 - F_c^2)^2]}{\sum [w(F_o^2)]} \right]^{1/2}; w = 1/[\sigma^2(F_o^2) + (aP)^2 + (bP)], \text{ where } P = [\max(F_o^2 \text{ or } 0) + 2(F_c^2)]/3$$

$$^c \text{Goodness-of-fit} = \left[\frac{\sum [w(F_o^2 - F_c^2)^2]}{(N_{\text{obs}} - N_{\text{param}})} \right]^{1/2}, \text{ based on all data}$$

Table 23. Selected Bond Distances (Å) and Angles (°) for [Au₂(*o*-Me₂-form)₂Cl₂], **21**.

Au2–N2	2.018(9)	Au1–N3	2.026(9)
Au2–N4	2.032(9)	Au1–Cl1	2.354(3)
Au2–Cl2	2.366(3)	N2–C1	1.328(14)
Au2–Au1	2.5176(7)	N2–C10	1.431(14)
Au1–N1	2.022(8)	N1–C1	1.318(14)
N2–Au2–N4	174.4(4)	N1–Au1–Au2	87.3(3)
N2–Au2–Cl2	92.6(3)	N3–Au1–Au2	87.7(3)
N4–Au2–Cl2	92.5(3)	Cl1–Au1–Au2	178.63(8)
N2–Au2–Au1	87.7(3)	C1–N2–Au2	120.1(7)
N4–Au2–Au1	87.3(3)	C1–N1–Au1	120.6(7)
Cl2–Au2–Au1	177.76(8)	N1–C1–N2	124.3(10)
N1–Au1–N3	175.0(4)		
N1–Au1–Cl1	92.6(3)		
N3–Au1–Cl1	92.4(3)		

Table 24. Selected Bond Distances (Å) and Angles (°) for [Au₂(*o*-Me₂-form)₂X₂][Au₂(*o*-Me₂-form)₂], X = Cl, **22**.

Au1–N1	1.99(3)	Au2–N4	2.03(3)
Au1–N2	2.01(3)	Au2–Au2A	2.7098(15)
Au1–Cl1	2.321(8)	C1–N2A	1.30(4)
Au1–Au1A	2.5671(19)	C1–N1	1.36(3)
Au2–N3	1.99(2)	N2–C1A	1.30(4)
N1–Au1–N2	174.6(10)	N3–Au2–N4	169.1(7)
N1–Au1–N2	174.6(10)	N3–Au2–Au2A	83.5(5)
N2–Au1–Cl1	92.1(7)	N4–Au2–Au2A	85.7(5)
N1–Au1–Au1	87.3(6)	N2–C1A–N1A	127(3)
N2–Au1–Au1A	87.4(7)	C1–N1–Au1	119(2)
Cl1–Au1–Au1A	178.5(3)		

Table 25. Selected Bond Distances (Å) and Angles (°) for [Au₂(*o*-Me₂-form)₂Br₂], **23**.

Au1–N1	2.004(17)	N1–C1	1.32(3)
Au1–N2	2.023(18)	N2–C1A	1.28(2)
Au1–Br1	2.470(2)	C1–N2A	1.28(2)
Au1–Au1A	2.5251(15)		
<hr/>			
N1–Au1–N2	173.4(6)	N2–Au1–Au1A	86.6(5)
N1–Au–Br1	93.1(4)	Br1–Au1–Au1A	179.62(10)
N2–Au1–Br1	93.4(5)	C1–N1–Au1	121.2(14)
N1–Au1–Au1A	86.9(4)	C1–N2A–Au1A	121.6(16)

Table 26. Selected Bond Distances (Å) and Angles (°) for [Au₂(*o*-Me₂-form)₂X₂][Au₂(*o*-Me₂-form)₂], X = Br, **24**.

Au1–N1	2.004(17)	Au2–Au2	2.706(2)
Au1–N2	2.023(18)	N1–C1	1.32(3)
Au1–Br1	2.470(2)	N1–C2	1.43(2)
Au1–Au1A	2.5251(15)	N2–C1	1.28(2) 3
Au2–N3	2.067(19)		
N1–Au1–N2	173.4(6)	N4–Au2–N3	165.0(10)
N1–Au1–Br1	93.1(4)	N4–Au2–Au2A	80.4(9)
N2–Au1–Br1	93.4(5)	N3–Au2–Au2A	84.6(5)
N1–Au1–Au1A	86.9(4)	C1–N1–Au1	121.2(14)
N2A–Au1A–Au1	86.6(5)	N2–C1A–N1	124(2)
Br1A–Au1A–Au1	179.62(10)		

Table 27. Selected Bond Distances (Å) and Angles (°) for [Au₂(*o*-Me₂-form)₂I₂], **25**.

Au1–N2	2.027(4)	Au1–I1	2.6828(4)
Au1–N1	2.027(4)	N1–C1	1.325(7)
Au1–Au1	2.5794(4)	N2–C1	1.310(7)
N2–Au1–N1	173.36(16)	Au1–Au1A–I1	176.947(12)
N2–Au1–Au1A	86.37(12)	C1–N1–Au1	119.6(3)
N1–Au1–Au1	87.10(12)	C2–N1–Au1	124.7(3)
N2–Au1–I1	93.70(12)	C1–N2A–Au1A	120.8(4)
N1–Au1–I1	92.88(12)	N2–C1A–N1A	126.1(5)

Table 28. Selected Bond Distances (Å) and Angles (°) for [Au₂(*o*-Me₂-form)₂CH₃I], **26**.

Au1A-N2A	2.011(10)	Au1A-Au1B	2.5293(11)
Au1A-N1A	2.021(11)	N1A-C10A	1.320(17)
Au1A-C1	2.120(10)	N2AA-C10A	1.318(16)
Au1B-I1	2.499(3)		
N2A-Au1A-N1A	174.8(4)	N1A-Au1A-Au1B	87.4(3)
N2A-Au1A-C1	92.6(3)	I1-Au1B-Au1A	178.72(7)
N1A-Au1A-C1	92.3(3)	C10A-N1A-Au1A	119.1(9)
N2AA-Au1B-I1	92.5(3)		

Table 29. Selected Bond Distances (Å) and Angles (°) for [Au₂(2,6-Me₂-form)₂] · 2Hg(CN)₂ · 2THF, **27**.

Au1–N3	2.096(16)	N6–C38A	1.19(4)
Au1–N1	2.11(2)	N5–C35	1.17(4)
Au1–N5	2.32(3)	N7–C37	1.17(4)
Au1–N6	2.51(3)	O1–C39	1.37(3)
Au1...Au2	2.9047(17)	O1–C42	1.41(4)
Au2–N4	2.11(2)	O2–C43	1.34(4)
Au2–N2	2.136(16)	O2–C46	1.40(4)
Au2–N7	2.32(3)	C46–C45	1.62(5)
Au2–N8	2.51(3)	C40–C41	1.47(5)
Hg2–C38	1.95(3)	C40–C39	1.50(5)
Hg2–C37	1.96(3)	C41–C42	1.57(5)
Hg1–C36	1.99(3)	C43–C44	1.56(5)
Hg1–C35	1.99(3)	C44–C45	1.47(5)
N3–Au1–N1	161.6(8)	C39–O1–C42	104(2)
N3–Au1–N5	96.0(8)	C43–O2–C46	103(2)
N1–Au1–N5	98.9(8)	C38A–N6–Au1	162(2)
N3–Au1–N6	93.9(7)	C35–N5–Au1	143(2)
N1–Au1–N6	94.3(8)	C37–N7–Au2	157(2)
N5–Au1–N6	99.2(9)	N5–C35–Hg1	170(2)
N3... Au1... Au2	81.5(5)	N6–C38A–Hg2	175(2)

Table 29**Continued**

N1...Au1...Au2	83.0(6)	N7-C37-Hg2	178(3)
N5...Au1...Au2	176.2(6)	O2-C46-C45	111(3)
N4-Au2-N2	160.1(8)	C41-C40-C39	105(3)
N4-Au2-N7	101.4(9)	O1-C39-C40	109(3)
N2-Au2-N7	94.4(8)	C40-C41-C42	102(3)
N4... Au2...Au1	80.5(7)	O2-C43-C44	107(3)
N2...Au2...Au1	81.9(5)	C45-C44-C43	106(3)
N7...Au2...Au1	169.9(7)	O1-C42-C41	104(3)
C38-Hg2-C37	176.5(10)	C44-C45-C46	98(3)
C36-Hg1-C35	178.0(10)		

Table 30. Selected Bond Distances (Å) and Angles (°) for [Au₂(*o*-Me₂-form)₂(PhCOO)₂], **28.**

Au1–N2	2.008(10)	N1–C1	1.323(16)
Au1–N1	2.010(10)	N2–C1A	1.315(15)
Au1–O1	2.045(8)	C18–O2	1.264(15)
Au1–Au1A	2.4899(10)	C1–N2A	1.315(15)
O1–C18	1.284(14)		
N2–Au1–N1	175.5(4)	C18–O1–Au1	112.6(7)
N2–Au1–O1	90.6(4)	C1–N1–Au1	120.1(8)
N1–Au1–O1	93.9(4)	C1A–N2–Au1	120.1(8)
N2–Au1–Au1A	87.9(3)	O2–C18–O1	130.4(11)
N1–Au1–Au1A	87.6(3)	N2–C1A–N1	124.2(11)
O1–Au1–Au1A	174.9(2)		

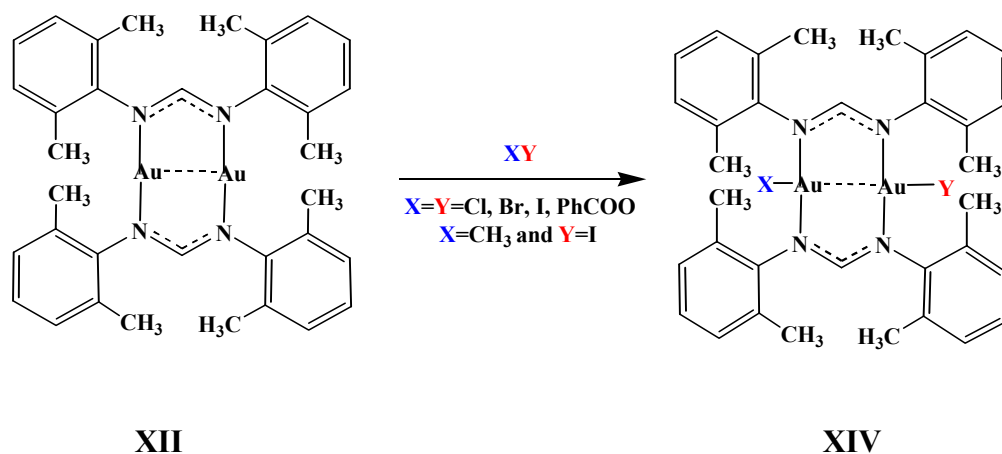
RESULTS AND DISCUSSION

Synthesis

The addition of 1 molar equivalent of Cl_2 , Br_2 , I_2 , to the dinuclear amidinate $[\text{Au}_2(o\text{-Me}_2\text{-form})_2]$, **XII**, in a THF solution at room temperature produced an immediate color change from colorless or light yellow to a very deep, dark green or brown. Recrystallization produced dark orange or brown crystals from which x-ray crystallography established Au(II) products, **21**, **23**, **25**, containing solvent such as THF or hexane in the lattice. Thermal gravimetric analysis and differential thermal analysis showed the release of the solvent followed by the loss of the halogen.

The reactions of the dinuclear complex with the halogenated solvents, CH_2X_2 , $\text{XCH}_2\text{CH}_2\text{X}$, CX_4 ($\text{X} = \text{Cl}, \text{Br}, \text{I}$) also formed Au (II) products. With the iodide derivative the reaction occurs in the time of mixing to give the Au(II) product. The analogous reactions with chloride and bromide derivatives takes approximately 2 to 3 days, and 7 days with CH_2Cl_2 in order to oxidize all the Au(I) material. A crystalline product in which there are an equal amount of oxidized and unoxidized complexes in the same unit cell, $[\text{Au}_2(o\text{-Me}_2\text{-form})_2\text{X}_2][\text{Au}_2(o\text{-Me}_2\text{-form})_2]$, $\text{X} = \text{Cl}$, **22** and $\text{X} = \text{Br}$, **24**, is isolated when the reaction is stopped after 3-4 h of stirring. Continued stirring of the reaction mixture for several days produced the completely oxidized products, $[\text{Au}_2(o\text{-Me}_2\text{-form})_2\text{X}_2]$, $\text{X} = \text{Cl}, \text{Br}$. The reaction was followed by UV-Vis for several days, the dinuclear peak at 255 nm decreased with time until it disappeared and new peaks of chloride, 346 nm, 456 nm (shoulder), and bromide derivatives, 379 nm, were formed. In the reaction of the halo alkyls CH_nX_m to produce the dihalides, the qualitative order of

reactivity with the gold complexes ($I > Br > Cl$) follows inversely the order of carbon-halogen bond dissociation energy, $C-Cl > C-Br > C-I$.



The replacement of the bromide in $[Au_2(o-Me_2-form)_2Br_2]$, **23**, by chloride is achieved by adding 1 mol of $PhICl_2$ to 1 mol of **23** in polar solvent, CH_3CN . After 30 minutes of mixing the UV-Vis peak of the bromide derivative, **23** at 379 nm in CH_2Cl_2 was shifted to 346 nm and 456 nm (shoulder) indicating the formation of the dichloride product, **21**.

The dropwise addition of methyl iodide, CH_3I , to a solution of $[Au_2(o-Me_2-form)_2]$ in ether generates $[CH_3Au(o-Me_2-form)_2 AuI]$, **26**, in quantitative yield under nitrogen at $0\text{ }^\circ\text{C}$ and in the absence of light. The dark orange brown crystals which form as large blocks are stable at room temperature. A gold metal forms around the wall of the reaction vessel if the reaction carried in the open air at room temperature. Growing crystals was successful at $0\text{ }^\circ\text{C}$ after one week.⁴⁵

The reaction of the dinuclear gold amidinate complex, **XII**, with $\text{Hg}(\text{CN})_2$ (1:2 stoichiometry) in THF forms a white product, **27**.⁴⁶ White crystals and a yellow powder are formed while crystals are grown. The white crystals change to yellow powder upon grinding, presumably with loss of THF and possibly some AuCN formation. The product was sparingly soluble in various organic solvents. The infrared spectrum of the adduct showed the cyanide frequency to be shifted from 2192 cm^{-1} in $\text{Hg}(\text{CN})_2$ to 2147 cm^{-1} in the adduct. The UV-vis spectrum of **27** in THF, although it was sparingly soluble, showed a red shift from 255 nm in the dinuclear gold amidinate complex, **XII**, to a broad band centered at 285 nm. The origin of this shift is uncertain but may be related to partial formation of the $\text{Hg}(\text{CN})_2$ adduct, **27**. Thermal gravimetric analysis of **27** showed the release of THF gradually at $>120\text{ }^\circ\text{C}$ followed by decomposition at $>200\text{ }^\circ\text{C}$. Powder diffraction of the yellow residue after heating above $265\text{ }^\circ\text{C}$ showed a diffraction pattern typical of AuCN (IR 2236 cm^{-1}). This result was confirmed by comparison with the powder diffraction pattern of a sample of AuCN obtained from the Aldrich Chemical Co.⁴⁶

The reaction of $\text{Hg}(\text{CN})_2$ resulted in the formation of the 2D complex $[\text{Au}_2(o\text{-Me}_2\text{-form})_2]\cdot 2\text{Hg}(\text{CN})_2\cdot 2\text{THF}$, **27**, not the expected oxidative-addition product, $[\text{NCAu}(o\text{-Me}_2\text{-form})_2\text{AuCN}]$, as in the case of the dinuclear gold(I) ylide, Figure 15.⁴⁷ The variable behavior of $\text{Hg}(\text{CN})_2$ toward dinuclear gold complexes requires comment. In the case of the mercury(II) cyanide reaction with the dinuclear gold(I) dithiophosphate, Figure 15, (b), the stability of the gold(I)-carbon bond compared with that of mercury(II)-carbon bond and the strength of the Hg(II)-S bonds compared with the labile

Au(I)-S bonds appear to lead to the metathesis products observed. In the case of the dinuclear gold(I) ylide, Figure 15, (a), oxidation of the Au(I) to Au(II) resulted in the formation of a reduced mercury product. With the adduct to the amidinate ligand complex, Figure 15, (c), the cyanide IR stretching frequency shifted to $\sim 2147\text{ cm}^{-1}$, a value very near to the CN stretching frequency found (2145 cm^{-1}) in the dinuclear Au(II) ylide dicyanide.⁴⁴ However, the oxidation of the dinuclear Au(I) amidinate by the $\text{Hg}(\text{CN})_2$ is much more difficult than the oxidation of the dinuclear Au(I) ylide. Cyclic voltammetric studies bear this out (vide infra).⁴⁸ The differences in the chemistry of these dinuclear gold(I) complexes may be understood by examining their respective HOMOs, which, in the ylide, is a metal-metal σ^* antibonding, while in the dinuclear gold(I) amidinate the HOMO is δ^* . Gold ylides are oxidized in 0.1 M $\text{Bu}_4\text{NBF}_4/\text{THF}$ at low potentials of +0.11 and +0.23 V vs. Ag/AgCl (quasi-reversible). The dinuclear amidinate, **XII**, oxidizes under the same conditions at +1.24 V vs. Ag/AgCl (reversible). These large differences in chemical character of the dinuclear gold(I) complexes appear to explain the widely different behavior of these compounds toward reaction with mercury cyanide.

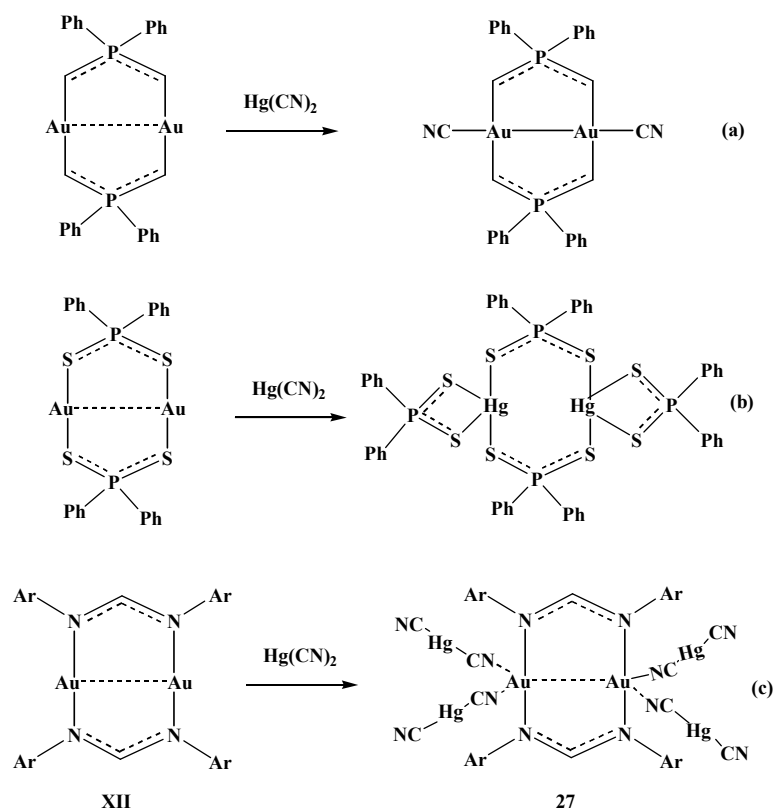


Figure 15. Schematic representation of the reactions between $\text{Hg}(\text{CN})_2$ and the dinuclear gold(I) dithiophosphinate, dinuclear gold(I) ylide and the dinuclear Au(I) amidinate complexes.

The benzoate product, **28** was obtained by adding an equivalent amount of benzoyl peroxide to a toluene solution of the dinuclear amidinate complex. The reaction was stirred for few hours before the solvent was slowly evaporated to form crystals. A brown product was isolated in a good yield. The reaction forming product happens rapidly after adding the benzoyl peroxide. The product is stable at room temperature. Infra-red spectroscopic studies of the gold benzoate complex showed two intense bands at 1628 and 1578 cm^{-1} due to $\nu(\text{C}=\text{O})$ and at 1320-1295 cm^{-1} due to $\nu(\text{C}-\text{O})$ frequencies. The separation between the two bands is $\sim 300 \text{ cm}^{-1}$, typical of unidentate benzoate bonding, pseudo ester character. The bonding of the benzoates to the dinuclear gold(I) amidinate is similar to the unidentate bonding observed in the ylide complexes, which adopt a trans geometry.⁴⁹

The facile replacement of the benzoate groups in $[\text{Au}_2(o\text{-Me}_2\text{-form})_2(\text{PhCOO})_2]$, **28**, by chloride or bromide was achieved by adding equivalent amounts of PhICl_2 or tetrabutylammonium bromide to **28** in polar solvents such as CH_3CN , Figure 16.

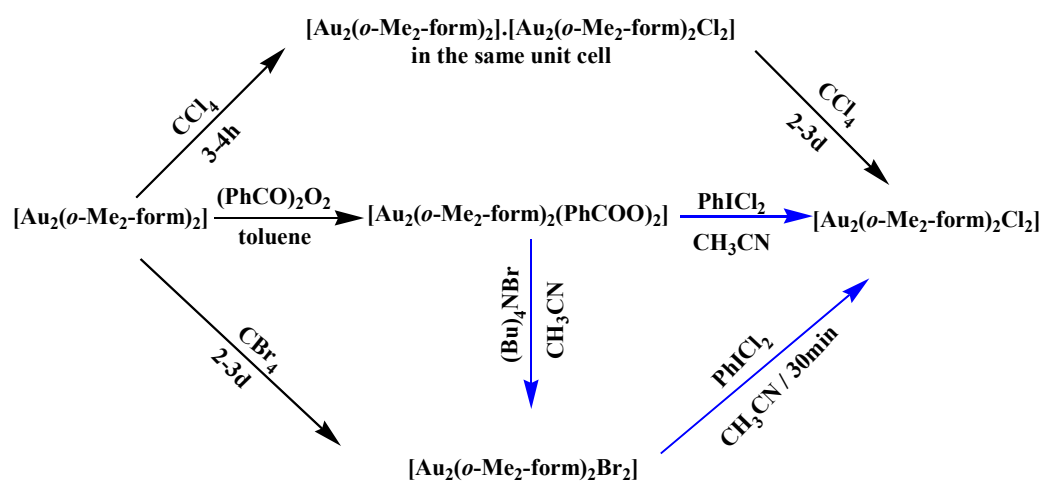


Figure 16. Schematic representation of the replacement reactions of $[\text{Au}_2(o\text{-Me}_2\text{-form})_2(\text{PhCOO})_2]$, **28** in CH_3CN .

The replacement of the benzoate groups by chloride is fast. After 5 minutes of mixing PhICl_2 with dinuclear amidinate $[\text{Au}_2(o\text{-Me}_2\text{-form})_2]$, **XII**, in $\text{CH}_3\text{CN}/\text{THF}$ the color of the reaction mixture changed from yellow to bright green. This result indicated the formation of the dichloride product, **21**, as also confirmed by the two UV-Vis peaks at 346 nm and 356 nm (shoulder) nm, in CH_2Cl_2 . With the tetrabutylammonium bromide, the UV-Vis peak of the benzoate derivative, **28**, at 345 nm in CH_2Cl_2 shifted to 379 nm after 7 days of mixing, which confirmed the formation of the dibromide product, **23**.

Crystallographic Studies

The gold(II) amidinate complexes **21**, **23**, and **25** readily form crystals suitable for X-ray diffraction. The X-ray crystallography established the formation of Au(II) products containing solvent such as THF or hexanes. The Au...Au distance decreases from 2.71 Å in the starting dinuclear complex to 2.51 - 2.57 Å in the oxidized species. The X-ray structures of **21** and **23** are shown in Figures 17, 18.²³ The X-ray structure of

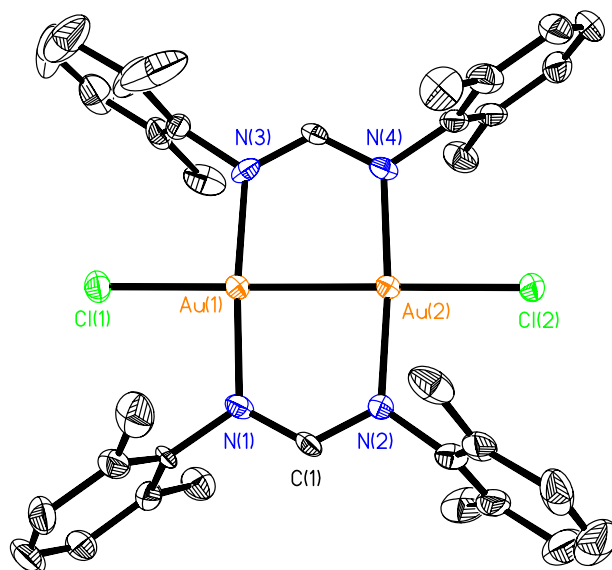


Figure 17. Thermal ellipsoid plot of **21** is drawn at the 50% probability level. Hydrogen atoms are removed for clarity.

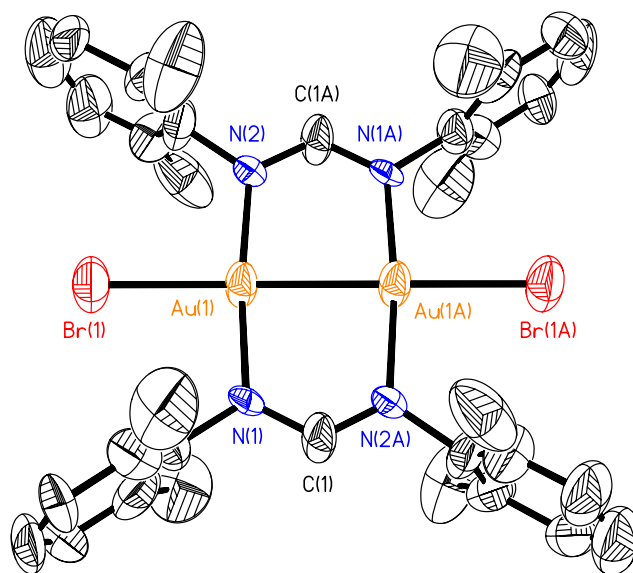


Figure 18. Thermal ellipsoid plot of **23** is drawn at the 50% probability level. Hydrogen atoms are removed for clarity.

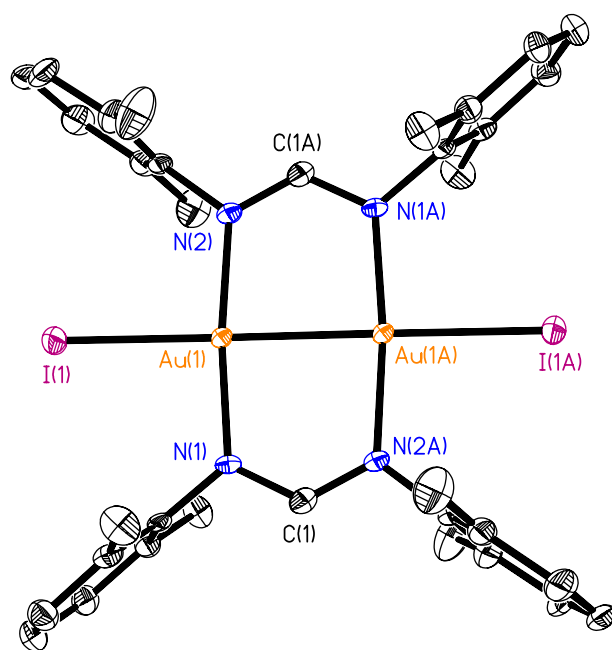


Figure 19. Thermal ellipsoid plot of **25** is drawn at the 50% probability level. Hydrogen atoms are removed for clarity.

25 is shown in Figure 19. The Au-X distances, Au-Cl = 2.36 Å, Au-Br = 2.47 Å, Au-I = 2.68 Å, are typical for these gold(I) halide distances. The N–Au–N angles of 173.9° (av.) show a deviation from linearity. The Au-N distances decreased from 2.035(7) Å in the dinuclear complex to 2.00 - 2.004 Å in the oxidative-addition products. The Au atoms have nearly square-planer coordination geometries with formation of bonds to a second Au center, two N atoms and one halide atom.

A crystalline product in which there is an equal amount of oxidized and unoxidized complexes in the same unit cell, $[\text{Au}_2(o\text{-Me}_2\text{-form})_2\text{X}_2][\text{Au}_2(o\text{-Me}_2\text{-form})_2]$, X = Cl, **22** or Br, **24**, was isolated when the reaction of dinuclear complex with the halogenated solvents, CH_2X_2 , $\text{XCH}_2\text{CH}_2\text{X}$, CX_4 (X = Cl, Br) was stopped after 3-4 h of stirring before oxidizing all the Au(I) material. An example of the chlorine oxidation product, $[\text{Au}_2(o\text{-Me}_2\text{-form})_2\text{X}_2][\text{Au}_2(o\text{-Me}_2\text{-form})_2]$, X = Cl, **22**, is shown in Figure 20 and the bromine oxidation product, X = Br, **24**, is shown in Figure 21 .

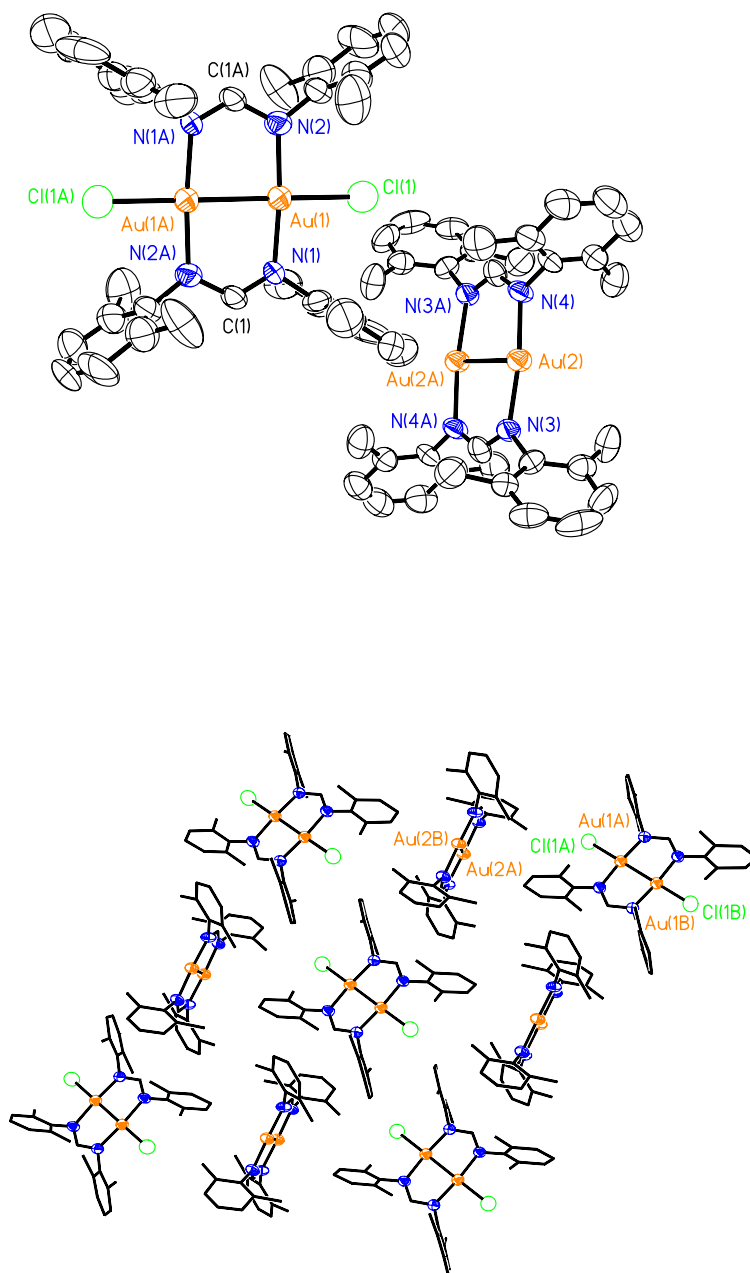


Figure 20. Thermal ellipsoid plot of **22** Ellipsoid is drawn at the 50% probability level. Hydrogen atoms are removed for clarity.

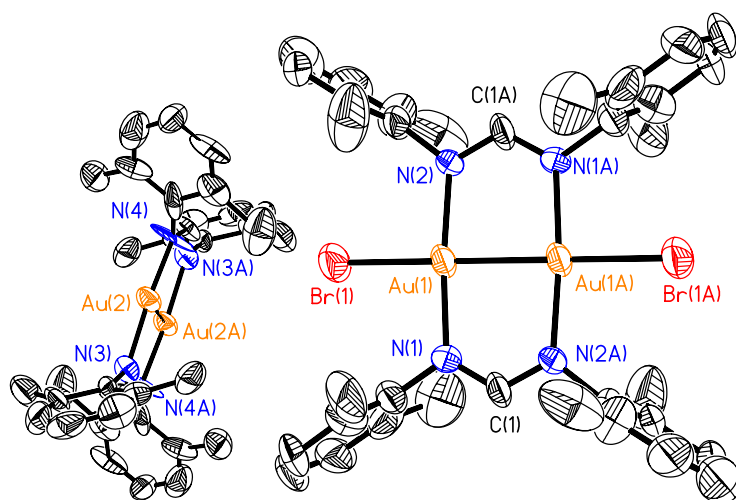


Figure 21. Thermal ellipsoid plot of **24** Ellipsoid is drawn at the 50% probability level. Hydrogen atoms are removed for clarity.

The Au...Au and the Au-Cl distances in **27** changed from 2.52 Å (av.) and 2.35 Å (av.) in the fully oxidized complex $[\text{Au}_2(o\text{-Me}_2\text{-form})_2\text{Cl}_2]$ to 2.55 Å (av.) and 2.34 Å (av.), respectively, in the $[\text{Au}_2(o\text{-Me}_2\text{-form})_2\text{Cl}_2][\text{Au}_2(o\text{-Me}_2\text{-form})_2]$, Table 31.

Table 31. Au(II)-Au(II), Au(I)...Au(I) and Au-Cl bond distances (Å) in $[\text{Au}_2(o\text{-Me}_2\text{-form})_2\text{X}_2][\text{Au}_2(o\text{-Me}_2\text{-form})_2]$, X = Cl, **22**, and $[\text{Au}_2(o\text{-Me}_2\text{-form})_2]$, **XII**.

Oxidizing reagent	Space group	AuII-AuII (Å)	AuI...AuI (Å)	Au-Cl (Å)
Cl ₂ and CH ₂ Cl ₂	<i>P2₁/c</i>	2.5176(7)		2.356(2)
Aqua regia	<i>P2₁/c</i>	2.5242(7)		2.355(3)
PhICl ₂	<i>P2₁/c</i>	2.523(2)		2.363(9)
ClCH ₂ CH ₂ Cl	<i>P2₁/n</i>	2.5671(19)	2.7098(15)	2.321(8)
CCl ₄	<i>P2₁/n</i>	2.5505(14)	2.7137(14)	2.349(6)

Growing crystals of the methyl iodide addition product, **26**, was successful at 0 °C over one week. Although well shaped, brown-black crystals were grown from ether which diffracted well, the spatial volume occupied by CH₃ and I is approximately identical. This leads to a disorder in the positions of the CH₃ and iodide atoms. While the Au(II) atoms and the amidinate ligand atoms refine well, Figure 22,⁴⁵ the CH₃ and I atom positions remain uncertain regarding their exact distances from the Au(II) atoms. The Au-CH₃ and Au-I distances in **26** appear to be 2.12 Å and 2.50 Å respectively, while in the dinuclear gold(I) ylide, $[(\text{CH}_3)\text{Au}(\text{CH}_2\text{PMe}_2\text{CH}_2)_2\text{AuI}]$, Au-CH₃ and Au-I

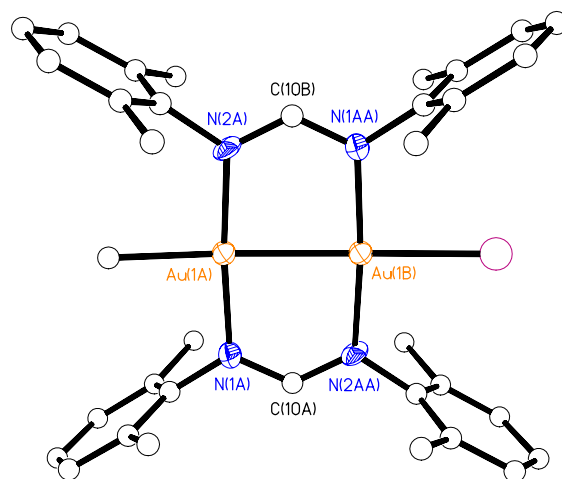


Figure 22. Thermal ellipsoid plot of **26** is drawn at the 50% probability level. Hydrogen atoms are removed for clarity. The structure has a disorder in the positions of the CH₃ and iodide atoms.

distances are 2.13(5) and 2.894(5), respectively.⁶ The Au(II)-Au(II) distance is 2.52 Å, is typical of the Au(II)-Au(II) distances observed in the halogen adducts.⁴⁶

Complex **27** crystallizes in the monoclinic space group $P2_1/c$. The N-Au-N angles associated with the amidinate ligands decreased from $\sim 170^\circ$ in the dinuclear starting material to $\sim 161^\circ$, with the N-C-N angles changing from 128° to 124 - 127° , Figure 23. The bonding to $\text{Hg}(\text{CN})_2$ increases the Au...Au distance from 2.7 Å in the dinuclear to 2.9 Å in the adduct, **27**. Gold centers are coordinated by four nitrogen atoms with Au-N distances in the range 2.09-2.51 Å, Figure 24, (a). The N-Au-N angles are in the range 95 - 100° (angles from the cyanide groups), Figure 24, (b). The C-Hg-C bond angle in $\text{Hg}(\text{CN})_2$ complex is $175.0(2)^\circ$ and is close to linear, 176 - 178 in **27**. The 2D lattice contains two THF solvent molecules in the large cavities (~ 10.2 Å X 13.7 Å), Figure 24, (c). The Hg-O distance is ~ 4.33 Å indicating that the interaction between the Hg and THF is not significant.⁴⁶

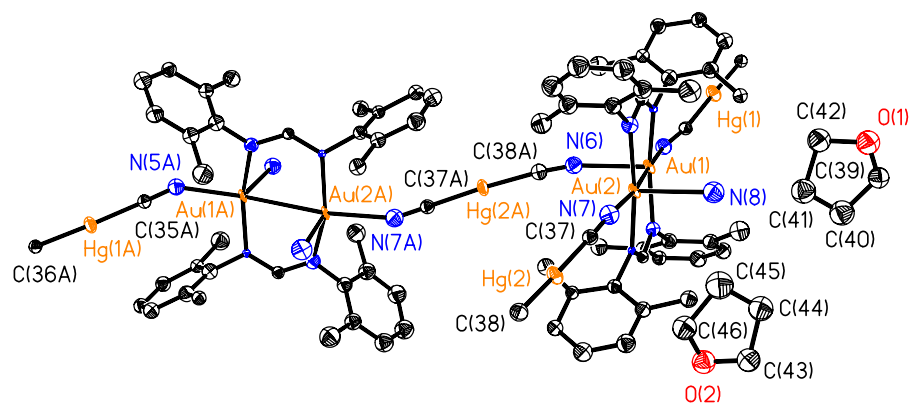


Figure 23. Thermal ellipsoid plot of **27** is drawn at the 50% probability level. Hydrogen atoms are removed for clarity.

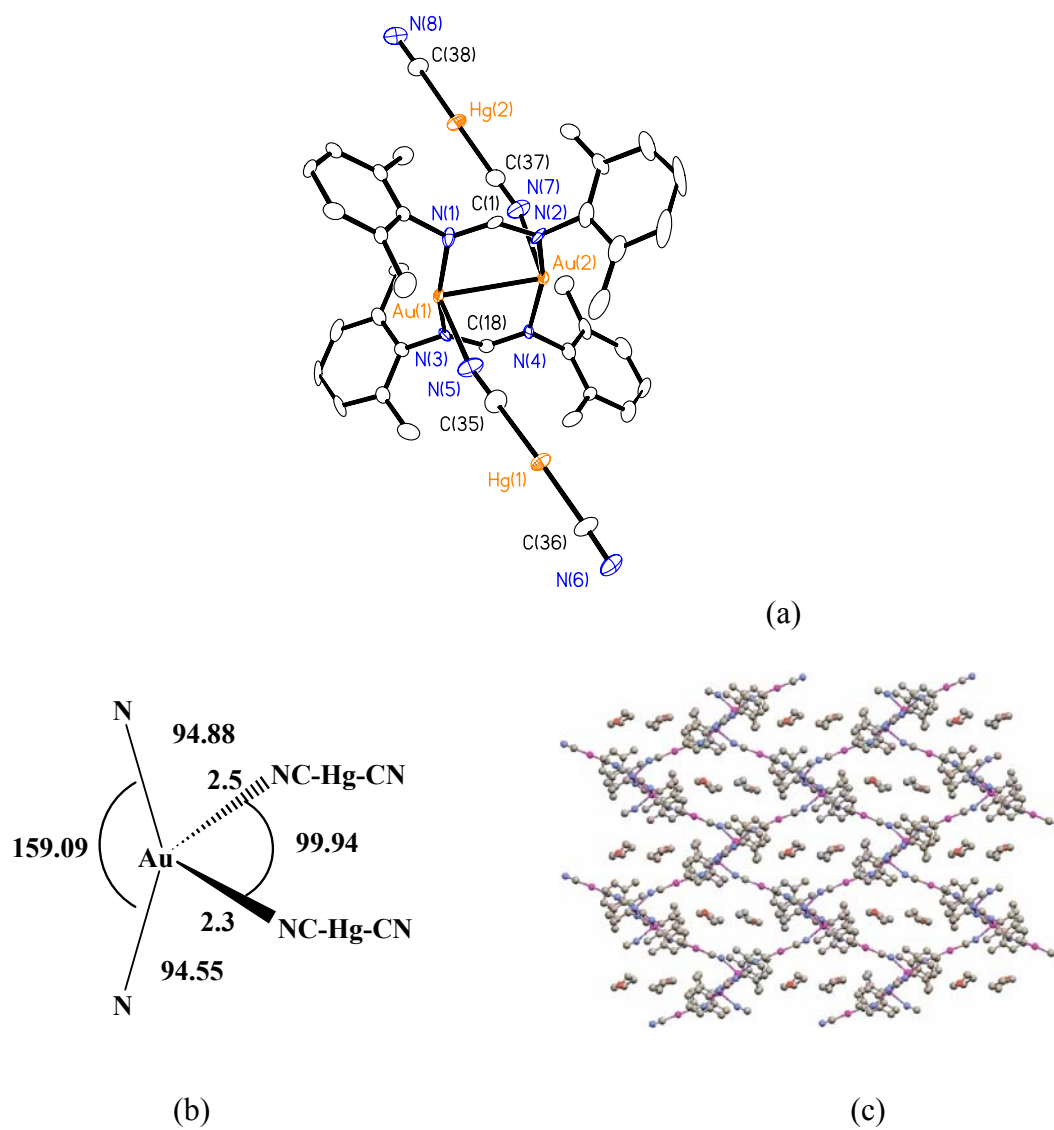


Figure 24. (a) Thermal ellipsoid plot of **27** is drawn at the 50% probability level. Hydrogen atoms are removed for clarity. (b) Coordination environment of gold with the four nitrogen atoms in **27**. (c) Packing diagram of **27** showing the THF solvent in the voids.

The structure of $[\text{Au}_2(o\text{-Me}_2\text{-form})_2(\text{PhCO})_2]$, **28**, figure 25, consists of unidentate benzoate units linked through oxygen to the gold(II) centers, the two benzoate units are trans to each other. The C-O bonds to O atoms coordinated to the Au are longer by 0.02 compared with those to free carbonyl O atoms (1.28 vs. 1.264). The Au-N distances decreased from 2.035(7) Å in the dinuclear complex to 2.01 and 2.008 in the oxidative-addition product. The Au -O distance is 2.045 Å. The Au atoms have nearly square-planar coordination geometries with formation of bonds to a second Au center, two N atoms and one O atom.

The oxidative addition of benzoyl peroxide to the dinuclear gold(I) ylide complexes, $\text{Au}_2(\text{CH}_2\text{Ph}_2\text{CH}_2)_2$ forms gold(II) ylide complexes with the shortest Au...Au distance observed, 2.56-2.58 Å,⁶ in the dinuclear Au(II) ylides complexes, Table 32. Similarly, the Au...Au distance in oxidized product, **28**, 2.48 Å is the shortest Au...Au distance in the Au(II) amidinate complexes. The length of the Au...Au distance in these complexes is may be due to the weak trans- directing ability of the carboxylate ligands compared with the halides.⁴⁹

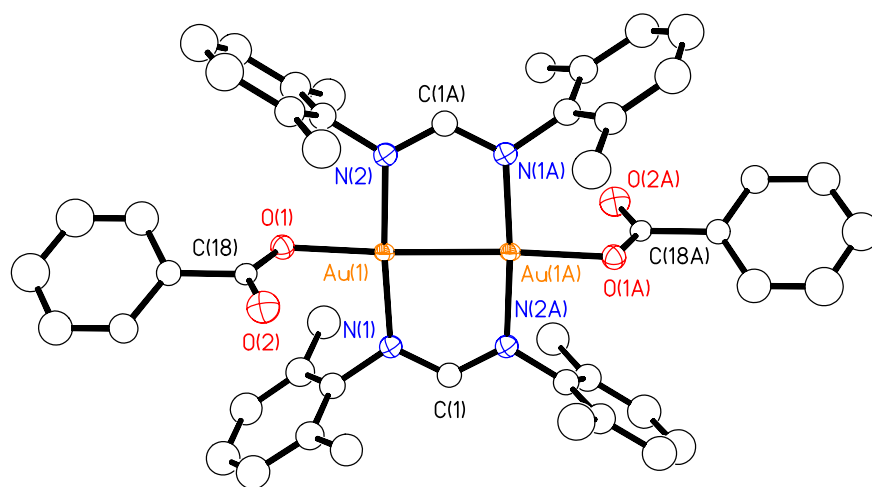


Figure 25. Thermal ellipsoid plot of **28** is drawn at the 50% probability level. Hydrogen atoms are removed for clarity.

Table 32. Dinuclear Au(II) ylide and amidinate complexes characterized by X-ray studies.

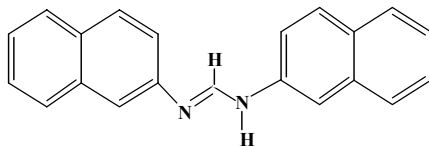
Complex	d(Au ^{II} ...Au ^{II})	d(Au-X)	d(Au-R)	Ref
[ClAu(CH ₂ PPh ₂ CH ₂) ₂ AuCl]	2.600(1)	2.388(8)		6
[BrAu(CH ₂ PPh ₂ CH ₂) ₂ AuBr]	2.614(1)	2.516(1)		6
[IAu(CH ₂ PPh ₂ CH ₂) ₂ AuI]	2.650	2.693(8)		6
[(CH ₃)Au(CH ₂ PPh ₂ CH ₂) ₂ AuI]	2.695(4)			6
[(CH ₃)Au(CH ₂ PMe ₂ CH ₂) ₂ AuI]	2.695(4)	2.894(5)	2.13(5)	6
[PhCO ₂ Au(CH ₂ PPh ₂ CH ₂) ₂ AuO ₂ CPh]	2.561(2)	2.117(13)		6
[ClAu(<i>o</i> -Me ₂ -form) ₂ AuCl], 21	2.517(7)	2.356(2)		this work
[BrAu(<i>o</i> -Me ₂ -form) ₂ AuBr], 22	2.525(15)	2.470(2)		this work
[IAu(<i>o</i> -Me ₂ -form) ₂ Au I], 25	2.579(4)	2.682(4)		this work
[(CH ₃)Au ₂ (<i>o</i> -Me ₂ -form) ₂ AuI], 26	2.529(11)	2.50	2.12	this work
[PhCO ₂ Au(<i>o</i> -Me ₂ form) ₂ AuO ₂ CPh], 28	2.489(10)	2.045(8)		this work

CHAPTER IV
ELECTROCHEMICAL AND PHOTOPHYSICAL STUDIES OF GOLD(I)
AMIDINATE COMPLEXES*

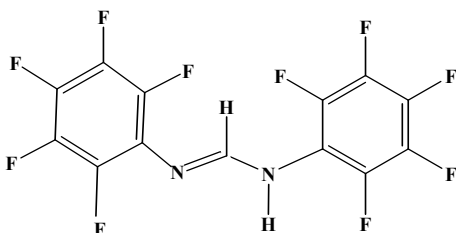
Electrochemical and photophysical studies of gold(I) amidinate complexes suggest that the electronic properties of the ligands play an important role in their chemistry.^{21,22} The tetranuclear gold(I) amidinate clusters $[\text{Au}_4(\text{ArNC}(\text{H})\text{NAr})_4]$, Ar = C_6H_4 -4-OMe, **12**, Ar = C_6H_4 -3-CF₃, **15**, and the previously reported from our group Ar = C_6H_4 -4-Me and Ar = C_6H_4 -3,5-Cl are the first tetranuclear gold(I) cluster species from group 11 elements that show fluorescence at room temperature.^{21, 22} The tetranuclear naphthyl derivative Ar = C_{10}H_7 , **13** is luminescent only at 77 K. Interestingly, and in spite of similar structures to these complexes, the pentafluorophenyl derivative Ar = C_6F_5 , **14**, does not show any photoluminescence in the solid state nor in the solution.¹⁹ The difference in the photophysical behavior is likely to be caused by the different substituents on the electron rich NCN linkage, **IV**, R = 2,3,4,5,6-pentafluoro, **IV**, R = 4-Me, 4-OMe, 3-CF₃, 3,5-Cl and **VII**. Electrochemical oxidation of the tetranuclear gold(I)

*Reproduced in part from *J. Cluster Sci.*, 15, 397-411, **2004**, Abdou, H. E.; Mohamed, A. A.; López-de-Luzuriaga, J. M.; Fackler, Jr., J. P., "Tetranuclear Gold(I) Clusters with Nitrogen Donor Ligands: Luminescence and X-Ray Structure of Gold(I) Naphthyl Amidinate Complex" copyright 2004 and from *J. Cluster Sci.*, 14, 253-266, **2003**, Mohamed, A. A.; Abdou, H. E.; Irwin, M. D.; López-de-Luzuriaga, J. M.; Fackler, J. P., Jr., "Gold(I) Formamidinate Clusters: The Structure, Luminescence, and Electrochemistry of the Tetranuclear, Base-Free $[\text{Au}_4(\text{ArNC}(\text{H})\text{NAr})_4]$ " copyright 2003 with kind permission of Springer Science and Business media.

amidinate complexes shows three reversible waves not seen in gold complexes before.

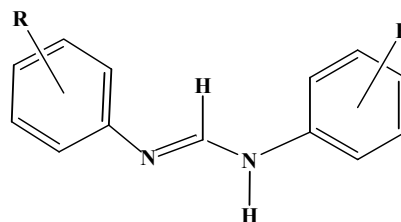


VII



IV

R = 2,3,4,5,6-pentafluoro



IV

R = 4-Me, 4-OMe, 3-CF₃, 3,5-Cl

EXPERIMENTAL

General Procedures

The solvents THF, CH₂Cl₂, were purchased from Aldrich and used as received. Bu₄NPF₆ was purchased from Aldrich. UV-Vis spectra were recorded on a Shimadzu UV-2501 PC spectrometer. Emission and excitation spectra were recorded on a SLM AMINCO, Model 8100 spectrofluorometer equipped with a xenon lamp. Solid-state low-temperature measurements were made using a cryogenic sample holder of local design. Powder samples were attached to the holder with a mixture of copper powder, Cryogen oil (used for mounting crystals for x-ray structures) and collodion (an ether and alcohol soluble transparent nitrocellulose). Liquid nitrogen was used to obtain the 77 K measurements. Cyclic voltammetry experiments were conducted using a Bioanalytical

Systems Inc. electrochemical analyzer, Model 100 under computer control. CV measurements were performed in methylene chloride with 0.1M Bu₄NPF₆ as supporting electrolyte. Fresh solutions containing supporting electrolyte (10 mL) were prepared prior to each CV experiment. Each solution was deoxygenated by purging with nitrogen for 2–5 minutes. Background CV's were acquired before the addition of the gold complexes. A three-electrode system was used, comprised of a platinum (1.6 mm diameter) working electrode, a platinum wire auxiliary electrode, and a silver/silver chloride (Ag/AgCl) reference electrode. The working electrode was wiped prior to each experiment and rinsed. Potentials are reported vs. Ag/AgCl at room temperature and are not corrected for junction potentials. Each CV experiment was repeated a number of times at different scan rates.

RESULTS AND DISCUSSION

Photoluminescence Studies

The absorption spectra of the ligand (Hform), **IV**, R = 4-OMe, show a high-energy (HE) peak centered at 290 nm and a low energy (LE) shoulder at 330 nm in CH₂Cl₂ and CH₃CN.²¹ These two bands in the spectrum of the ligand are red shifted in the cluster [Au₄(ArNC(H)NAr)₄], Ar = C₆H₄-4-Ome, **12**, to 315 nm (ϵ_{\max} =28,000 L/M-cm) and 360 nm (ϵ_{\max} =12,800 L/M-cm) in CH₂Cl₂ (300 and 375 nm in CH₃CN) with a third band in CH₂Cl₂ at 260 nm (ϵ_{\max} =50,000 L/M-cm), Figure 26.²¹ The excitation spectrum is consistent with the low energy absorption spectrum, near 375 nm. The absorption spectra of sodium formamidinate in CH₂Cl₂ and CH₃CN show profiles typical

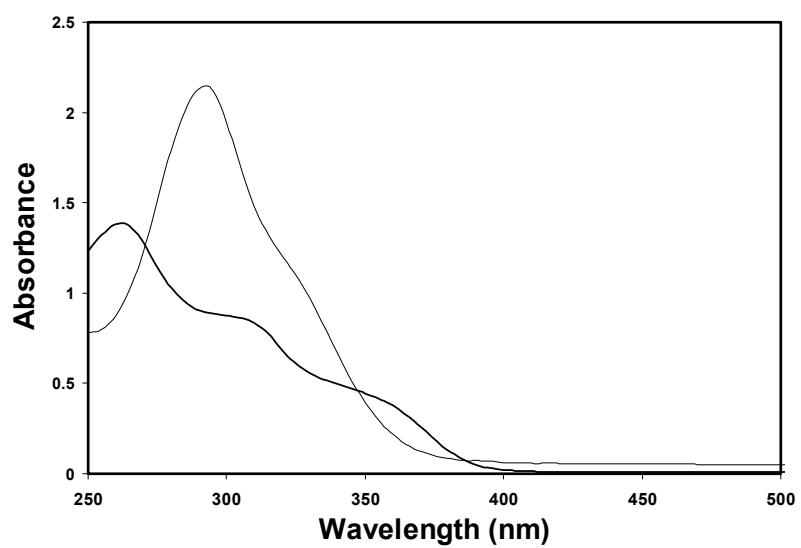


Figure 26. UV-Vis spectra of the ligand (Hform), **IV**, R = 4-OMe and **12**, (1.8×10^{-5} M) in CH₂Cl₂.

of formamidine (Hform) with a slight red shift. The tetranuclear gold(I) complexes, **12**, show a bright blue-green luminescence under UV light, with an emission at ~ 490 nm and a weak emission at ~ 530 nm in the solid state, at room temp and 77 K, Figure 27. Solutions of **12** in CH_2Cl_2 , THF, and acetone are non-emissive at room temperature but emit when frozen.²¹ Evaporation of the solvent forms a film that emits at room temperature. The small Stokes shift and symmetric band profiles between the excitation and emission spectra suggest the high energy emission to be fluorescence. Preliminary lifetime data for **12** at 77 K suggests the presence of two lifetimes, one with a 2.28 ns lifetime and another (a lower energy emission) with a 5 μs lifetime upon excitation at 350 nm. The intensity of the emission at ~ 490 nm is enhanced and sharpened by lowering the temp to 77 K. The low energy emission (shoulder in Fig. 27) may be associated with a triplet excited state. It dominates the emission when a 400 nm excitation is used.²¹ Emission spectra of $[\text{Cu}_2(\text{PhNNPh})_2]^{50}$ and $\text{Ag}_2(\text{form})_2^{51}$ were assigned to a fluorescence using a $\pi-\pi^*$ intraligand/MLCT model based on the vibronic structure that is observed. In silver(I) formamidinate the small Stokes shift between excitation and emission spectra (the separation between the maxima, 2210 cm^{-1}), and the emission life-time (≤ 1 ns) support fluorescence. However, the $[\text{Au}_4\text{Cl}_4(\text{piperidine})_4]$ emits at 700 nm and the rhomboidal $[\text{Au}_4(\text{dithioacetate})_4]$ emits at 743 nm with an emission assigned to a metal-centered 5d-6s transition which is modified by the metal-metal interaction in the Au_4 unit

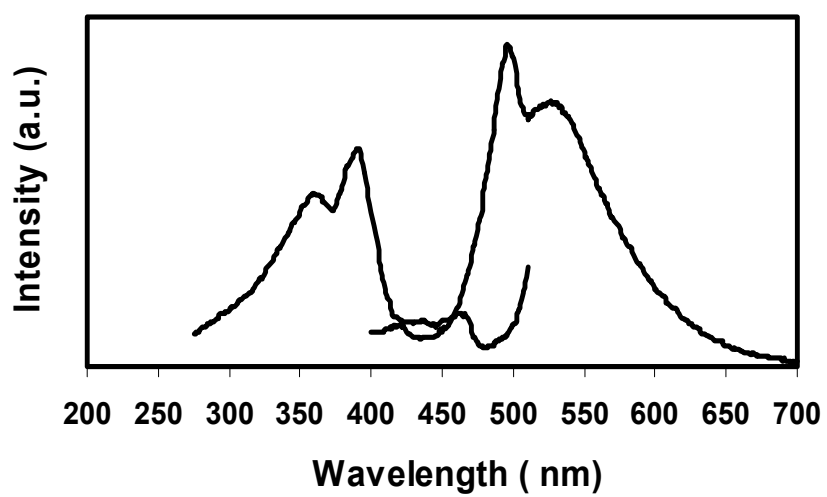


Figure 27. Excitation and emission spectrum of **12**, at 77 K.

The tetranuclear gold(I) amidinate clusters $[\text{Au}_4(\text{ArNC}(\text{H})\text{NAr})_4]$, $\text{Ar} = \text{C}_{10}\text{H}_7$, **13** and the trifluoromethylphenyl amidinate $\text{Ar} = \text{C}_6\text{H}_4\text{-3-CF}_3$, **15** are strongly luminescent at 77 K and, in addition, the trifluoromethyl complex displays also luminescence at room temperature.²² The pentafluorophenyl amidinate derivative $\text{Ar} = \text{C}_6\text{F}_5$, **14**, does not show any photoluminescence in the solid state nor in the solution. For complex **13** (naphthyl amidinate), excitation at 375 nm gives rise to a very broad emission with maximum at 538 nm, Figure 28.²² For complex **15** (trifluoromethyl amidinate), excitation at 365 nm leads to a room temperature emission at 468 nm, which is shifted to 473 nm at 77 K, Figure 29. This asymmetry in the emission bands in complex **13** and **15** suggests a major contribution from the ligands to the emission process. In the case of the trifluoromethylphenyl complex **15**, the energies of the excitation and emission bands are not very different from the other gold amidinates $[\text{Au}_4(\text{ArNC}(\text{H})\text{NAr})_4]$ ($\text{Ar} = \text{C}_6\text{H}_4\text{-4-OMe}$, **12**, and the previously reported by our group, $\text{Ar} = \text{C}_6\text{H}_3\text{-3,5-Cl}_2$ and $\text{Ar} = \text{C}_6\text{H}_4\text{-4-Me}$).²¹ In spite of the relatively small Stokes shift (6000 cm^{-1}) found in **15**, the very long lifetime (within the milliseconds range 0.21 ms, $R = 0:98$), seems to suggest phosphorescence from a triplet state. The structure less profile, even at cryogenic temperatures, for the emission bands does not allow us to establish the atoms or groups involved in the emission process.²²

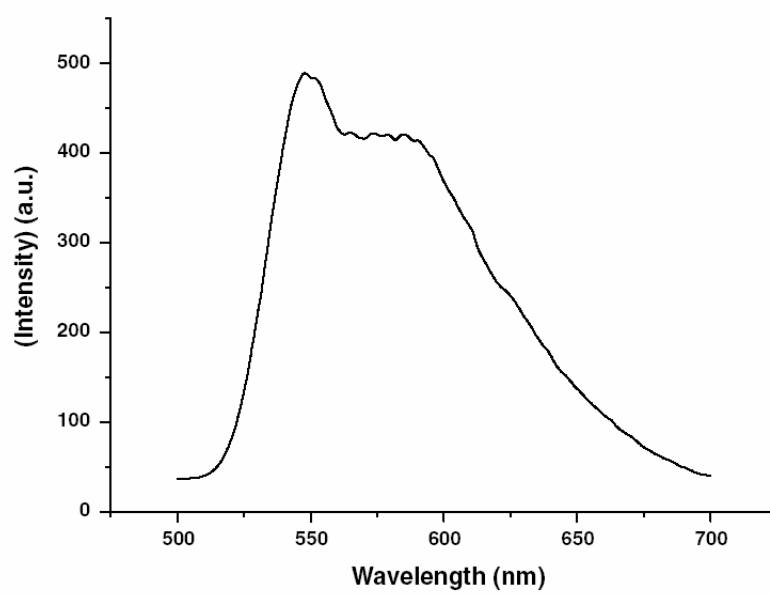


Figure 28. Emission spectrum of **13**, at 77 K.

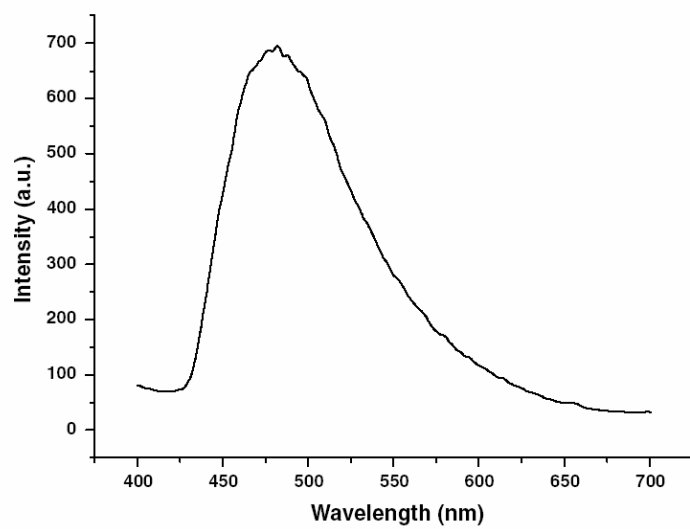


Figure 29. Emission spectrum of **15**, at 77 K.

The different luminescence behavior of the tetranuclear naphthyl amidinate derivative **13**, pentafluorophenyl, **14**, and trifluoromethyl, **15**, with respect to the previously reported amidinates is likely to be related to the substituents on the electron rich NCN linkage.²² The effect of the substituents on the optical behavior is more pronounced in the naphthyl amidinate complex, **13**. In this case the lifetime is longer (1.17 ms, R = 0.99) and the emission band is broader and shifted to lower energy than in the other complexes **12** and **15**. The shift and the spectral width perhaps is related to a higher contribution from the orbitals of the gold centers to the emissive excited state, since gold centered phosphorescence is reported at similar energies.⁵³ Another possibility is that the different electron donor abilities of these groups produce different photoluminescence behavior of the amidinate ligands. This electronic structural change is responsible for the shift in the emission energies from the MLCT excited state in both complexes, and even the absence of luminescence properties in the pentafluorophenyl derivative, a worst case electron donor.²²

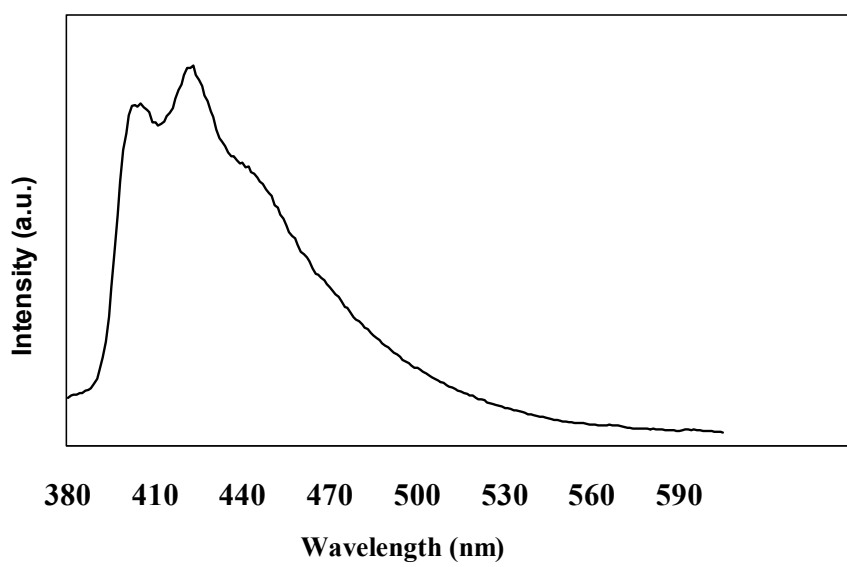


Figure 30. Emission spectrum of **20**, at 77 K.

The dinuclear gold(I) amidinate complex, $[\text{Au}_2(2,6\text{-Me}_2\text{-form})_2]$, **20**, did not show visible emission under UV-Vis light at RT. The formamidine ligand $\text{ArNH}(\text{CH})\text{NAr}$, $\text{Ar} = 2,6\text{-Me}_2\text{-C}_6\text{H}_3$, **VIII** did not emit under UV-Vis light at RT either. Complex **20** shows a high-energy (HE) vibronic emission at 430 nm at 77 K in the solid state but not at ambient temperature, Figure 30. The emission of the tetranuclear gold(I) amidinate clusters is at lower energy, $\sim 490\text{-}530$ nm, compared with the vibronic emission of **20** ~ 430 nm, indicating more contribution from the metal to the system.

Electrochemical Oxidation

The oxidation of the gold(I) amidinate clusters has been studied electrochemically in 0.1M $\text{Bu}_4\text{NPF}_6/\text{CH}_2\text{Cl}_2$ at a Pt working electrode with different scan rates.²¹ The tetranuclear complex $[\text{Au}_4(\text{ArNC}(\text{H})\text{NAr})_4]$, $\text{Ar} = \text{C}_6\text{H}_4\text{-4-OMe}$, **12**, showed three reversible waves at 0.75, 0.95, 1.09 V vs. Ag/AgCl at a scan rate of 500 mV/s. The three waves are reversible, and the current for the third wave is larger than those at the first two waves, Figure 31. Similar results were obtained from the tetranuclear complexes $[\text{Au}_4(\text{ArNC}(\text{H})\text{NAr})_4]$, $\text{Ar} = \text{C}_6\text{H}_4\text{-4-Me}$ and $\text{Ar} = \text{C}_6\text{H}_3\text{-3,5-Cl}$, previously synthesized in our group.²¹ Three reversible waves at 0.87, 1.19, 1.42 V vs. Ag/AgCl at a scan rate of 100 mV/s was also obtained from the tetranuclear complex $[\text{Au}_4(\text{ArNC}(\text{Ph})\text{NAr})_4]$ $\text{Ar} = \text{C}_6\text{H}_5$, **16**, Figure 32. The amidine ligands $\text{ArNH}(\text{CH})\text{NAr}$, $\text{Ar} = \text{C}_6\text{H}_4\text{-4-Me}$, $\text{Ar} = \text{C}_6\text{H}_4\text{-4-OMe}$ and $\text{ArNH}(\text{Ph})\text{NAr}$ showed one irreversible wave at ~ 1.24 V vs. Ag/AgCl at a scan rate of 100 mV/s. The pentafluorophenyl amidinate derivative, $[\text{Au}_4(\text{ArNC}(\text{H})\text{NAr})_4]$, $\text{Ar} = \text{C}_6\text{F}_5$, **14**, did not show any oxidation below 1.8 V.

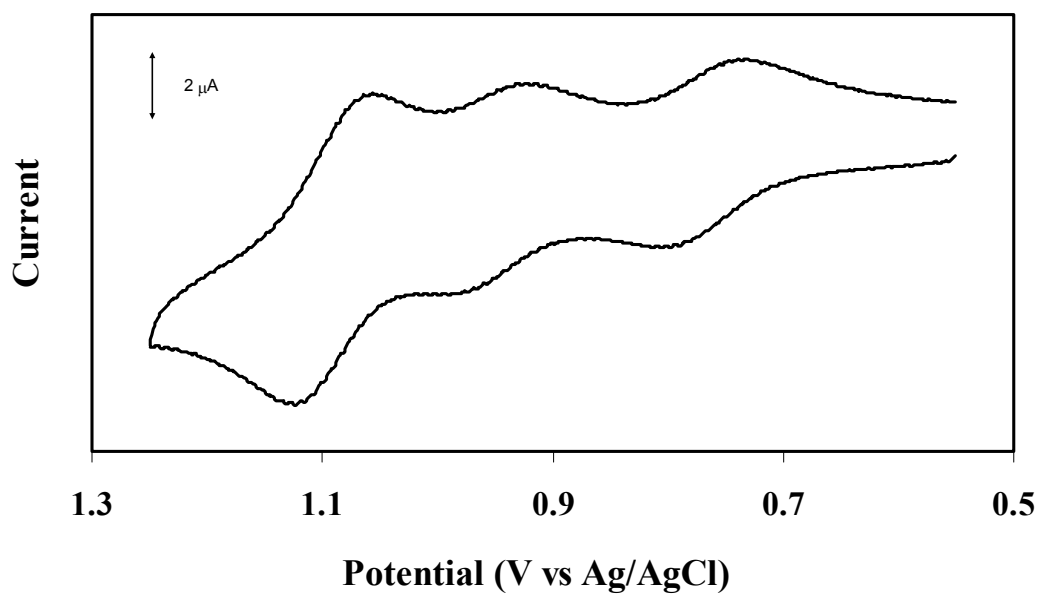


Figure 31. Cyclic voltammogram of **12** in CH_2Cl_2 with 0.1M NBu_4PF_6 electrolyte. The potentials are referenced to the Ag/AgCl electrode.

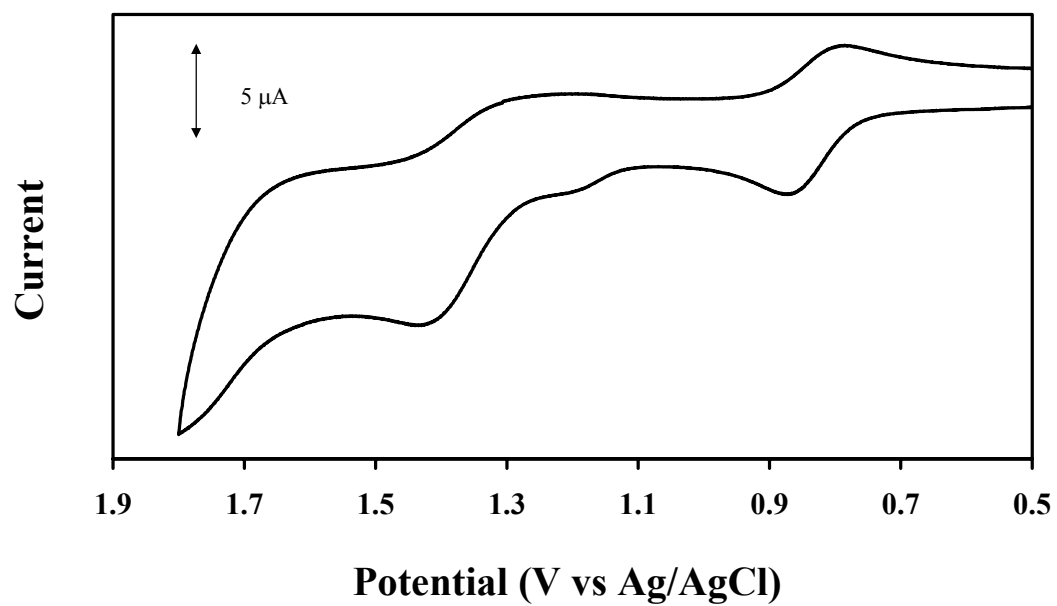


Figure 32. Cyclic voltammogram of **16**, in CH_2Cl_2 with 0.1M NBu_4PF_6 electrolyte. The potentials are referenced to the Ag/AgCl electrode.

The cyclic voltamogram of the dinuclear gold(I) amidinate complex, $[\text{Au}_2(2,6\text{-Me}_2\text{-form})_2]$, **20**, showed a reversible wave at 1.24 V vs. Ag/AgCl at a scan rate of 100 mV/s, Figure 33. The formamidine ligand $\text{ArNH}(\text{CH})\text{NAr}$, $\text{Ar} = 2,6\text{-Me}_2\text{-C}_6\text{H}_3$, showed one irreversible wave at 1.32 V vs. Ag/AgCl with a scan rate of 100 mV/s.

The oxidation of the dinuclear amidinate is much more difficult than the oxidation of the dinuclear gold(I) ylide complex. Gold ylides are oxidized in 0.1 M $\text{Bu}_4\text{NBF}_4/\text{THF}$ at low potentials of +0.11 and +0.23 V vs. Ag/AgCl (quasi-reversible).⁴⁸ The dinuclear amidinate, **20**, oxidizes under the same conditions at +1.24 V vs. Ag/AgCl (reversible). The differences in the chemistry of these dinuclear gold(I) complexes may be understood by examining their respective HOMOs, which, in the ylide, is a metal-metal σ^* anti-bonding, while in the dinuclear gold(I) amidinates the HOMO is metal-ligand δ^* .

Chemical Oxidation

Trials to oxidize the tetranuclear complex $[\text{Au}_4(\text{ArNC}(\text{H})\text{NAr})_4]$, $\text{Ar} = \text{C}_6\text{H}_4\text{-4-OMe}$ and $\text{Ar} = \text{C}_6\text{H}_4\text{-4-Me}$ derivatives using chemical oxidants such as FcPF_6 , aqua regia, TCNQ and $\text{PhI}\cdot\text{Cl}_2$ resulted in the recover of the starting materials. The NOPF_6 oxidant failed also to oxidize the tetranuclear clusters.

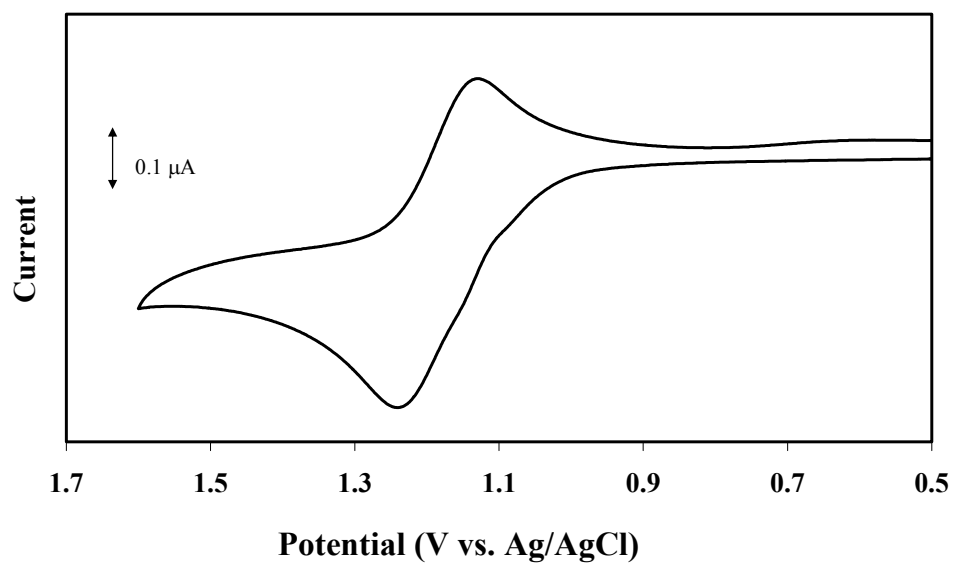


Figure 33. Cyclic voltammogram of **20** in CH_2Cl_2 with 0.1M NBu_4PF_6 electrolyte. The potentials are referenced to the Ag/AgCl electrode.

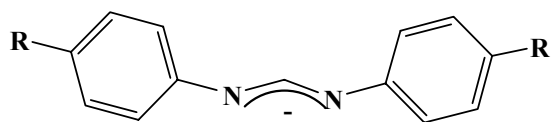
CHAPTER V

**FORMATION OF MIXED LIGAND MIXED METAL TETRANUCLEAR
GOLD(I)-NITROGEN CLUSTERS FROM LIGAND EXCHANGE REACTION
WITH THE DINUCLEAR GOLD(I) AMIDINATE COMPLEX**



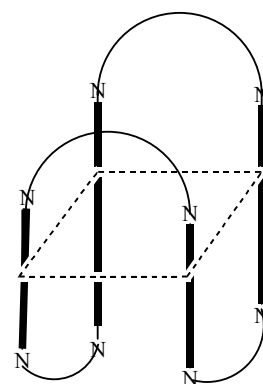
Density Functional Theory calculations show that a dinuclear gold(I) is less stable than a tetranuclear gold(I) amidinate clusters. Chapter II concluded that steric factors has influence the preference for the dinuclear gold(I) amidinate complex $[\text{Au}_2(2,6\text{-Me}_2\text{-form})_2]$, **XII**, over the tetranuclear species $[\text{Au}_4(4\text{-Me-form})_4]$, **XVI**. Chapter V describes a new approach to change the nuclearity of the dinuclear complex, **XII**, it is based on exchanging the sterically bulky ligand 2,6-Me₂-form, **XVII**, with less bulky anionic ligands such as ArNHC(H)NAr, Ar = C₆H₄-4-Me, Ar = C₆H₄-4-OMe, **I** and 3,5-diphenylpyrazolate, **II**. Introducing less bulky anionic ligands to react with the dinuclear complex, **XII**, causes the gold to rearrange and form more stable tetranuclear gold(I) amidinate complex, **30**, and the tetranuclear mixed ligands complexes, **31**, **32**.

The ligand exchange of the sterically bulky ligand, **XVII**, to form mixed ligand species provides a facile procedure for the synthesis of mixed ligand complexes with increased nuclearity. Chapter V describes the utilization of this approach to synthesize tetranuclear mixed Au-Ag complexes of pyrazolate and amidinate ligands, **33**, by reacting the trinuclear silver(I) pyrazolate, $[\text{Ag}(\mu\text{-}3,5\text{-Ph}_2\text{Pz})]_3$, **XVIII**, with the dinuclear complex, **XII**.

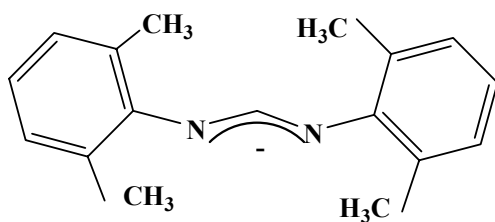


R = Me, OMe

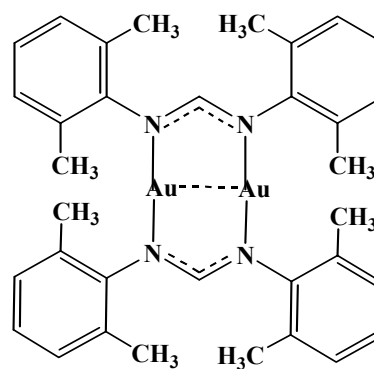
I



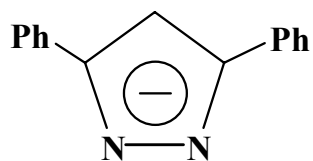
XVI



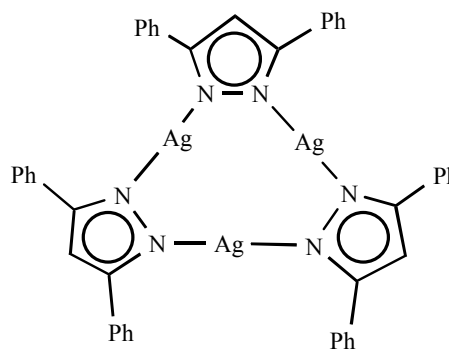
XVII



XII



II



XVIII

EXPERIMENTAL

General Procedures

All glassware was oven-dried prior to use. Triethyl orthoformate (orthoester), *p*-toluidine, 2,6-dimethylaniline, *o*-anisidine (4-methoxyaniline), 3,5-diphenylpyrazolate, KOH and NaOH were purchased from Aldrich. Tetrahydrothiophene was purchased from TCI, Tokyo. The solvents THF, CH₂Cl₂, hexanes, toluene, ethanol and ether were purchased from Aldrich and used as received. The dinuclear gold(I) amidinate complex, [Au₂(2,6-Me₂-form)₂], **XII**, was prepared as explained in chapter II. Trinuclear silver(I) pyrazolate, [Ag(μ -3,5-Ph₂Pz)]₃, **XVIII**, was prepared following a literature procedure.¹³ Elemental analyses were performed by Guelph Chemical laboratories Ltd. & Chemisar Laboratories Inc, Guelph, Ontario, Canada. UV-Vis spectra were recorded on a Shimadzu UV-2501 PC spectrometer. ¹H spectra were recorded on a Unity Plus 300 NMR spectrometer using solvent peaks to reference the chemical shifts (δ). Emission and excitation spectra were recorded on a SLM AMINCO, Model 8100 spectrofluorometer equipped with a xenon lamp. Spectra were corrected for instrumental response. Solid-state low-temperature measurements were made using a cryogenic sample holder of local design. Powder samples were attached to the holder with a mixture of copper paste. Mass spectrometry data (electrospray ionization) were recorded at the Laboratory for Biological Mass Spectrometry at Texas A&M University, using an MDS Series Qstar Pulsar with a spray voltage of 5 keV.

Preparation of $[\text{Au}_2(2,6\text{-Me}_2\text{-form})_2][\text{Au}_4(4\text{-Me-form})_4]$, 29. N,N' -di(4-Me)phenylformamidine (56 mg, 0.25 mmol) was stirred with (14 mg, 0.25 mmol) of KOH in THF for 24 hr. Gradually, the colorless solution turned yellow. $[\text{Au}_2(2,6\text{-Me}_2\text{-form})_2]$ (220 mg, 0.25 mmol) was added and stirring continued for an additional 12 hr. The solvent was removed under vacuum and the crude product dissolved in CH_2Cl_2 , placed in a separatory funnel and layered with ethanol-water mixture to extract the salt of the exchanged ligand. The CH_2Cl_2 layer was separated, dried under vacuum and recrystallized from THF/hexanes and left overnight at room temperature for slow evaporation to form colorless crystals of **29**·2THF. ^1H NMR (CDCl_3 , ppm): 8.25 (s, 4H (CH, amidinate tetranuclear)), 2.23 (s, 24H (CH_3 , tetranuclear)), 7.43 (s, 2H (CH, amidinate dinuclear)), 2.47 (s, 24H (CH_3 , dinuclear)).

Preparation of $[\text{Au}_4(4\text{-Me-form})_4]$, 30. N,N' -di(4-Me)phenylformamidine (226 mg, 1 mmol) was stirred with (56 mg, 1 mmol) of KOH in THF for 24 hr. The colorless solution turned yellow. $[\text{Au}_2(2,6\text{-Me}_2\text{-form})_2]$ (450 mg, 0.5 mmol) was added and stirring continued for additional 24 hr. The solvent was removed under vacuum and the crude product dissolved in CH_2Cl_2 , placed in a separatory funnel and layered with ethanol-water mixture to extract the salt of the exchanged ligand. The CH_2Cl_2 layer was separated, dried under vacuum and recrystallized from THF/hexanes and left overnight at room temperature for slow evaporation to form colorless crystals of **30**. ^1H NMR (CDCl_3 , ppm): 8.25 (s, 4H (CH amidinate)), 2.23 (s, 24H (CH_3))

Preparation of $[\text{Au}_4(3,5\text{-Ph}_2\text{pz})_2(2,6\text{-Me}_2\text{-form})_2]$, 31. 3,5-diphenylpyrazolate 110 mg (0.5 mmol) was stirred with 20 mg (0.5 mmol) of NaOH in THF for 24 hr.

[Au₂(2,6-Me₂-form)₂] 450 mg (0.5 mmol) was added and stirring continued for additional 12 hr. The solvent was removed under vacuum and the crude product dissolved in CH₂Cl₂, placed in a separatory funnel and layered with ethanol-water mixture to extract the salt of the exchanged ligand. The CH₂Cl₂ layer was separated, dried under vacuum and recrystallized from THF/hexanes and left overnight at room temperature for slow evaporation to form colorless crystals. Two different crystals were formed as blocks, **31·2THF** and needles, **32·THF**. Complex **31·2THF**, ¹H NMR (CDCl₃, ppm): 8.11 (br, 8H (Ph rings pyrazolate)), 7.84 (t, 8H (Ph ring pyrazolate)), 6.69 (s, 2H (CH pyrazolate)), 7.45 (br, 2H (CH amidinate)), 2.50 (s, 24H (CH₃ amidinate)).

Preparation of [Au₄(3,5-Ph₂pz)₃(2,6-Me₂-form)], 32. 3,5-diphenylpyrazolate (80 mg, 0.38 mmol) was stirred with 22 mg (0.38 mmol) of NaOH in THF for 24 hr. [Au₂(2,6-Me₂-form)₂] 220 mg (0.25 mmol) was added and stirring continued for additional 12 hr. The solvent was removed under vacuum and the crude product dissolved in CH₂Cl₂, placed in a separatory funnel and layered with ethanol-water mixture to extract the salt of the exchanged ligand. The CH₂Cl₂ layer was separated, dried under vacuum and recrystallized from THF/hexanes and left overnight at room temperature for slow evaporation to form colorless crystals of **32·THF**. ¹H NMR (CDCl₃, ppm): 8.12- 8.15 (d, 12H (ph ring pyrazolate)), 7.82- 7.87 (t, 12H (ph ring pyrazolate)), 6.75 (s, 3H (CH pyrazolate)), 7.47 (s, 1H (CH amidinate)), 2.50 (s, 12H (CH₃ amidinate)).

Preparation of [Au₂(3,5-Ph₂pz)₂ Ag₂ (2,6-Me₂-form)₂], 33. [Ag(μ-3,5-Ph₂Pz)]₃ 246 mg (0.25 mmol) was stirred with [Au₂(2,6-Me₂-form)₂] 112 mg (0.12 mmol) in THF

for 24 h, in the dark. The reaction mixture was filtered and the filtrate left overnight in the refrigerator to form colorless crystals of **33**·2THF. ¹H NMR (CDCl₃, ppm): 7.65 (br, 8H (Ph rings pyrazolate)), 7.00 (s, 2H (CH pyrazolate)), 7.52 (br, 2H (CH amidinate)), 2.59 (s, 24H (CH₃ amidinate)).

CRYSTALLOGRAPHIC STUDIES

Cell parameters and refinement results of gold(I) amidinate complexes **29**, **31**, **32**, and **33** are summarized in Tables 33 and 34. Tables 35-38 show the important interatomic distances and angles. X-ray data were collected using a Siemens (Bruker) SMART CCD (charge coupled device) based diffractometer equipped with a LT-2 low temperature apparatus operating at 110 K. A suitable crystal was chosen and mounted on a glass fiber using cryogenic grease. Data were measured using omega scans of 0.3° per frame for 60 s, such that a hemisphere was collected. The first 50 frames were recollected at the end of data collection as a monitor for decay. No decay was detected. Cell parameters were retrieved using SMART software and refined using SAINT on all observed reflections.²⁸ Data reductions were performed using SAINT software.²⁹ The structures were solved by direct methods using SHELXS-97 and refined by least squares on F², with SHELXL-97 incorporated in SHELXTL-PC V 5.03.^{30, 31} The structures were determined in the space groups reported in Tables 33 and 34 by analysis of systematic absences. Hydrogen atom positions were calculated by geometrical methods and refined as a riding model.

Table 33. Crystal Data and Structure Refinement for [Au₂(2,6-Me₂-form)₂][Au₄(4-Me-form)₄] \cdot 2THF, **29** \cdot 2THF, and [Au₂(3,5-Ph₂pz)₂ Ag₂ (2,6-Me₂-form)₂] \cdot 2THF, **33** \cdot 2THF.

compound	29 \cdot 2THF	33 \cdot 2THF
empirical formula	C ₈₅ H ₉₅ Au ₅ N ₁₀ O ₂	C ₇₄ H ₈₀ Au ₂ Ag ₂ N ₈ O ₂
fw	2273.53	1833.6
crystal system	triclinic	Monoclinic
space group	<i>P</i> $\bar{1}$	<i>P</i> 2 ₁ / <i>c</i>
<i>A</i> (Å)	10.794(11)	14.0038(10)
<i>B</i> (Å)	14.392(15)	51.586(4)
<i>C</i> (Å)	25.75(3)	17.7422(12)
α	82.564(17)	90.00
<i>B</i> (°)	85.443(18)	92.00(10)
γ	82.614(19)	90.00
<i>V</i> (Å ³)	3926(7)	12799(15)
<i>Z</i>	2	6
<i>d</i> _{calc} (g/cm ⁻³)	1.922	1.472
<i>M</i> (mm ⁻¹)	9.363	2.012
<i>T</i> (K)	110(2)	110(2)
R1 ^a , wR2 ^b	0.0924, 0.1595	0.0955, 0.2728
Goodness-of-fit ^c	0.985	1.019

$$^a R1 = \frac{\sum \|F_o\| - |F_c|}{\sum |F_o|}$$

$$^b wR2 = \left[\frac{\sum [w(F_o^2 - F_c^2)^2]}{\sum [w(F_o^2)^2]} \right]^{1/2}; w = 1/[\sigma^2(F_o^2) + (aP)^2 + (bP)], \text{ where } P = [\max(F_o^2 \text{ or } 0) + 2(F_c^2)]/3$$

$$^c \text{Goodness-of-fit} = \left[\frac{\sum [w(F_o^2 - F_c^2)^2]}{(N_{\text{obs}} - N_{\text{param}})} \right]^{1/2}, \text{ based on all data}$$

Table 34. Crystal Data and Structure Refinement for $[\text{Au}_4(3,5\text{-Ph}_2\text{pz})_2(2,6\text{-Me}_2\text{-form})_2]\cdot 2\text{THF}$, **31** $\cdot 2\text{THF}$, and $[\text{Au}_4(3,5\text{-Ph}_2\text{pz})_3(2,6\text{-Me}_2\text{-form})]\cdot \text{THF}$, **32** $\cdot \text{THF}$.

compound	31 $\cdot 2\text{THF}$	32 $\cdot \text{THF}$
empirical formula	$\text{C}_{70}\text{H}_{60}\text{Au}_4\text{N}_8\text{O}$	$\text{C}_{66}\text{H}_{60}\text{Au}_4\text{N}_8\text{O}$
fw	1825.14	1769.10
crystal system	monoclinic	monoclinic
space group	$P2_1/c$	$P2_1/c$
A (Å)	11.5747(19)	23.058(5)
B (Å)	25.497(4)	14.314(3)
C (Å)	21.221(3)	18.528(4)
α	90.00	90.00
B (°)	96.979(3)	90.94(3)
γ	90.00	90.00
V (Å ³)	6216.3(18)	6114(2)
Z	4	4
d_{calc} (g/cm ⁻³)	1.950	1.922
M (mm ⁻¹)	9.462	9.616
T (K)	110(2)	110(2)
$R1^a$, $wR2^b$	0.0566, 0.1227	0.0589, 0.1374
Goodness-of-fit ^c	0.770	1.178

$$^a R1 = \frac{\sum ||F_o| - |F_c||}{\sum |F_o|}$$

$$^b wR2 = \frac{[\sum [w(F_o^2 - F_c^2)^2] / \sum [w(F_o^2)]]^{1/2}}{[\max(F_o^2 \text{ or } 0) + 2(F_c^2)]/3}$$

$$^c \text{Goodness-of-fit} = \frac{[\sum [w(F_o^2 - F_c^2)^2] / (N_{\text{obs}} - N_{\text{param}})]^{1/2}}{}$$

Table 35. Selected Bond Distances (Å) and Angles (°) for [Au₂(2,6-Me₂-form)₂][Au₄(4-Me-form)₄]·2THF, **29**·2THF.

Au1...Au2	3.057(2)	Au3–N4	2.007(13)
Au1...Au2	2.926(3)	Au4–N7	2.015(13)
Au3...Au4	3.007(2)	C2–C3	1.34(2)
Au1...Au4	3.006(3)	Au4–N6	2.047(14)
Au5...Au5A	2.701(2)	Au5–N10	2.015(14)
Au1–N1	2.044(13)	Au5–N9	2.031(14)
Au2–N2	2.025(13)	C1–N1	1.309(19)
Au2–N3	2.033(13)	C1–N2	1.381(19)
Au3–N5	2.000(14)		
Au1...Au2...Au3	63.47(4)	C3–C2–N1	120.6(15)
Au4...Au1...Au2	114.30(5)	C7–C2–N1	119.9(15)
N9–Au5–N10	169.0(5)	C2–C3–C4	122.3(18)
Au2...Au3...Au4	118.27(4)	C3–C4–C5	119.7(18)
N7...Au4... Au3	104.3(4)	C6–C5–C8	123.4(17)
N6...Au4...Au3	79.8(4)	C4–C5–C8	119.3(17)
N10–Au5–N9	169.0(5)	C5–C6–C7	124.0(18)
N1–C1–N2	125.8(14)	C2–C7–C6	117.4(17)

Table 36. Selected Bond Distances (Å) and Angles (°) for [Au₄(3,5-Ph₂pz)₂(2,6-Me₂-form)₂] \cdot 2THF, **31** \cdot 2THF.

Au1–N1	2.044(13)	Au3–N4	2.022(15)
Au1–N5	2.047(11)	Au3...Au4	3.1153(9)
Au1...Au2	3.1149(9)	Au4–N8	2.017(15)
Au1...Au4	3.1482(9)	Au4–N6	2.021(12)
Au2–N3	1.995(14)	N1–C1	1.28(2)
Au2–N2	2.039(13)	N2–C1	1.32(2)
Au2...Au3	3.1020(9)	N5–N6	1.370(16)
Au3–N7	1.979(15)	N7–N8	1.369(19)
N1–Au1–N5	172.2(5)	Au3...Au2...Au1	94.93(2)
N1...Au1...Au2	78.1(4)	N7–Au3–N4	174.0(6)
N5...Au1...Au2	108.9(3)	N7...Au3...Au2	107.0(4)
N1...Au1...Au4	114.5(4)	N4...Au3...Au2	78.7(4)
N5...Au1...Au4	64.1(3)	N7...Au3...Au4	63.1(4)
Au2...Au1...Au4	84.62(2)	N4...Au3...Au4	116.1(5)
N3–Au2–N2	165.9(6)	Au2...Au3...Au4	85.39(2)
N3...Au2...Au3	78.9(4)	N8–Au4–N6	174.2(5)
N2...Au2...Au3	111.5(4)	N8...Au4...Au3	65.0(4)
N3...Au2...Au1	111.3(4)	N6...Au4...Au3	109.3(3)
N2...Au2...Au1	78.2(4)	Au3 Au4 Au1	94.00(2)

Table 37. Selected Bond Distances (Å) and Angles (°) for [Au₄(3,5-Ph₂pz)₃(2,6-Me₂-form)]·THF, **32**·THF.

Au1–N1	2.023(11)	Au3–N5	2.006(13)
Au1–N8	2.029(10)	Au3...Au4	3.1870(10)
Au1...Au4	3.0277(9)	Au4–N7	2.008(11)
Au1...Au2	3.2075(10)	Au4–N6	2.014(11)
Au2–N2	2.006(14)	N1–N2	1.362(18)
Au2–N3	2.018(13)	N3–N4	1.404(16)
Au2...Au3	3.0541(9)	N5–N6	1.361(17)
Au3–N4	2.004(13)		
N1–Au1–N8	174.6(5)	N4...Au3...Au4	117.0(3)
N1...Au1...Au4	105.8(3)	N5...Au3...Au4	62.7(4)
N8...Au1...Au4	79.2(3)	Au2...Au3...Au4	93.05(3)
N1...Au1...Au2	62.6(4)	N7–Au4–N6	171.8(5)
N8...Au1...Au2	115.9(3)	N7...Au4...Au1	80.7(3)
Au4...Au1...Au2	93.14(3)	N6...Au4...Au1	105.2(3)
N2–Au2–N3	176.3(5)	N7...Au4...Au3	112.8(3)
N2...Au2...Au3	111.2(4)	N6...Au4...Au3	62.6(4)
N3...Au2...Au3	65.8(3)	Au1...Au4...Au3	86.94(3)
N2...Au2...Au1	62.8(4)	N2–N1–Au1	116.8(9)
N3...Au2...Au1	114.2(3)	N1–N2–Au2	117.4(9)
Au3...Au2...Au1	86.13(3)	N4–N3–Au2	112.6(9)

Table 37 Continued

N4–Au3–N5	174.5(5)	N3–N4–Au3	114.7(9)
N4...Au3...Au2	65.3(3)	N6–N5–Au3	116.3(9)
N5...Au3...Au2	109.3(4)		

Table 38. Selected Bond Distances (Å) and Angles (°) for [Au₂(3,5-Ph₂pz)₂ Ag₂ (2,6-Me₂-form)₂] \cdot 2THF, **33** \cdot 2THF.

Au1–N1	2.017(12)	C1–N2	1.300(19)
Au1–N8	2.025(13)	C1–N1	1.31(2)
Au1...Ag1	2.9543(11)	C18–C26	1.38(2)
Au1...Ag2	3.3349(12)	C18–C19	1.39(2)
Ag1–N2	2.063(14)	C19–N3	1.33(2)
Ag1–N3	2.089(12)	C26–N4	1.353(18)
Ag1...Au2	3.3173(12)	C33–N6	1.29(2)
Au2–N5	1.992(14)	C33–N5	1.35(2)
Au2–N4	2.016(13)	C50–C51	1.42(3)
Au2...Ag2	2.9037(11)	C51–N7	1.39(2)
Ag2–N6	2.053(13)	N3–N4	1.355(18)
Ag2–N7	2.057(13)	N7–N8	1.349(18)
N1–Au1–N8	176.4(5)	N5...Au2...Ag1	118.4(4)
N1...Au1...Ag1	82.1(4)	N4...Au2...Ag1	62.4(4)

Table 38

Continued

N8...Au1...Ag1	96.3(4)	Ag2...Au2...Ag1	73.63(3)
N1...Au1...Ag2	121.4(4)	N6–Ag2–N7	172.8(6)
N8...Au1...Ag2	60.8(4)	N6...Ag2...Au2	79.9(4)
Ag1...Au1...Ag2	72.75(3)	N7...Ag2...Au2	104.9(4)
N2–Ag1–N3	171.8(5)	N6...Ag2...Au1	123.5(4)
N2...Ag1...Au1	79.7(4)	N7...Ag2...Au1	60.8(4)
N3...Ag1...Au1	104.8(4)	Au2...Ag2...Au1	107.00(3)
N2...Ag1...Au2	125.4(4)	N2–C1–N1	125.8(15)
N3...Ag1...Au2	60.5(4)	N7–C51–C50	104.4(15)
Au1...Ag1...Au2	106.25(3)	N6–C33–N5	125.3(15)
N5–Au2–N4	177.8(6)	N4–C26–C18	110.7(13)
N5...Au2...Ag2	84.1(4)	N3–C19–C18	109.6(14)
N4...Au2...Ag2	94.3(4)	C26–C18–C19	103.6(13)

RESULTS AND DISCUSSION

Synthesis

Reacting the potassium salt of the amidinate, K[4-Me-form], **I**, with the dinuclear gold(I) complex, $[\text{Au}_2(2,6\text{-Me}_2\text{-form})_2]$, **XII**, in a 1:1 stoichiometry ratio in THF forms the dinuclear-tetranuclear complex $[\text{Au}_2(2,6\text{-Me}_2\text{-form})_2][\text{Au}_4(4\text{-Me-form})_4]\cdot 2\text{THF}$, **29**, with one tetranuclear and one dinuclear molecules in the same unit cell. The potassium salt of the exchanged bulky ligand, K[(2,6-Me₂-form)], **XVII**, formed as a byproduct. ¹H NMR spectra of the crude product showed the spectra, a combination of the independent dinuclear and the tetranuclear complex, (CDCl₃, methine: 8.26 ppm, tetranuclear; 7.43 ppm, dinuclear), in addition to the exchanged bulky ligand, **XVII**, methine peak at 7.38 ppm. Adding more K[4-Me-form] to the NMR tube exchanged the remaining of the bulky ligand, **XVII**, in the dinuclear complex in **29** and produced the tetranuclear complex, $[\text{Au}_4(4\text{-Me-form})_4]$, **30**, Figure 34. The dinuclear methine peak at 7.44 ppm disappeared completely and the intensity of the tetranuclear product methine peak increased. Adjusting the reaction ratio to 1:2 of the amidinate potassium salt, K[4-Me-form], **I**, formed the tetranuclear complex, **30**, only. The exchange reaction was studied by ¹H NMR. After 10 min of mixing a new resonance at 8.62 was formed. Its intensity started to decrease after ~ 4h until it disappeared completely after 24h while the intensity of the tetranuclear product, **30**, at 8.26 ppm increased, Figure 35. Similar results were also obtained from the reaction of the amidinate potassium salt, K[4-OMe-form], **I**, with the dinuclear complex, **XII**.

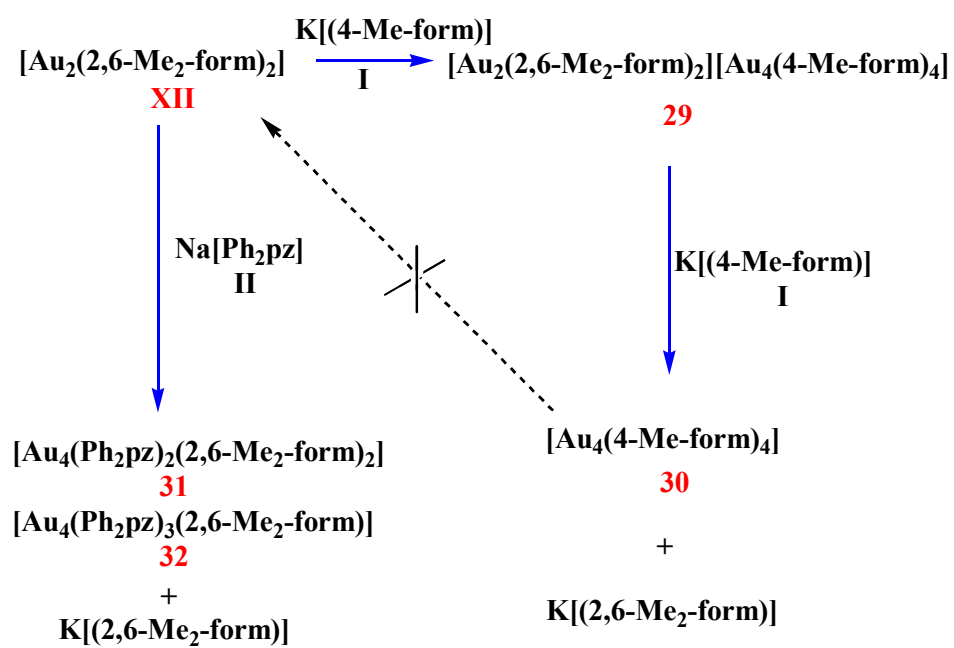


Figure 34. Schematic representation of the exchange reactions between XII, I and II.

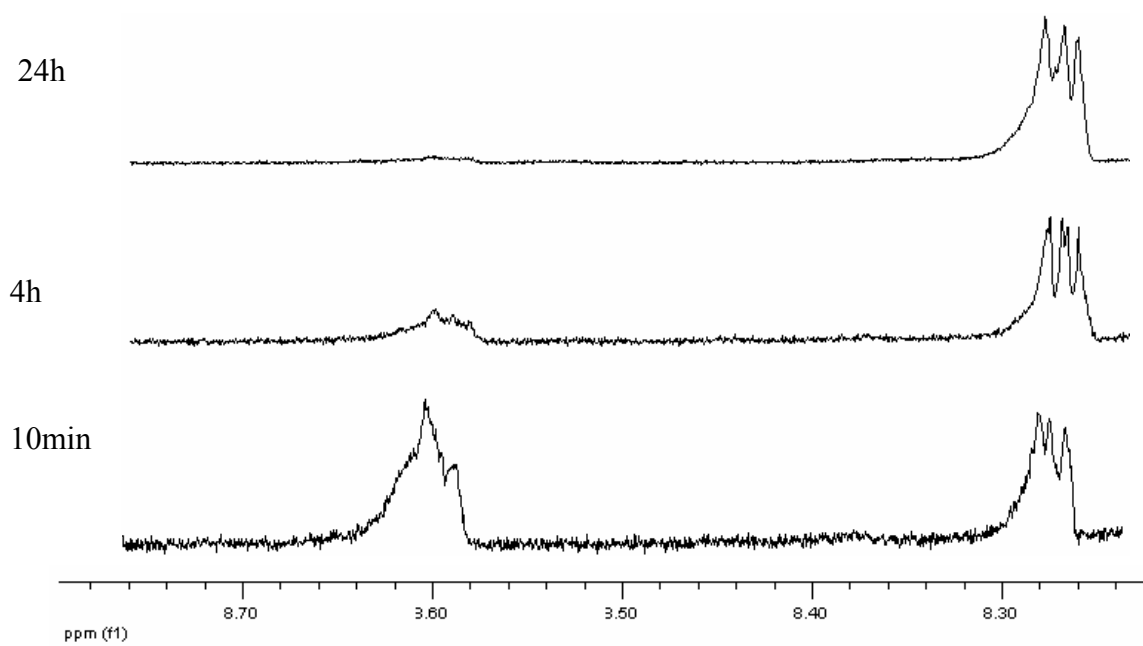


Figure 35. ^1H NMR spectra of **30** in CDCl_3 at 25°C .

The tetranuclear amidinate complex $[\text{Au}_4(4\text{-OMe-form})_4]$, formed after 10 min of mixing as indicated by its ^1H NMR methine peak at 8.20 ppm. A resonance at 8.49 ppm formed during the reaction time and disappeared completely when the exchange reaction was completed.

The new resonances formed during the exchange reactions of the dinuclear amidinate complex, **XII**, with the amidinate potassium salts $\text{K}[4\text{-OMe-form}]$ at 8.62 ppm and $\text{K}[4\text{-Me-form}]$ at 8.49 ppm could be related to an intermediate formed after mixing. Similar peaks were obtained during the synthesis of the tetranuclear $[\text{Au}_4(4\text{-Me-form})_4]$ and $[\text{Au}_4(4\text{-OMe-form})_4]$ by reacting their potassium amidinate salts with $\text{Au}(\text{THT})\text{Cl}$.^{21,22}

Mass spectra (ESI^+) of the tetranuclear complex $[\text{Au}_4(4\text{-OMe-form})_4]$, **XV**, in CH_3CN showed peaks from $[\text{Au}_2\text{L}_2]^+$ ($m/z = 904$), $[[\text{Au}_2\text{L}_2] - \text{OMe}]^+$ ($m/z = 879$) and $[[\text{Au}_2\text{L}_2]\text{CH}_3\text{CN}]^+$ ($m/z = 950$) in addition to $[[\text{Au}_3\text{L}_2] - \text{OMe}]^+$ ($m/z = 1064$). The mass spectra for the dinuclear complex $[\text{Au}_2(2,6\text{-Me}_2\text{-form})_2]$ and the tetranuclear complex, $[\text{Au}_4(4\text{-Me-form})_4]$, **30** produced two similar peaks, although in low intensity, at $m/z = 701$ and 676 , respectively, which could be related to a structure similar to $[\text{AuL}_2]^+$ with $\text{fw} = 701$, $\text{L} = (2,6\text{-Me}_2\text{-form})$ and $\text{fw} = 680$, $\text{L} = (4\text{-Me-form})$.

The reaction of the diphenylpyrazolate salt, $\text{Na}[3,5\text{-Ph}_2\text{pz}]$, **II**, with the dinuclear gold(I) complex $[\text{Au}_2(2,6\text{-Me}_2\text{-form})_2]$, **XII**, in a 1:1 stoichiometric ratio resulted in the formation of two tetranuclear products, blocks, $[\text{Au}_4(\text{Ph}_2\text{pz})_2(2,6\text{-Me}_2\text{-form})_2] \cdot 2\text{TTHF}$, **31**, and needles, $[\text{Au}_4(\text{Ph}_2\text{pz})_3(2,6\text{-Me}_2\text{-form})] \cdot \text{TTHF}$, **32**, Figure 33. The product, **31**, is mixed ligands with each pyrazolate ring facing amidinate. Adjusting the reaction ratio to

1:1.5 of the diphenylpyrazolate anion salt resulted in the isolation of the tetranuclear mixed ligands complex **32** only. The reaction was followed by ^1H NMR. A new resonance at 7.56 ppm formed during the exchange reaction and disappeared completely when the reaction was completed.

The potassium salt of the exchanged bulky ligand $\text{K}[(2,6\text{-Me}_2\text{-form})]$, **XVII**, was extracted using separatory funnel. The crude product was dissolved in CH_2Cl_2 , and the solution was layered with ethanol/water mixture. The CH_2Cl_2 layer was separated, dried under vacuum and recrystallized from THF/hexanes, and left over night at room temperature for slow evaporation to form crystals. The ^1H NMR spectra of the product after extraction showed the disappearance of the exchanged salt, **XVII**, peak at 7.38 ppm. The yield of the tetranuclear mixed ligands complexes **31**, **32** and **33** is small ~14%.

The exchange reaction of the bulky amidinate anionic ligand, 2,6-Me₂-form, **XVII**, by the less steric anionic ligand **I** and **II** is irreversible, Figure 34. These results indicate that the gold centers prefer a tetranuclear over the dinuclear arrangement. The influence of the steric effect give preference to the formation of the dinuclear gold (I) amidinate complex, $[\text{Au}_2(2,6\text{-Me}_2\text{-form})_2]$, **XII** over the tetranuclear species, **XVI**. Density Functional Theory calculations show that a dinuclear gold(I) is less stable than a tetranuclear gold(I) amidinate clusters. The tetramer is much more stable than the dimer at both Gaussian 98 and ADF levels. Replacing C by Si in the Backbone reduces strain and makes the energies similar, Figure 36.⁵⁴

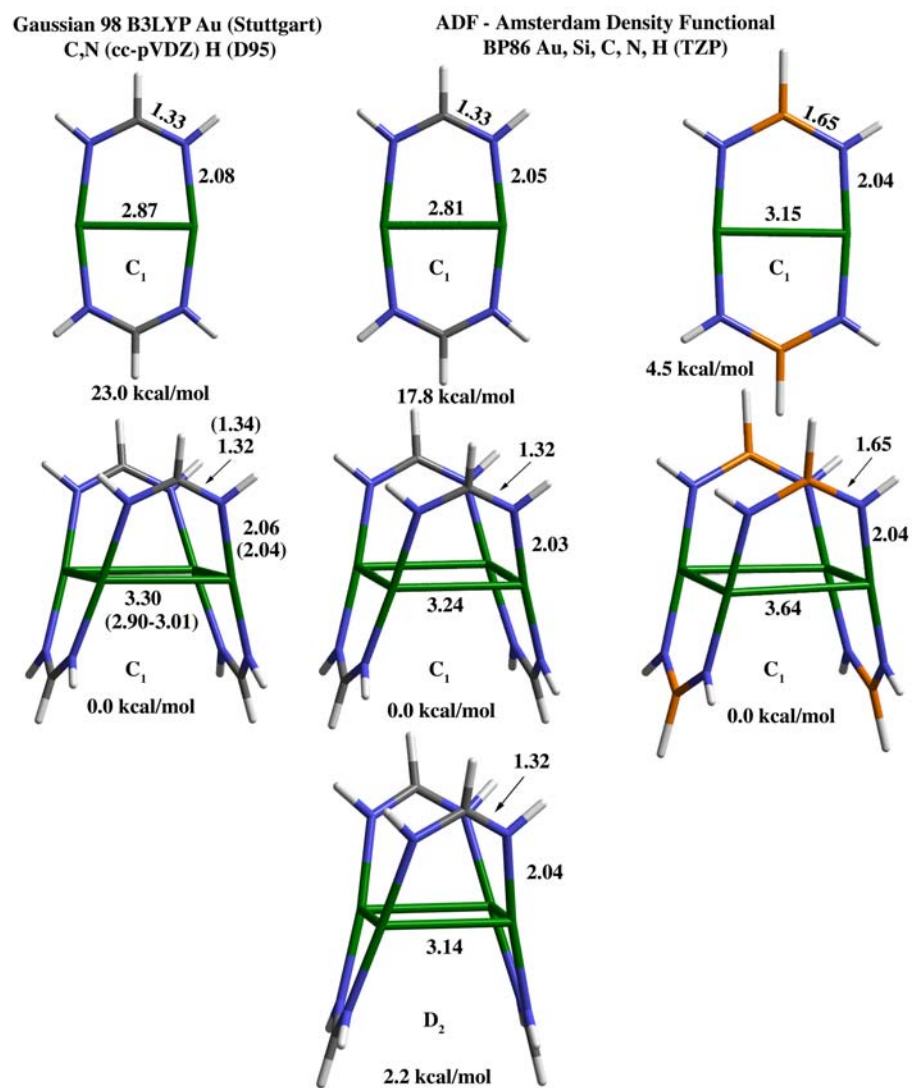


Figure 36. Density Functional Theory calculations of the tetranuclear and dinuclear amidinate complexes at both the Gaussian 98 and ADF levels.

The ligand exchange of the sterically bulky ligands to form mixed ligand species provides a facile procedure for the synthesis of mixed ligand mixed metal complexes of high nuclearity. The tetranuclear gold-silver complex, **33**, was synthesized by reacting the dinuclear gold(I) amidinate complex, **XII**, with the trinuclear silver(I) pyrazolate complex, $[\text{Ag}(\mu\text{-}3,5\text{-Ph}_2\text{Pz})]_3$, **XVIII**, in 1:1 stoichiometric ratio in THF. The tetranuclear gold-silver complex, **33**, is the only tetranuclear mixed ligand complex formed with two amidinate ligands facing each other.

Crystallographic Studies

The needle crystals from **29** were grown by slow evaporation of the THF solution at room temperature. The X-ray structure is shown in Figure 37. The structure is dinuclear-tetranuclear Au_2Au_4 with similar bond distances and angles, $\text{Au}\dots\text{Au} = \sim 2.7$ Å in the dinuclear complex and ~ 3.0 Å in the tetranuclear complex, to their parent complexes reported before.^{21, 22} The crystals from **29** crystallize in the triclinic space group $\text{P}\bar{1}$ (the tetranuclear complex space group is $\text{C}2/\text{c}$ and the dinuclear complex is $\text{P}\bar{1}$). The blocks product, **31**, is mixed ligands $[\text{Au}_4(\text{Ph}_2\text{pz})_2(2,6\text{-Me}_2\text{-form})_2]\cdot 2\text{THF}$. Each

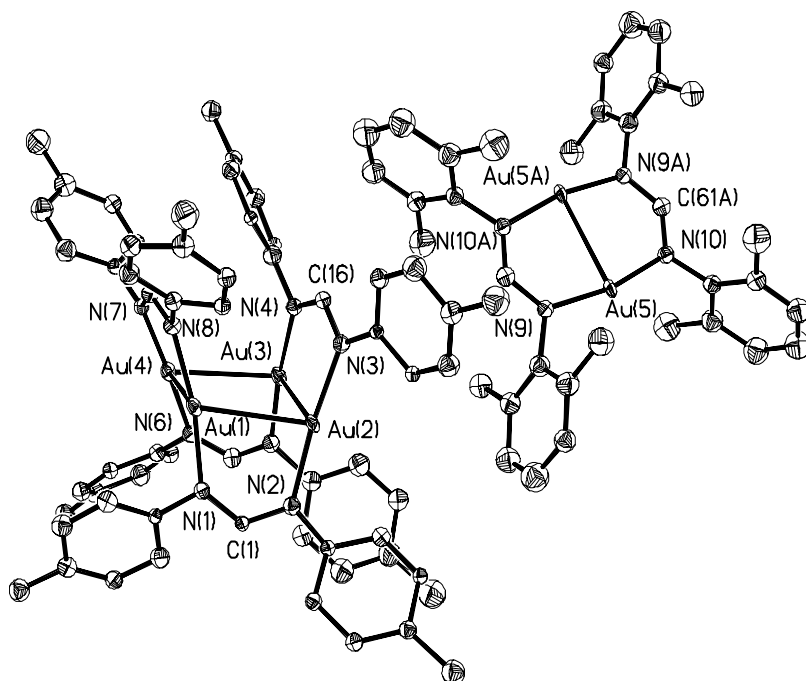


Figure 37. Thermal ellipsoid plot of **29** is drawn at the 50% probability level. Hydrogen atoms are removed for clarity.

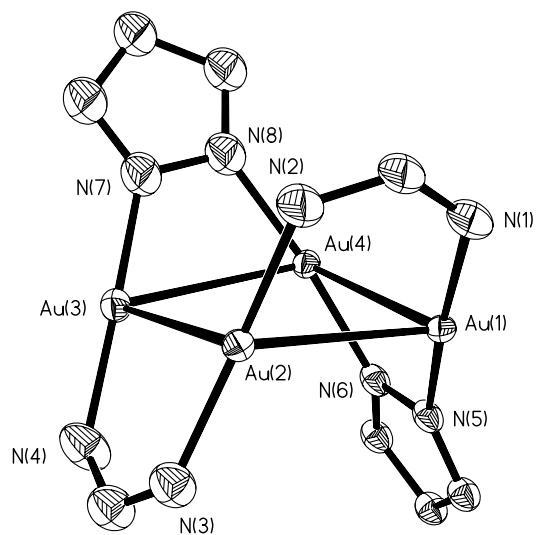


Figure 38. Thermal ellipsoid plot of **31** is drawn at the 50% probability level. Hydrogen atoms are removed for clarity.

pyrazolate ring in **31** is facing amidinate ligand, i.e. anti, to avoid the steric bulk amidinate ligand, Figure 38. The Au...Au distances are ~ 3.1 Å, slightly longer than those in the gold(I) amidinates $[\text{Au}_4(\text{ArNC}(\text{H})\text{NAr})_4]$.

Complex $[\text{Au}_4(\text{Ph}_2\text{pz})_3(2,6\text{-Me}_2\text{-form})]\cdot\text{THF}$, **32**, was isolated from 1:1.5 stoichiometry from sodium pyrazolate as needles. The structure shows the ligands above and below the Au_4 plane, Figure 39. In the tetranuclear gold(I) pyrazolate complex, $[\text{Au}_4(t\text{-Bu-pz})_4]$ the Au...Au distances range is 3.11-3.18 Å.¹³ In complexes **31** and **32**, the Au...Au distances range are 3.10-3.14 and 3.02-3.20 Å, respectively. In clusters **31** and **32**, the Au...Au distances linked by the pyrazolate ligands are slightly longer than those linked by the amidinate ligands. The tetranuclear complex $[\text{Au}_2(3,5\text{-Ph}_2\text{pz})_2(2,6\text{-Me}_2\text{-form})_2\text{Ag}_2]\cdot 2\text{THF}$, **33**, is mixed-ligand mixed-metal with two amidinate ligands facing each other. Apparently, the long Au...Ag distances, ~ 3.3 Å between the two amidinate allow the bulky amidinate ligands to be in a syn arrangement to each other. The four gold and silver atoms are arranged in a parallelogram ($\text{Au}\dots\text{Ag}\dots\text{Au} = 73\text{--}106^\circ$), Figure 40.

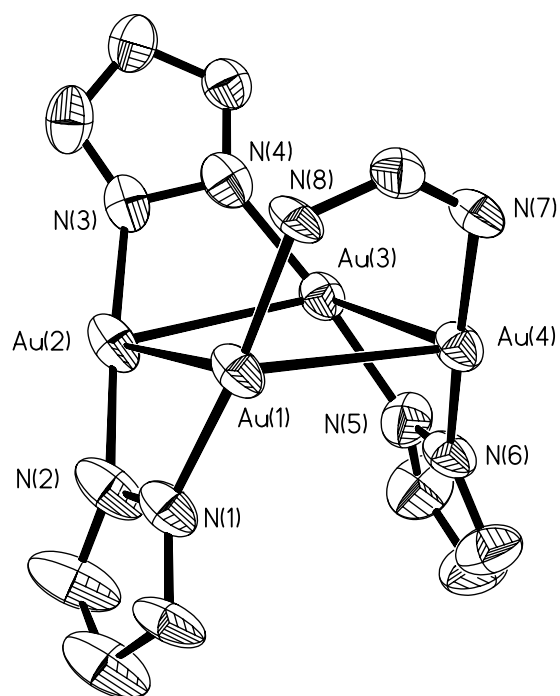


Figure 39. Thermal ellipsoid plot of **32** is drawn at the 50% probability level. Hydrogen atoms are removed for clarity.

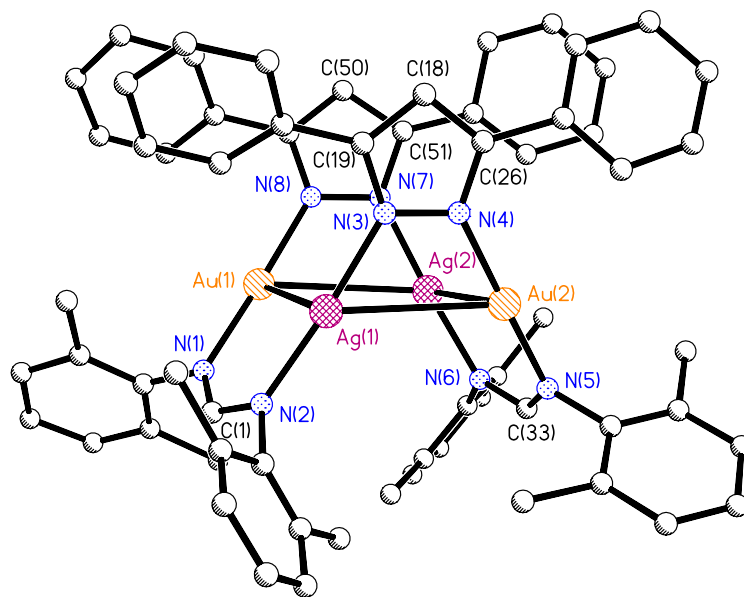


Figure 40. Thermal ellipsoid plot of **33** is drawn at the 50% probability level. Hydrogen atoms are removed for clarity.

Photophysical Properties

Solution studies of **29** using UV-Vis techniques show the spectra combined of the independent dinuclear, **XII** and tetranuclear complexes, **30**, UV-vis (CH_2Cl_2 : 265, 310, 360 nm; tetranuclear; 255 nm, dinuclear), Figure 41.

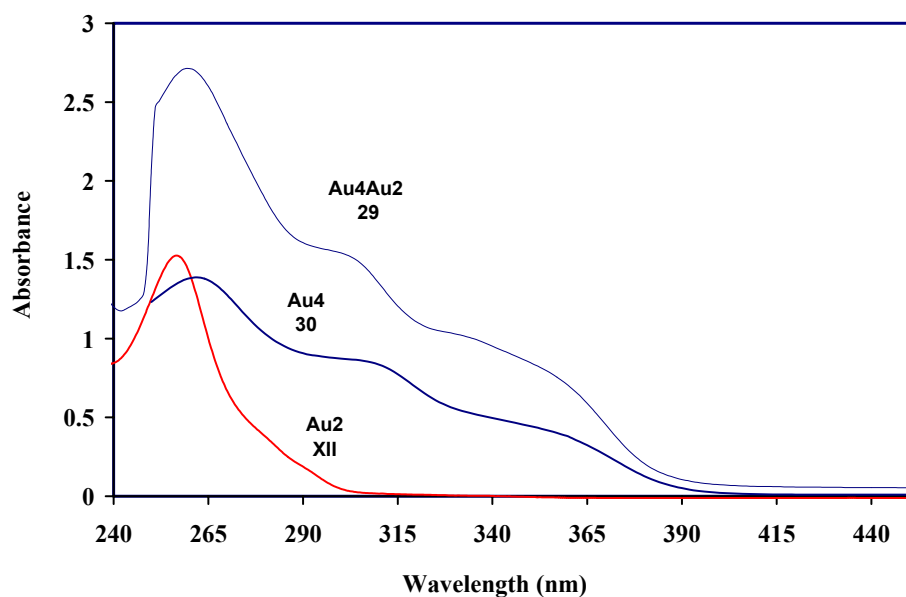


Figure 41. UV -Vis spectra of **XII**, **29**, and **30** in CH_2Cl_2 .

Complex **29** shows a blue-green luminescence under UV-Vis light at RT and 77K. The dinuclear complex, **XII**, emits at ~ 430 nm at 77 K in the solid state but not at ambient temperature. The tetranuclear gold(I) complex **30** shows a bright blue-green luminescence under UV light, with an emission at ~ 490 nm and a weak emission at ~ 530 nm in the solid state, at room temp and 77K, Figure 42. The emission of **29** at RT and

77K shows two components, a broad emission at 465 nm and a weak emission at 530 nm in the solid state at RT and 77K. The luminescence of **29** in the solid state is dominated by the tetranuclear species, Figure 42.

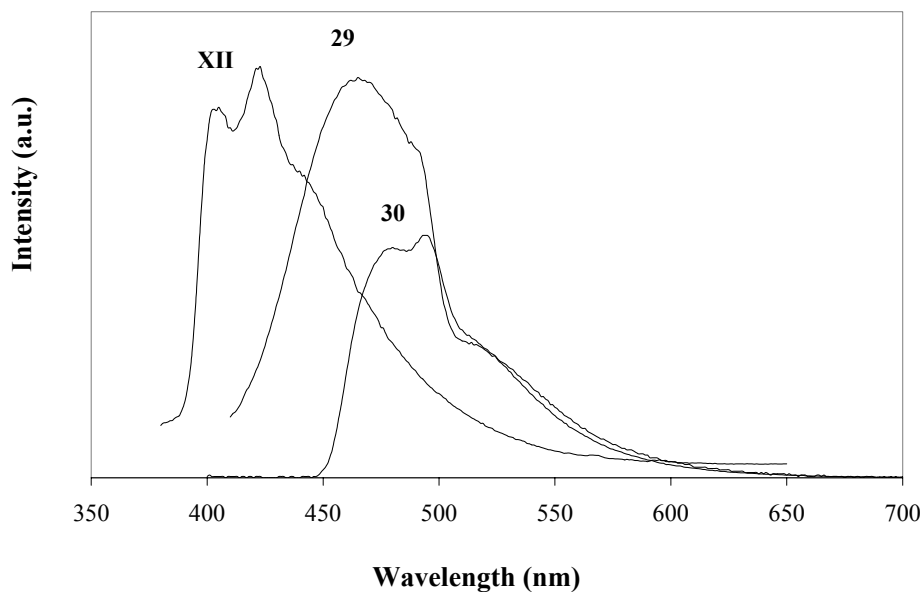


Figure 42. Emission spectra of **XII**, **29**, and **30** in the solid state at 77K.

The ligands themselves do not show visible emission under these experimental conditions. The luminescence studies of several tetranuclear gold(I) amidinate complexes show a bright blue-green luminescence under UV light, with an emission at ~ 490 nm and a weak emission at ~ 530 nm in the solid state, at room temp and 77K.^{21, 22} The life-time measurements of the tetranuclear gold(I) amidinates at 77K suggests metal contribution at the lower energy side.^{21, 22} The small Stokes shift and symmetric band profiles between the excitation and emission spectra suggest the emission at ~ 490 nm to be fluorescence.

The emission from various coinage metals pyrazolate complexes is structured, typical of a ligand-based emission.^{13,55,56} There is a vibronic structure in the emission spectrum which probably corresponds to the stretching (C=N) or (N=N) vibrational modes of the pyrazolate ligand. Based upon these observations, the emission appears to be ligand to metal charge transfer, LMCT, involving the pi electronic ground state of the ligand. The tetranuclear gold(I) pyrazolate [Au₄(*t*-Bu-pz)₄] emit at 541 nm in the solid state at ambient temp. The gold pyrazolates **31** and **32** emit at 490 with a weak emission at 530. The emission at 530 nm is more apparent in complex **32** than it is in **31**, Figure 43. While the dinuclear gold(I) amidinate complex, [Au₂(2,6-Me₂-form)₂], **XII**, shows a vibronic emission at higher energy, 430 nm, complexes **31** and **32** presents emissions at lower energy. The low energy emissions from **31** and **32** suggested more gold contribution in the HOMO energy level.

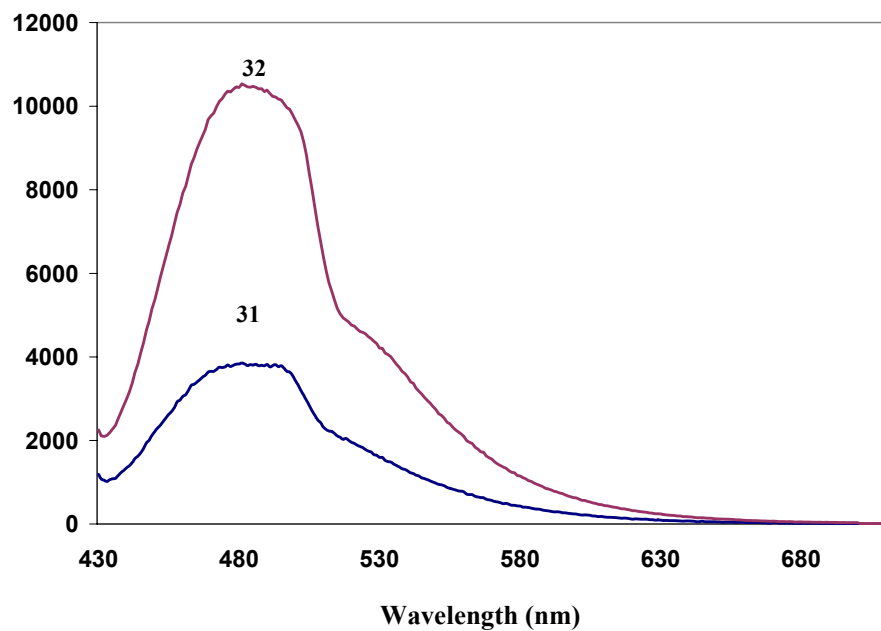


Figure 43. Emission spectra of **31** and **32** in the solid state at 77K.

CHAPTER VI

CONCLUSIONS AND SUGGESTIONS FOR FUTURE WORK

From the work presented here, several important conclusions can be drawn;

The structural arrangement of gold(I) amidinate complexes is determined by the substituents on the amidine ligand, ArNH(CH)NAr. Based on the number of X-ray structures presented in chapter II, we tentatively concluded that the 2,6-substituents on the ligand N-aryl groups play a key role in determining the gold(I) amidinate clusters nuclearity. The electronic vs. steric effect of the substituents on the molecular arrangement of gold(I) amidinates complexes was studied in detail. Syntheses involving various substituted amidinates resulted in tetranuclear gold(I) amidinate clusters, $[\text{Au}_4(\text{ArNC}(\text{H})\text{NAr})_4]$. No change in the nuclearity was found by using substituents such as electron donating or electron withdrawing groups. The tetranuclear gold(I) amidinate clusters and their Au...Au distances are summarized in Table 39 .

Table 39. Tetranuclear Gold(I) Amidinate Cluster.

$[\text{Au}_4(\text{ArNC}(\text{H})\text{NAr})_4]$, Ar =	Au...Au Å
C ₆ H ₄ -4-OMe	2.94
C ₆ H ₄ -3-CF ₃	2.92
C ₆ F ₅	2.96
C ₁₀ H ₇	2.98
C ₆ H ₄ -4-Me	2.96
C ₆ H ₃ -3,5-Cl	2.96
$[\text{Au}_4(\text{ArNC}(\text{Ph})\text{NAr})_4]$, Ar = Ph	2.92
$[\text{Au}_4(\text{ArNC}(\text{CH}_3)\text{NAr})_4]$ Ar = C ₆ H ₅	2.94

Using sterically bulky groups in the 2,6 positions of the N-aryl groups showed that steric factors lead to the formation of di- and trinuclear gold(I) amidinates by preventing the formation of the tetranuclear species suggested to be more stable by DFT calculations with less sterically crowded amidinates.⁵⁴

Electrochemical and photophysical studies of gold(I) amidinate complexes suggest that the electronic properties of the ligands play an important role in their chemistry.^{21,22} The tetranuclear gold(I) amidinate clusters $[\text{Au}_4(\text{ArNC}(\text{H})\text{NAr})_4]$ are the first tetranuclear gold(I) cluster species from group 11 elements that show fluorescence at room temperature. Electrochemical oxidation of the tetranuclear gold(I) amidinate complexes shows three reversible waves not seen in gold complexes before. The oxidation of the dinuclear amidinate is much more difficult than the oxidation of the dinuclear gold(I) ylide complex. Gold ylides are oxidized in 0.1 M $\text{Bu}_4\text{NBF}_4/\text{THF}$ at low potentials of +0.11 and +0.23 V vs. Ag/AgCl .⁴⁸ The dinuclear amidinate, **20**, oxidizes under the same conditions at +1.24 V vs. Ag/AgCl . The differences in the chemistry of these dinuclear gold(I) complexes may be understood by examining their respective HOMOs, which, in the ylide, is a metal-metal σ^* anti-bonding,⁴⁷ while in the dinuclear gold(I) amidinates the HOMO is metal-ligand δ^* . The dinuclear gold(I) amidinate complex $[\text{Au}_2(2,6\text{-Me}_2\text{-form})_2]$ with a Au...Au distance 2.711(3) Å is rare. To our knowledge, there is only one other example of a symmetrical dinuclear gold(I) nitrogen complex, $\{\text{Au}_2[(\text{Me}_3\text{SiN})_2\text{C}(\text{Ph})]_2\}$, which has a Au...Au distance of 2.646 Å.²⁴

The gold(II) amidinate complexes are the first formed with nitrogen ligands. Oxidative-addition reactions to the dinuclear gold(I) amidinate complex were studied

thoroughly. Various reagents such as Cl_2 , Br_2 , I_2 , benzoyl peroxide and CH_3I add to the dinuclear gold(I) amidinate complex to form oxidative addition gold (II) metal-metal bonded complexes, **21**, **22**, **25**, **26**, **28**, Table 40.^{23,45} The Au(II) amidinate complexes are stable at room temperature.

The oxidative addition of benzoyl peroxide leads to the isolation of the first stable dinuclear gold (II) nitrogen complex possessing Au-O bonds, $[\text{Au}_2(o\text{-Me}_2\text{-form})_2(\text{PhCO}_2)_2]$, **28**. Complex **28** has the shortest Au...Au distance in all the Au(II) amidinate complexes, 2.48 Å. Similarly the oxidative addition of benzoyl peroxide to the dinuclear gold(I) ylide complexes, $\text{Au}_2(\text{CH}_2\text{Ph}_2\text{CH}_2)_2$ forms gold(II) ylide complexes with the shortest Au...Au distance observed, 2.56-2.58 Å,⁶ in the dinuclear Au(II) ylides complexes. The facile replacement of the benzoate groups in $[\text{Au}_2(o\text{-Me}_2\text{-form})_2(\text{PhCOO})_2]$, **28**, by chloride or bromide was also studied. Adding equivalent amounts of PhICl_2 or tetrabutylammonium bromide to **28** in polar solvents such as CH_3CN resulted in the replacement of the benzoate groups in **28** by chloride or bromide.

Table 40. Dinuclear Au(II) Amidinate Complexes Characterized by X-ray Studies.

Complex	$d(\text{Au}^{\text{II}} \dots \text{Au}^{\text{II}})$	$d(\text{Au-X})$	$d(\text{Au-R})$
$[\text{ClAu}(o\text{-Me}_2\text{form})_2\text{AuCl}]$, 21	2.517(7)	2.356(2)	
$[\text{BrAu}(o\text{-Me}_2\text{-form})_2\text{AuBr}]$, 22	2.525(15)	2.470(2)	
$[\text{IAu}(o\text{-Me}_2\text{-form})_2 \text{Au I}]$, 25	2.579(4)	2.682(4)	
$[(\text{CH}_3)\text{Au}_2(o\text{-Me}_2\text{-form})_2 \text{AuI}]$, 26	2.529(11)	2.50	2.12
$[\text{PhCO}_2\text{Au}(o\text{-Me}_2\text{form})_2\text{AuO}_2\text{CPh}]$, 28	2.489(10)	2.045(8)	

The reaction with $\text{Hg}(\text{CN})_2$ results in the formation of the 2D mercury(II) cyanide coordination polymer, $[\text{Au}_2(o\text{-Me}_2\text{-form})_2] \cdot 2\text{Hg}(\text{CN})_2 \cdot 2\text{THF}$, **27**, not the expected oxidative-addition product $[\text{NCAu}(o\text{-Me}_2\text{-form})_2\text{AuCN}]$, as in the case of the dinuclear gold(I) ylide.⁴⁶

A new approach for changing the nuclearity of the dinuclear gold(I) amidinate complexes based on the anionic ligand exchange was introduced in chapter V. Density Functional Theory calculations show that a dinuclear gold(I), $[\text{Au}_2(o\text{-Me}_2\text{-form})_2]$, is less stable than a tetranuclear gold(I) amidinate clusters, $[\text{Au}_4(\text{ArNC}(\text{H})\text{NAr})_4]$.⁵⁴ Introducing less bulky anionic ligands to react with the dinuclear complex causes the gold to rearrange and form more stable tetranuclear gold(I) amidinate complex. Tetranuclear gold(I) complexes with mixed amidinate and pyrazolate ligands were formed, $[\text{Au}_4(3,5\text{-Ph}_2\text{pz})_2(2,6\text{-Me}_2\text{-form})_2]$, **31** and $[\text{Au}_4(3,5\text{-Ph}_2\text{pz})_3(2,6\text{-Me}_2\text{-form})]$, **32**. The idea was extended to the synthesis of tetranuclear mixed Au-Ag metal complex of pyrazolate and amidinate ligands $[\text{Au}_2(3,5\text{-Ph}_2\text{pz})_2\text{Ag}_2(2,6\text{-Me}_2\text{-form})_2]$, **33**. Complex **33** is the only tetranuclear amidinate complex with two of the bulky amidinate ligands facing each other. Apparently, the long Au...Ag distances, $\sim 3.3 \text{ \AA}$ between the two amidinate allow the bulky amidinate ligands to be in a syn arrangement to each other for the first time.

Mixed Au-Pd metal complexes could be synthesized using the same procedure explained in chapter V. The mixed Au-Ag and Au-Pd complexes are very effective catalysts for CO oxidation.

Catalytic studies, in collaboration with Professor D. W. Goodman's group, suggest that gold amidinates and related gold nitrogen complexes are the best catalyst precursors for CO oxidation on a TiO₂ surface reported to date (87% conversion).¹⁸ In the past few years, Au(I) and Au(III) have proved to be an efficient homogeneous catalysts to activate the triple bonds for the addition of various nucleophiles.⁵⁷ The gold amidinate complexes could be used as catalysts for similar organic reactions. This project is already under investigation in our laboratory.

The interesting chemistry of the gold amidinate complexes presented in this dissertation; variable nuclearities, high catalytic activity for CO oxidation, 2-D supramolecular formation with Hg(CN)₂, oxidative-addition with Au(II)-Au(II) bond formation, reversible electrochemical oxidation, luminescence at room temperature and formation of mixed gold-silver metal complexes open a new area in gold nitrogen chemistry. Many opportunities exist for other classes of nitrogen ligands such as guanidates, which are expected to produce interesting chemistry with gold as well.

REFERENCES

- (1) Schmidbaur, H. (Ed.), *Gold Progress in Chemistry, Biochemistry, and Technology*; Wiley: West Sussex, England, 1999.
- (2) Cotton, F. A.; *Basic Inorganic Chemistry*; Wiley: New York, 1995; Vol. 3.
- (3) Clerac, R.; Cotton, F. A.; Dunbar, R. A.; Murillo, C. A.; Wang, X. *Inorg. Chem.* **2001**, *40*, 420–426. (b) Cotton, F. A.; Lin, C.; Murillo, C. A. *Inorg. Chem.*, **2000**, *39*, 4574–4578. (c) Cotton, F. A.; Daniels, L. M.; Murillo, C. A.; Schooler, P. J. *Chem. Soc. Dalton Trans.*, **2000**, 2007–2012. (d) Cotton, F. A.; Daniels, L. M.; Murillo, C. A.; Schooler, P. J. *Chem. Soc. Dalton Trans.*, **2000**, 2001–2005. (e) Cotton, F. A.; Daniels, L. M.; Matonic, J. H.; Murillo, C.A. *Inorg. Chim. Acta*, **1997**, *256*, 277–282.
- (4) Cotton, F. A.; Feng, X.; Matusz, M.; Poli, R. *J. Am. Chem. Soc.* **1988**, *110*, 7077–7083.
- (5) Pyykko, P.; Mendizabal, F. *Inorg. Chem. Commun.*, **1998**, *37*, 3018–3025.
- (6) Laguna, A.; Laguna, M., *Coord. Chem. Rev.*, **1999**, *193-195*, 837-856.
- (7) (a) Barker, J.; Kilner, M. *Coord. Chem. Rev.* **1994**, *133*, 219–300 and references cited therein. (b) Patai, S.; *The Chemistry of Amidines and Imidates*; Wiley: New York, 1975; Vol. 1.
- (8) Murray, H. H.; Briggs, D. A.; Garzon Guillermo; Raptis Raphael; Porter, L. C.; Fackler, J. P. Jr. *Organometallics*, **1987**, *6*, 1992.
- (9) Ren, T.; Lin, C.; Amalberti, P.; Macikenas, D.; Protasiewicz, J. D.; Baum, J. C.; Gibson, T. L. *Inorg. Chem. Commun.*, **1998**, *1*, 23–26.
- (10) Archibald, S. J.; Alcock, N. W.; Busch, D. H.; Whitcomb, D. R. *Inorg. Chem.*, **1999**, *38*, 5571–5578.
- (11) Archibald, S. J.; Alcock, N. W.; Busch, D. H.; Whitcomb, D. R.; *J. Cluster Sci.*, **2000**, *11*, 261–283.
- (12) (a) Raptis R. G.; Murray, H. H.; Fackler J. P., Jr. *J. Chem. Soc. Chem. Commun.* **1987**, *10*, 737-739. (b) Murray, H. H.; Raptis, R. G.; Fackler, J. P., Jr. *Inorg. Chem.* **1988**, *27*, 26-33. (c) Raptis R. G.; Fackler J. P., Jr. *Inorg. Chem.* **1988**, *27*, 4179-4182.

- (13) Yang, G.; Raptis, R. G. *Inorg. Chem. Acta* **2003**, *352*, 98-104.
- (14) (a) Clerac, R.; Cotton, F. A.; Dunbar, K. R.; Murillo, C. A.; Wang, X. *Inorg. Chem.* **2001**, *40*, 420-426. (b) Cotton, F. A.; Lin, C.; Murillo, C. A. *Inorg. Chem.* **2000**, *39*, 4574-4578.
- (15) Irwin, M. D.; Abdou, H. E.; Mohamed, A. A.; Fackler, J. P., Jr. *Chem. Commun.* **2003**, 2882-2883.
- (16) Mohamed, A. A.; Fackler, J. P., Jr. Unpublished results.
- (17) Hutchings, G. J. *Gold Bull.* **2004**, *37*, 3-11.
- (18) Choudhary, V.; Sivadinarayana, C.; Chusuei, C. C.; Datye, A. A. K.; Fackler, Jr., J. P.; Goodman, D. W., *J. Catal.*, **2002**, *297*, 247.
- (19) Schmidbaur, H. *The Chemistry of Organic Derivatives of Gold and Silver*; Patai, S.; Wiley: New York, 1999; Vol. 100.
- (20) Hayashi, A.; Olmstead, M. M.; Attar, S.; Balch, A. L. *J. Am. Chem. Soc.* **2002**, *124*, 5791-5795.
- (21) Mohamed, A. A.; Abdou, H. E.; Irwin, M. D.; López-de-Luzuriaga, J. M.; Fackler, J. P., Jr. *J. Cluster Sci.* **2003**, *14*, 253-266.
- (22) Abdou, H. E.; Mohamed, A. A.; López-de-Luzuriaga, J. M.; Fackler, Jr., J. P., *J. Cluster Sci.* **2004**, *15*, 397-411.
- (23) Abdou, H. E.; Mohamed, A. A.; Fackler, Jr., J. P. *Inorg. Chem.* **2005**, *44*, 166-168
- (24) Fenske, D.; Baum, G.; Zinn, A.; Dehnicke, K. *Z. Naturforsch., B: Chem. Sci.* **1990**, *45*, 1273-1278.
- (25) Carlson, T. G.; Fackler, J. P., Jr.; Staples, R. J.; Winpenny, R. E. *Inorg. Chem.* **1995**, *34*, 426.
- (26) (a) Fackler, J. P., *Polyhedron*, **1997**, *16*, 1. (b) Fackler, J. P., *Inorg. Chem.* **2002**, *41*, 6959. (c) Grohman, A.; Schmidbaur, H. in Abel, E. W.; Stone, F. G.; Wilkinson G., Eds; *Comprehensive Organometallic Chemistry II*, **1995**, *3*, 1-56, Pergamon, Oxford.
- (27) SMART V 4.043 Software for the CCD Detector System, Bruker Analytical X-Ray Systems, Madison, WI, 1995.

- (28) SAINT V 4.035 Software for the CCD Detector System, Bruker Analytical X-Ray Systems, Madison, WI, 1995.
- (29) Scheldrick, G. M., SHELXS-97, Program for the Solution of Crystal Structure, University of Göttingen, Germany, 1997.
- (30) SHELXTL 5.03 (PC-Version), Program Library for Structure Solution and Molecular Graphics, Bruker Analytical X-ray Systems, Madison, WI, 1995.
- (31) Patai, S. *The Chemistry of Amidines and Imidates Vol 1*; Wiley: New York, 1975.
- (32) Van Vliet, P.I.; Van Koten, G.; Vrieze, K. *J. Organomet. Chem.* **1979**, *179*, 89-100.
- (33) Anulewicz, R.; Wawer, I.; Krygowski, T. M.; Maennle, F.; Limbach, H. H. *J. Am. Chem. Soc.* **1997**, *119*, 12223–12230.
- (34) Beck, J.; Strahle, J. *Angew. Chem. Int. Ed. Engl.* **1986**, *25*, 95.
- (35) Chiari, B.; Piovesana, O.; Tarantelli, T.; Zanazzi, P. F. *Inorg. Chem.* **1985**, *24*, 366.
- (36) Archibald, S. J.; Alcock, N. W.; Busch, D. H.; Whitcomb, D. R. *J. Cluster Sci.* **2000**, *11*, 261-283.
- (37) Examples of Au-N complexes:(a) Barbera, J.; Elduque, A.; Gimenez, R. F.; Lahoz, J.; Oro, L.; Serrano, J. L. *Inorg. Chem.* **1998**, *37*, 2960. (b) Balch, A. L.; Olmstead, M.; Vickery, J. C. *Inorg. Chem.* **1999**, *38*, 3494. (c) Bovio, B.; Burini, A.; Pietroni, B. R. *J. Organomet. Chem.* **1993**, *452*, 287.
- (38) Mohamed, A. A.; Kani, I.; Ramirez, A. O.; Fackler, Jr., J. P. *Inorg. Chem.* **2004**, *43*, 3833-3839.
- (39) Van Zyl, W. E.; López-de-Luzuriga, J. M.; Fackler, Jr., J. P.; Staples, R. J. *Can. J. Chem.* **2001**, *79*, 896-903.
- (40) King, C.; Wang, J. -C.; Khan, M. N. I.; Fackler, Jr., J. P. *Inorg. Chem.* **1989**, *28*, 2145-2149.
- (41) Van Zyl, W. E.; Staples, R. J.; Fackler, Jr., J. P. *Inorg. Chem. Commun.* **1998**, *1*, 51-54. (b) Van Zyl, W. E.; Lopez-de-Luzuriaga, J. M.; Fackler, Jr., J. P. *J. Mol. Struct.* **2000**, *516*, 99-106.
- (42) Vicente, J.; Chicote, M.-T.; Herrero, G. P.; Jones, P. G. *J. Chem. Soc., Chem.* **1995**, 745-746.

- (43) Nazrul, Md.; Khan, I.; Wang, S.; Fackler, Jr., J. P. *Inorg. Chem.* **1989**, *28*, 3579-3588.
- (44) Mansour, M. A.; Connick, W. B.; Lachicotte, R. J.; Gysling, H. J.; Eisenberg, R. *J. Am. Chem. Soc.* **1998**, *120*, 1329-1330.
- (45) Abdou, H. E.; Mohamed, A. A.; Fackler, J. P., Jr. *Z. Naturforsch., B:Chem. Sci.* **2004**, *59B*, 1480-1482.
- (46) Mohamed, A. A.; Abdou, H. E.; Fackler, Jr., J. P. *Inorg. Chem.* **2006**, *45*, 11-12.
- (47) Murray, H. H.; Mazany, A. M.; Fackler, J. P., Jr., *Organometallics*, **1985**, *4*, 154-157.
- (48) Mohamed, A. A.; Bruce, A. E.; Bruce, M. R. M. In *Chemistry of Organic Derivatives of Gold and Silver*; Patai, S., Ed.; John Wiley and Sons: New York, 1999.
- (49) Porter, L. C.; Fackler, Jr., J. P. *Acta Cryst.* **1986**, *42*, 1128-1131.
- (50) Harvey, P. D. *Inorg. Chem.* **1995**, *34*, 2019-2024.
- (51) Ren, T.; Lin, C.; Amalberti, P.; Macikenas, D.; Protasiewicz, J. D.; Baum, J. C.; Gibson, T. L. *Inorg. Chem. Commun.* **1998**, *1*, 23-26.
- (52) Vogler, A.; Kunkley, H. *Chem. Phys. Lett.* **1988**, *150*, 135-137.
- (53) Forward, J. M.; Fackler, J. P., Jr.; Assefa, Z. In Roundhill, D. M.; Fackler, J. P. Jr.; Eds; *Optoelectronic Properties of Inorganic Compounds*; Plenum Press: New York, 1999, 195-220.
- (54) Mohamed, A. A, Pérez, L. M., Fackler, J. P., Jr. Unpublished results.
- (55) Omary, M.A.; R.-Omary, M. A., Diyabalanage, H. V.; Dias, H. V *Inorg. Chem.* **2003**, *42*, 8612-8614.
- (56) Dias, H. V. Rasika; Diyabalanage, H. V. K.; Eldabaja, M. G.; Elbjeirami, O.; Rawashdeh-Omary, M. A.; Omary, M. A. *J. Am. Chem. Soc.* **2005**, *127*, 7489-7501.
- (57) Georgy, M.; Boucard, V.; Campagne, J. *J. Am. Chem. Soc.* **2005**, *127(41)*, 14180-14181.
- (58) The ligand 1,3,6-triazabicyclo[3.3.0]oct-4-ene, tbo, was given to us by Chad Wilkinson from the LMSB.

(59) Heinrich, D. D.; Staples, R. J.; Fackler, J. P., Jr. *Inorg. Chim. Acta.* **1995**, *229*, 61–75.

(60) Heinrich, D. D.; Wang, J.; Fackler, J. P., Jr. *Acta Cryst.* **1990**, *46*, 1444-1447.

APPENDIX A
SYNTHESIS AND CHARACTERIZATION OF TETRANUCLEAR GOLD(I)
GUANIDINATE COMPLEX

EXPERIMENTAL

Synthesis

Preparation of [Au₄(tbo)₄], tbo =1,3,6-triazabicyclo[3.3.0]oct-4-ene, **34.** tbo (111 mg, 1 mmol) was stirred with (40 mg, 1 mmol) of NaOH in 20 mL of THF for 24 hr. The ligand was not completely soluble. CH₂Cl₂, 5 mL, was added to help increase the solubility. Au(THT)Cl (320 mg, 1 mmol) was added and stirring continued for additional 3 hr. The volume was decreased under vacuum. The product was filtered and the yellow filtrate left overnight in the refrigerator for slow evaporation to form colorless crystals of the tetranuclear gold(I) cluster [Au₄(tbo)₄], **34**.⁵⁸

Crystal Structure

Cell parameters and refinement results of the tetranuclear gold(I) cluster [Au₄(tbo)₄], **34**, are summarized in Table 41. Table 42 shows the important interatomic distances and angles. Thermal ellipsoid plots of the tetranuclear gold(I) cluster [Au₄(tbo)₄] is shown in Figure 44. The tetranuclear Au(I) complex, **34**, crystallizes as colorless needles in the triclinic space group P $\bar{1}$. The four gold atoms are located at the corner of a rhomboid with the tbo ligands bridged above and below the near plane of the four Au(I) atoms. The NC bond length in NCN is ~1.32 Å, indicating delocalization across the NCN bridge. The average Au...Au distance is 2.94 Å, typical of Au(I)...Au(I)

interactions. The angles at Au...Au...Au are acute ($66.03(3)$ – $66.12(3)^\circ$) and obtuse ($111.92(3)$ – $115.82(3)^\circ$). The N–Au–N angles of 177.2° (av.) show a deviation from linearity consistent with Au...Au interactions.

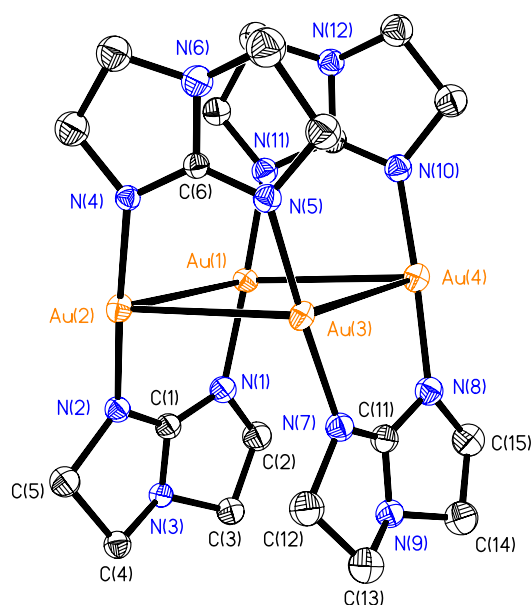


Figure 44. Thermal ellipsoid plot of **34** is drawn at the 50% probability level. Hydrogen atoms are removed for clarity.

Table 41. Crystal Data and Structure Refinement for $[\text{Au}_4(\text{tbo})_4]$, tbo = 1,3,6-triazabicyclo[3.3.0]oct-4-ene, **34**.

Compound	$[\text{Au}_4(\text{tbo})_4]$
Formula	$\text{C}_{20}\text{H}_{36}\text{Au}_4\text{N}_{12}$
FW	1232
Space Group	$\text{P}\bar{1}$
a (Å)	11.476(3)
b (Å)	15.033(4)
c (Å)	17.185(5)
α	112.028(5)
B	105.673(5)
γ	91.165(5)
V (Å ³)	2621.5(13)
Z	4
d_{calc} (g/cm ⁻³)	3.113
μ (mm ⁻¹)	22.351
λ (Å)	0.71073
T (K)	110(2)
R1, wR2	0.7072, 0.2801

$$^a \text{R1} = \frac{\sum \left| |F_o| - |F_c| \right|}{\sum |F_o|}$$

$$^b \text{wR2} = \left[\frac{\sum [w(F_o^2 - F_c^2)^2]}{\sum [w(F_o^2)]} \right]^{1/2}; w = 1/[\sigma^2(F_o^2) + (aP)^2 + (bP)], \text{ where } P = [\max(F_o^2 \text{ or } 0) + 2(F_c^2)]/3$$

Table 42. Selected Bond Distances (Å) and Angles (°) for [Au₄(tbo)₄], tbo =1,3,6-triazabicyclo[3.3.0]oct-4-ene, **34**.

Au1–N11	2.011(16)	N2–C1	1.32(3)
Au1–N1	2.039(16)	N4–C6	1.29(2)
Au1...Au2	3.1139(12)	N8–C11	1.33(3)
Au1...Au4	3.1563(13)	N1–C1	1.28(3)
Au3–N7	2.026(18)	N5–C6	1.32(3)
Au3–N5	2.037(17)	N3–C1	1.37(2)
Au3...Au4	3.1889(12)	N3–C4	1.49(3)
Au3...Au2	3.2220(13)	N6–C6	1.35(2)
Au2–N2	1.984(15)	N8–C11	1.33(3)
Au2–N4	2.017(15)	N7–C11	1.28(3)
Au1...Au2...Au3	66.12(3)	N1–C1–N2	131.1(18)
Au4...Au3...Au2	111.92(3)	N1–C1–N3	112.9(18)
Au1...Au4...Au3	66.03(3)	N2–C1–N3	115.9(17)
Au2...Au1...Au4	115.82(3)	N11–Au1–N1	177.2(7)
N7–Au3–N5	177.7(7)	N11...Au1...Au2	103.3(5)
N7...Au3...Au4	77.9(5)	N1...Au1...Au4	103.5(5)
N7...Au3...Au2	104.4(5)	C6–N4–Au2	124.1(14)
C1–N2–Au2	123.2(12)	C6–N5–Au3	124.0(13)
N2–Au2–N4	176.6(7)		

APPENDIX B

SYNTHESIS OF BIS(DIETHYLDITHIOCARBAMATO)DIGOLD(I) COMPLEX BY THE LIGAND EXCHANGE OF THE DINUCLEAR GOLD(I) AMIDINATE COMPLEX, $[\text{Au}_2(o\text{-Me}_2\text{-form})_2]$

EXPERIMENTAL

Synthesis

Preparation of $\text{Au}_2[\text{S}_2\text{CN}(\text{C}_2\text{H}_5)_2]_2$, **35.** $[\text{Au}_2(o\text{-Me}_2\text{-form})_2]$, (60 mg, 0.067 mmol) was dissolved in 10 mL THF and stirred for 10 min., tetraethylthiuram disulfide (20 mg, 0.067 mmol) was added. The color of the reaction mixture gradually changed from yellow to orange with the formation of a white precipitate. The reaction mixture was stirred for 24 h, filtered and the orange-yellow filtrate was left overnight at room temperature for slow evaporation. Yellow crystals of **35** formed after two days.

RESULTS AND DISCUSSION

Synthesis

The reaction of the dinuclear amidinate complex $[\text{Au}_2(2,6\text{-Me}_2\text{-form})_2]$, **20**, with tetraethylthiuram disulfide in THF results in the formation of the dinuclear complex $\text{Au}_2[\text{S}_2\text{CN}(\text{C}_2\text{H}_5)_2]_2$, **35**, not the expected oxidative-addition product, $[\text{Au}_2(2,6\text{-Me}_2\text{-form})_2][\text{S}_2\text{CNEt}_2]_2$, as in the case of the dinuclear gold(I) ylide, $[\text{Au}(\text{CH}_2)_2\text{PPhMe}]_2[\text{S}_2\text{CNEt}_2]_2$.⁵⁹ Tetraethylthiuram disulfide replaced the bulky amidinate ligand, 2,6-Me₂-

form. The same structure was reported previously, obtained by the reaction of Au(THT)Cl with $\text{KS}_2\text{CN}(\text{C}_2\text{H}_5)_2$ in THF.⁶⁰

Crystal Structure

Thermal ellipsoid plot of **35** is shown in Figure 45. $\text{C}_{10} \text{H}_{20} \text{Au}_2 \text{N}_2 \text{S}_4$, $M = 690.45$, tetragonal, $a = 17.936(7)$, $b = 17.936(7)$, $c = 22.734(12)$, $\alpha = 90.00$, $\beta = 90.00$, $\gamma = 90.00$, $V = 7313(5) \text{ \AA}^3$, $T = 110(2) \text{ K}$, space group $I4_1/a$, $Z = 16$. The intramolecular Au...Au distance is $2.7799(15) \text{ \AA}$, the intermolecular Au...Au distance is $2.9795(16) \text{ \AA}$ and the Au-S distance is $\sim 2.294 \text{ \AA}$. In the previously reported structure the intramolecular Au-Au distance is $2.782(1) \text{ \AA}$ and the intermolecular Au-Au distance is $3.004(1) \text{ \AA}$.⁶⁰

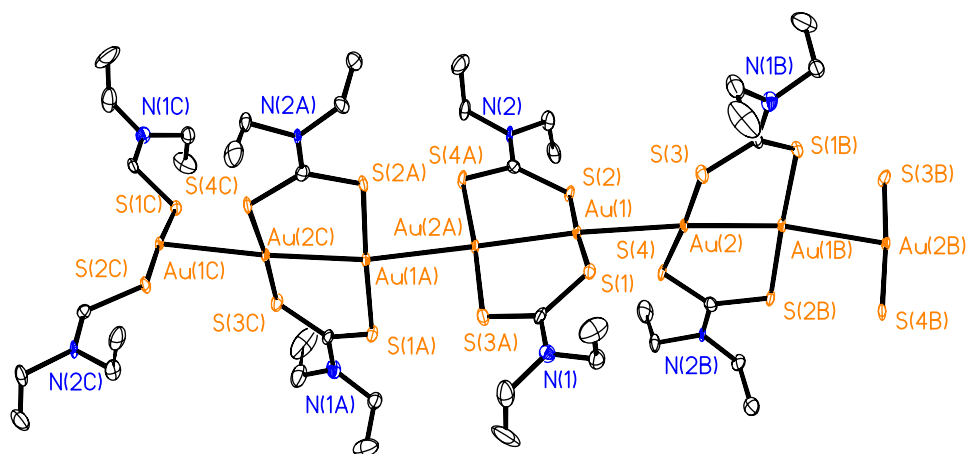


Figure 45. Thermal ellipsoid plot of **35** is drawn at the 50% probability level. Hydrogen atoms are removed for clarity.

VITA

Hanan Elsayed Abdou received her B.S. in chemistry from Zagazig University, Egypt in 1991. In January 1999 she was enrolled for graduate study in chemistry at the University of Maine and served as a Teaching Assistant in the department of chemistry. She received her M.S. in chemistry from the University of Maine in May 2001.

Her permanent address is:

502 Al-Saleem Tower

Al-Qawmya Square

Zagazig, Egypt